

## INFORMATION TO USERS

This reproduction was made from a copy of a document sent to us for microfilming. While the most advanced technology has been used to photograph and reproduce this document, the quality of the reproduction is heavily dependent upon the quality of the material submitted.

The following explanation of techniques is provided to help clarify markings or notations which may appear on this reproduction.

1. The sign or "target" for pages apparently lacking from the document photographed is "Missing Page(s)". If it was possible to obtain the missing page(s) or section, they are spliced into the film along with adjacent pages. This may have necessitated cutting through an image and duplicating adjacent pages to assure complete continuity.
2. When an image on the film is obliterated with a round black mark, it is an indication of either blurred copy because of movement during exposure, duplicate copy, or copyrighted materials that should not have been filmed. For blurred pages, a good image of the page can be found in the adjacent frame. If copyrighted materials were deleted, a target note will appear listing the pages in the adjacent frame.
3. When a map, drawing or chart, etc., is part of the material being photographed, a definite method of "sectioning" the material has been followed. It is customary to begin filming at the upper left hand corner of a large sheet and to continue from left to right in equal sections with small overlaps. If necessary, sectioning is continued again—beginning below the first row and continuing on until complete.
4. For illustrations that cannot be satisfactorily reproduced by xerographic means, photographic prints can be purchased at additional cost and inserted into your xerographic copy. These prints are available upon request from the Dissertations Customer Services Department.
5. Some pages in any document may have indistinct print. In all cases the best available copy has been filmed.

**University  
Microfilms  
International**

300 N. Zeeb Road  
Ann Arbor, MI 48106



8323747

**Rogers, Ralph David**

STRUCTURAL AND GEOCHEMICAL EVOLUTION OF A MINERALIZED  
VOLCANIC VENT AT CERRO DE PASCO, PERU

*The University of Arizona*

PH.D. 1983

**University  
Microfilms  
International** 300 N. Zeeb Road, Ann Arbor, MI 48106

Copyright 1983

by

Rogers, Ralph David

All Rights Reserved



PLEASE NOTE:

In all cases this material has been filmed in the best possible way from the available copy.  
Problems encountered with this document have been identified here with a check mark ☒.

1. Glossy photographs or pages ☒
2. Colored illustrations, paper or print ☒
3. Photographs with dark background ☒
4. Illustrations are poor copy \_\_\_\_\_
5. Pages with black marks, not original copy \_\_\_\_\_
6. Print shows through as there is text on both sides of page \_\_\_\_\_
7. Indistinct, broken or small print on several pages \_\_\_\_\_
8. Print exceeds margin requirements \_\_\_\_\_
9. Tightly bound copy with print lost in spine \_\_\_\_\_
10. Computer printout pages with indistinct print \_\_\_\_\_
11. Page(s) \_\_\_\_\_ lacking when material received, and not available from school or author.
12. Page(s) \_\_\_\_\_ seem to be missing in numbering only as text follows.
13. Two pages numbered \_\_\_\_\_. Text follows.
14. Curling and wrinkled pages \_\_\_\_\_
15. Other \_\_\_\_\_

University  
Microfilms  
International



STRUCTURAL AND GEOCHEMICAL EVOLUTION OF A  
MINERALIZED VOLCANIC VENT AT  
CERRO DE PASCO, PERU

by

Ralph David Rogers

---

A Dissertation Submitted to the Faculty of the  
DEPARTMENT OF GEOSCIENCES  
In Partial Fulfillment of the Requirements  
For the Degree of  
DOCTOR OF PHILOSOPHY  
In the Graduate College  
THE UNIVERSITY OF ARIZONA

1 9 8 3

Copyright 1983 Ralph David Rogers

THE UNIVERSITY OF ARIZONA  
GRADUATE COLLEGE

As members of the Final Examination Committee, we certify that we have read  
the dissertation prepared by Ralph David Rogers

entitled STRUCTURAL AND GEOCHEMICAL EVOLUTION OF A MINERALIZED VOLCANIC  
VENT AT CERRO DE PASCO, PERU

and recommend that it be accepted as fulfilling the dissertation requirement  
for the Degree of Doctor of Philosophy.

John M. Guilbert  
Francis J. Goff  
Carol A. Davis  
E. J. Essene  
Paul H. Paster

6/24/83  
Date

6/24/83  
Date

6/24/83  
Date

6/24/83  
Date

6/24/83  
Date

Date

Final approval and acceptance of this dissertation is contingent upon the  
candidate's submission of the final copy of the dissertation to the Graduate  
College.

I hereby certify that I have read this dissertation prepared under my  
direction and recommend that it be accepted as fulfilling the dissertation  
requirement.

John M. Guilbert  
Dissertation Director

June 24, 1983  
Date



STATEMENT BY AUTHOR

This dissertation has been submitted in partial fulfillment of requirements for an advanced degree at The University of Arizona and is deposited in the University Library to be made available to borrowers under rules of the Library.

Brief quotations from this dissertation are allowable without special permission, provided that accurate acknowledgment of source is made. Requests for permission for extended quotation from or reproduction of this manuscript in whole or in part may be granted by the copyright holder.

SIGNED: \_\_\_\_\_



## ACKNOWLEDGMENTS

This research was supported intellectually, financially and logistically by numerous people. Logistical support for the fieldwork in Peru was provided by Centromin Peru. In particular the help of Julio Pastor, chief geologist, and Rolando Luna, mine geologist at Cerro de Pasco, is gratefully acknowledged. Numerous discussions with assistant mine geologists on the staff at Cerro de Pasco were also very helpful. Financial support for this research was provided by NSF grant number INT-7908669 to John Guilbert and, for one year, by a research fellowship from Phillips Petroleum Company.

The help and guidance given by Drs. Peter Coney, George Davis, Chris Eastoe, Denis Norton and Spencer Titley of The University of Arizona during the dissertation research are gratefully acknowledged. The guidance of, and critical discussions with, Dr. John Guilbert, my dissertation director, were particularly helpful. As were Dr. Guilbert's undying efforts to improve my grammar and composition, especially his endless injunctions to not split my infinitives.

## TABLE OF CONTENTS

	Page
LIST OF ILLUSTRATIONS . . . . .	vii
LIST OF TABLES . . . . .	x
ABSTRACT . . . . .	xi
 INTRODUCTION . . . . .	 1
Location . . . . .	2
Previous Work . . . . .	4
Scope of Study . . . . .	5
 DISTRICT GEOLOGY . . . . .	 7
Geologic Setting . . . . .	7
Mineralization . . . . .	9
Surface Effects . . . . .	12
Sedimentary Textures in Sulfide . . . . .	13
 THE VOLCANIC SYSTEM . . . . .	 17
Ring Fault System . . . . .	17
Rootless Blocks . . . . .	19
Volcaniclastic Rocks . . . . .	22
Intrusive Rocks . . . . .	25
Fractures and Hydrothermal Alteration . . . . .	28
Summary . . . . .	29
 STRUCTURAL GEOLOGY OF THE VOLCANIC SYSTEM . . . . .	 31
Bedding Orientations . . . . .	31
Foliation Orientation . . . . .	35
Fracture and Vein Systems . . . . .	40
Summary . . . . .	45
 ALTERATION . . . . .	 47
Distribution . . . . .	48
Quartz-Alunite-Kaoline Zone . . . . .	49

TABLE OF CONTENTS--Continued

	Page
Quartz-Phyllosilicate Zone . . . . .	52
Calcite-Chlorite-Epidote Zone . . . . .	52
Alteration Marginal to the Pyrite-Silica Body . . . . .	54
Alteration in Limestone . . . . .	54
X-ray and Microprobe Studies . . . . .	55
Variations within the Phyllosilicate Zone . . . . .	56
Geometry of Alteration Zones . . . . .	62
Disruption of the Alteration Patterns . . . . .	63
Lourdes Fragmental . . . . .	63
Summary . . . . .	64
GEOCHEMISTRY . . . . .	66
General Conditions . . . . .	67
Geochemical Systems . . . . .	71
Phase Relations . . . . .	73
Cu-Fe Sulfides and Cu-As Sulfosalts . . . . .	78
OTHER FELSIC VOLCANIC SYSTEMS . . . . .	82
DISCUSSION . . . . .	85
Initial Phases . . . . .	85
Infilling of the Vent . . . . .	88
Structural Collapse and Fracturing . . . . .	92
Hydrothermal System . . . . .	97
Level of Exposure . . . . .	104
CONCLUSIONS . . . . .	107
LIST OF REFERENCES . . . . .	110

## LIST OF ILLUSTRATIONS

Figure	Page
1. Location map . . . . .	3
2. Geologic map and cross sections of the Cerro de Pasco district, Peru . . . . .	In Pocket
3. Slab A: "sedimentary pyrite" from Cerro de Pasco . . . . .	14
4. Slab B: "sedimentary pyrite" from Cerro de Pasco . . . . .	16
5. The vent margin, looking west . . . . .	18
6. Rootless block in the Cerro de Pasco vent . . . . .	21
7. Outcrop expression of bedding in the Rumiallana Agglomerate . . . . .	23
8. Outcrop expression of the foliation in the dacite unit (Tvd) . . . . .	27
9. Relation of bedding orientations to spatial location within the vent at Cerro de Pasco . . . . .	33
10. Lower hemisphere stereographic projection of poles to bedding orientations . . . . .	34
11. Fold in the dacite unit (Tvd) . . . . .	36
12. Foliation orientations, folds, and form lines defining the morphology of the southernmost "diapiric structure" shown on Figure 2 . . . . .	37
13. Rose diagrams showing the orientation of mineralized fractures measured in the field (A) and the orientation of vein segments measured from mine level maps (B) . . . . .	41
14. North-south cross-section, looking, east, through the vein system at Cerro de Pasco . . . . .	42

LIST OF ILLUSTRATIONS--Continued

Figure	Page
15. Rose diagrams showing orientations of mineralized fractures and vein segments by domain as described in the text . . . . .	44
16. Quartz-alunite-kaolinite alteration zone, altered Rumiallana Agglomerate (100x) . . . . .	50
17. Part of the gradational boundary between the quartz-alunite-kaolinite zone and the quartz-pyrophyllite-kaolinite zone, altered Rumiallana Agglomerate (100x) . .	51
18. Quartz-muscovite-kaolinite zone, altered Rumiallana Agglomerate (100x) . . . . .	53
19. Components of fine-grained white micas calculated from microprobe analyses . . . . .	58
20. Schematic diagram of alteration zonation . . . . .	60
21. Activity-temperature diagram for the system $\text{Al}_2\text{O}_3\text{-SiO}_2\text{-H}_2\text{O}$ .	74
22. Activity-activity diagrams for the system $\text{K}_2\text{O-Al}_2\text{O}_3\text{-SiO}_2\text{-SO}_3\text{-HCl-H}_2\text{O}$ . . . . .	76
23. Activity-activity diagrams for the system $\text{K}_2\text{O-Al}_2\text{O}_3\text{-SiO}_2\text{-SO}_3\text{-HCl-H}_2\text{O}$ . . . . .	77
24. Activity-activity diagrams for the system $\text{Fe}_2\text{O}_3\text{-FeO-Cu}_2\text{O-As}_2\text{O}_3\text{-H}_2\text{S-SO}_3\text{-H}_2\text{O}$ . . . . .	80
25. Initial phase of vent development as seen in a schematic east-west section . . . . .	89
26. Infilling of the vent structure . . . . .	91
27. Structural collapse of the system . . . . .	93
28. Activity-activity diagram for the system $\text{K}_2\text{O-Al}_2\text{O}_3\text{-SiO}_2\text{-HCl-H}_2\text{O}$ . . . . .	101

LIST OF ILLUSTRATIONS--Continued

	Page
Figure	
29. Activity-activity diagrams for the system $\text{CaO-MgO-Al}_2\text{O}_3\text{-SiO}_2\text{-H}_2\text{O}$ . . . . .	103
30. Late stage hydrothermal activity resulted in ore deposition . . . . .	105

## LIST OF TABLES

	Page
Table	
1. Microprobe Analyses . . . . .	57
2. Fluid Inclusion Filling Temperatures . . . . .	68



## ABSTRACT

Major Cu-Pb-Zn-Ag mineralization is associated with a dissected volcanic vent, approximately 2 Km in diameter, at Cerro de Pasco, Peru. Vent fill material, including volcanoclastic agglomerate, bedded and welded tuff, and rootless blocks, document more than one kilometer of subsidence of the floor of the vent. A concave-upward conical fold distorts the vent-fill material, thus recording a late structural collapse. Resurgent igneous activity is evidenced by quartz monzonite porphyry dikes and a group of interpenetrating dacite domes intruded along the vent margin. Hydrothermal ore deposition occurred during the final stage in the evolution of this volcanic system. The volcanic system is best described as a caldera system that has experienced igneous resurgence.

Mineralization is associated with three distinctive fracture sets. Fractures in Set I parallel the strike and dip of the vent margin and formed as a result of slumping along the vent margin. Fractures in Set II occur between the vent margin and the Longitudinal Fault and formed as a result of strike-slip motion along that fault. Fractures in Set III have a consistent east-west strike, converge at depth to a quartz monzonite porphyry dike, and formed in response to emplacement of the dike.

Alteration zones have developed parallel to fracture-controlled flow channels. Quartz-alunite-kaolinite is developed

closest to vein mineralization. This assemblage grades into quartz-phylosilicate-kaolinite away from the veins, and this latter zone in turn grades into calcite-chlorite-epidote further from the veins.

Hydrothermal solutions were localized by the permeable zones along the vent margin. The first hydrothermal minerals deposited were pyrite and silica. These formed a large massive sulfide replacement body. Subsequently, ~300°C solutions equilibrated with the early formed pyrite and continued to ascend upward and outward into what would become the main ore zone. As these solutions moved into the oxidized environment of the upper levels of the volcanic vent they deposited pyrite and enargite in veins and generated hydrogen ions that hydrolytically altered the adjacent wallrocks. Changes in solution composition accompanying alteration are discussed.

## INTRODUCTION

Mineralization at Cerro de Pasco, Peru is shown to be the product of the structural and geochemical evolution of a volcanic and subvolcanic to plutonic system, demonstrating a relationship between volcanism and mineralization that was not previously appreciated. Erosion has breached the volcanic vent such that the present level of exposure provides opportunity to study the interior of a volcanic system. This study investigates the evolution of the volcanic system at Cerro de Pasco, the geochemistry of the (spatially) associated hydrothermal system, and the relationship of the volcanic system to the hydrothermal system which formed the ore deposit.

Many hydrothermal ore deposits are spatially associated with felsic volcanic systems. The Kuroko systems of Japan are examples of systems developed on the sea floor (Lambert and Sato, 1974; Ohmoto, 1978). Other systems evolved in a subaerial setting, such as those found in the San Juan Mountains of Colorado (Steven and Lipman, 1976). Evolution of the subaerial felsic volcanic systems commonly includes one or more episode of caldera formation (Smith and Bailey, 1968).

In their classic model of resurgent cauldrons, Smith and Bailey (1968) suggested that hydrothermal systems might be characteristic of the late stages of the caldera cycle. In the San Juan Mountains, hydrothermal ore deposits are spatially related to

calderas (Steven, Luedke and Lipman, 1974). Caldera development has been important in generation of the structures that have localized mineralization, but the age of the mineralization is significantly younger than that of caldera formation (Lipman et al., 1976; Doe et al., 1979).

#### Location

Cerro de Pasco, located in the high sierra of central Peru (Figure 1), is part of the polymetallic province of central Peru (Cobbing et al., 1981). This Cu-Pb-Zn-Ag province trends north-northwest through the central Andes. The rich variety of deposit types present was summarized by the Geological Staff of Cerro de Pasco Corporation (1950) and Petersen (1965). The province is probably most famous for its base metal Cordilleran veins and manto massive sulfide bodies. These deposits are commonly associated with anticlines and regional strike-slip faults (Peterson, 1965).

The ore deposit at Cerro de Pasco has been worked continuously since the early 1920's, and several studies have been conducted, investigating various aspects of the geology. Boutwell, McLaughlin and Walker (1920) produced the first detailed map of the district. The spatial association between the ore deposit and the volcanic vent was recognized early (Bowditch, 1935), as was the possibility of a genetic link. Bowditch (1935) reported L. C. Graton's comment that "When the top blows off a steam boiler there is no reason to expect the steam to go anywhere else."

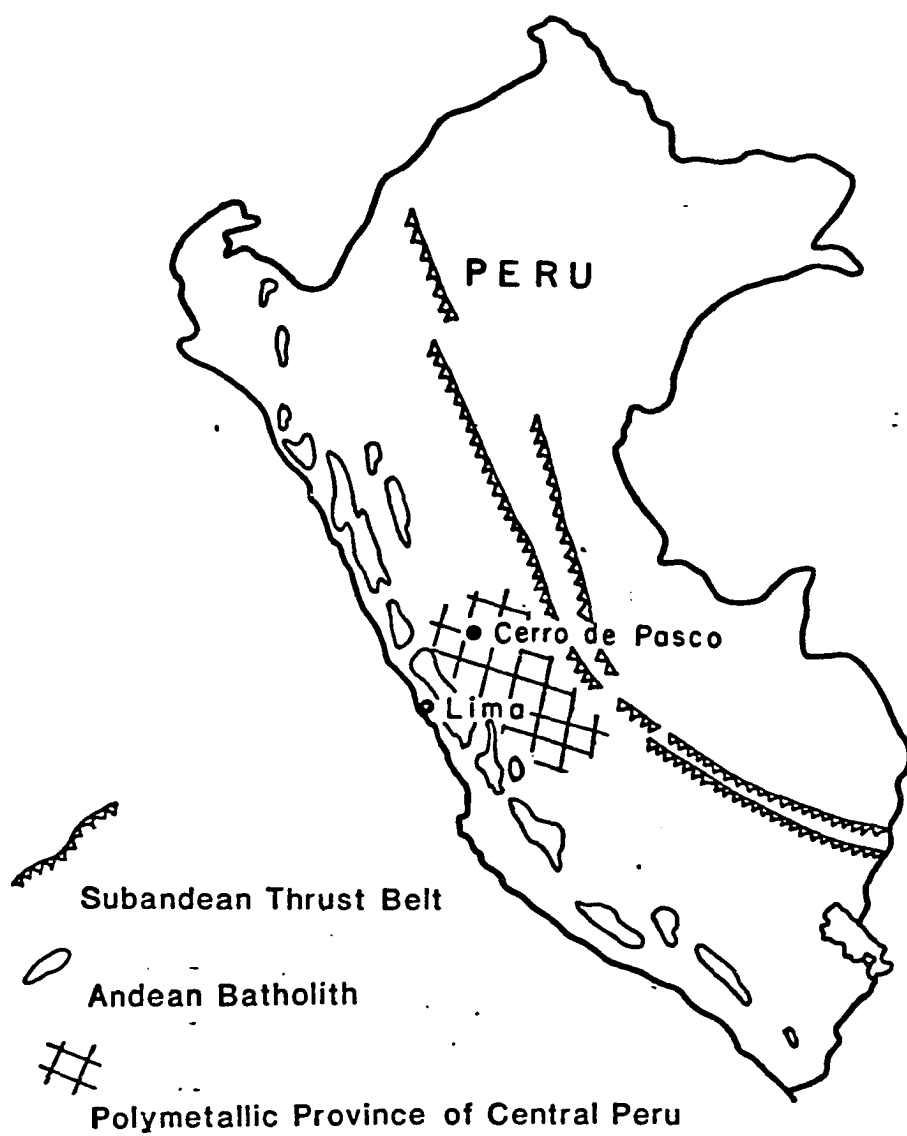


Figure 1. Location map.

### Previous Work

Extensive earlier research has concentrated on mineralogical aspects of the deposit. Bowditch (1935) studied the mineralogy of the vein ores and the associated minerals. Zonation of alteration minerals associated with vein mineralization was reported by Graton and Bowditch (1936). Lacy (1949) delineated six types of pyrite, all of different textural ages, and studied the mineralogy of the massive sulfide body. Of particular interest are pyrrhotite and galena-sphalerite pipes which drill the sulfide body; they were studied in detail by Einaudi (1968, 1977). An array of unusual Cu-Pb-Zn-Ag-As-S base and precious metal sulfide and sulfosalt minerals was found to be associated with the late stages of the hydrothermal system (Lacy and Hosmer, 1956). The general geology of the deposit has been summarized in three excellent reports (McLaughlin et al., 1933; Geological Staff, 1950; Rivera, 1970) which contain descriptions of the ore deposit and the immediately enclosing rocks, but report little or nothing about the volcanic system and associated volcanic rocks. The structural framework of the district was reported by Ward (1961).

The association of intrusive rocks with mineralization in central Peru has been stressed by a number of workers (Geological Staff, 1950; Lacy, 1953). Lacy (1953) in particular emphasized the relation of mineralization to intrusions rather than volcanic systems. Studies in other districts and terrains, however, have emphasized the relationship between mineralization and the evolution of volcanic systems.

Cerro de Pasco therefore provides a provocative setting for the study of the interrelationships between volcanism, plutonism, and ore deposition.

The detailed geology of the volcanic vent at Cerro de Pasco has not been studied or reported previously. Early studies suggested that a volcanic cone may have once stood above the vent (Bowditch, 1935), but the vent structure has been infilled by volcanoclastic and sedimentary material, which has in turn been intruded by volcanic domes and dikes. Detailed mapping conducted during the field seasons of 1980 and 1981 has revealed important aspects of lithologic variation and internal geometry within this volcanic system (Figure 2).

#### Scope of Study

The purpose of this study is to investigate the interrelationships between the evolution of the volcanic system and the development of the hydrothermal system at Cerro de Pasco. Pursuant to this purpose, the volcanic system will be described in detail. First, the district scale structural setting of the volcanic system and the general characteristics of the ore deposit will be described. Second, the details of the volcanoclastic, volcanic, and intrusive rocks that fill the vent structure will be described. Then the structures within and immediately adjacent to the vent will be described and interpreted. Particular attention will be paid to the relations of those structures to the ore deposit. Next, the alteration associated with

the ore deposit will be described and investigated to constrain physico-chemical conditions at the time of mineralization. The alteration can, thus, be used to identify the level of the system that is presently exposed. Finally, the structural evolution of the system will be integrated with the processes of ore deposition. Briefly, Cerro de Pasco will be shown to provide an excellent locale to study caldera formation and its relation to late-stage hydrothermal activity. It will also be seen that collapse of the floor of the volcanic vent was followed by slumping along the vent margin and infilling by volcanic and volcanoclastic material. The ring fault system and fracturing formed by slumping were important in localizing later hydrothermal mineralization. Subsequent to the collapse, resurgent igneous activity included the intrusion of dacite domes along the western margin of the vent and quartz monzonite porphyry dikes into the central portion of the vent. Intrusion of the quartz monzonite porphyry created additional fractures and led to the development of a hydrothermal system (Rogers, 1982).



## DISTRICT GEOLOGY

Cerro de Pasco is located in the central part of a regional structural dome, the northernmost of three such domes in central Peru (Megard, 1979). The southernmost of the three domes, the Yauli Dome, is associated with the famous mining districts at San Cristobal and Morococha. All three domes are cored by low-grade metamorphic rocks of the Excelsior Group of Devonian age (McLaughlin, 1924; Jenks, 1951). Flanking the northernmost dome are deformed rocks of Paleozoic, Mesozoic, and Cenozoic age, part of the Cenozoic fold and thrust belt of central Peru (Figure 1). Piercing it is a nearly cylindrical volcanic vent containing igneous, volcanoclastic, and sedimentary rocks. K-Ar dates on mineral separates from igneous rocks within the vent fall between 14 and 15 million years (Silberman and Noble, 1977). The surficial expression and extrusive manifestations of this ancient volcano have been completely removed by erosion, and the interior portion of the vent has been exposed for study.

### Geologic Setting

The normal stratigraphic succession near Cerro de Pasco is characterized by miogeosynclinal, dominantly marine sedimentary rocks. The Lower Paleozoic Excelsior Group, which forms the regional basement, is composed of quartzite and biotite-muscovite phyllites and schists with minor andesites and limestone. The rock is penetratively

foliated, with foliation strictly parallel to lithologic banding. Foliation is defined by parallel alignment of micaceous minerals and by compositional banding defined by quartzite and phyllite layers. The Permian Mitu Group (Newell, Chronic and Roberts, 1953) unconformably overlies the Excelsior Group and is composed of andesite flows, volcanic agglomerates, and breccias. The Triassic-Jurassic Pucara' Group, the next unit upwards, varies from impure sandy limestone to pure micrite, with interbeds of shale, chert, and limestone pebble conglomerate (Jenks, 1951; Szekely and Grose, 1972). The remainder of the Mesozoic section characteristic of central Peru is absent from the immediate vicinity of Cerro de Pasco (Megard, 1979). Locally the Shuco limestone conglomerate member of the Tertiary Pocabamba Formation rests unconformably on the Devonian Excelsior Group (Noble, McKee and Megard, 1979). It is composed of angular clasts of pink and gray sandy limestone up to 25 centimeters across set in a matrix of similar composition.

The dome is flanked by north-south trending anticlines and synclines that can be traced for several kilometers along strike (Jenks, 1951). Locally, the N-S regional trends have been disrupted by cross folds which produce smaller domes and east-west trending folds (Geological Staff, 1950). These folds are cut by several northwest trending faults and the Longitudinal Fault (Figure 2) which strikes slightly west of north (Ward, 1961). The Longitudinal Fault has experienced both reverse and strike-slip motion and may form a

decollement separating folded sedimentary rocks from the metasediments of the Excelsior Group below (Jenks, 1951). The north-west striking faults are vertical and have experienced strike-slip displacement. The fault and fold orientations suggest deformation in response to east-west compression.

The vent is filled with varied volcanoclastic rocks, to be described below, which have been intruded by later igneous bodies. The igneous rocks were originally mapped as a single quartz porphyry by Boutwell et al. (1920), and they have subsequently been referred to as the Cerro Quartz Monzonite. The intrusions have the general form of plugs and dikes, with the largest quantity of igneous material localized in the western portion of the vent.

#### Mineralization

The major mineralization of the district is localized in and along the southeastern portion of the vent (Figure 2), but iron oxides and hydrothermal alteration are found at localities scattered throughout the vent. Mineralization shows strong fracture control, including vein structures within the vent and the ring-fault which forms the vent margin.

Mineralization and hydrothermal alteration exhibit a variety of forms and mineral associations. Replacement and vein mineralization have been estimated originally to have totalled 100 million tons of pyrite, with 4 million tons of zinc, 2 million tons of lead, over a million tons of copper, 10 thousand tons of silver, and significant

gold and bismuth (Peterson, 1954; Einaudi, 1977). Most of the mineralization occurs within a massive replacement body that occupies a position tangential to the vent margin on its east side. This sulfide body has the geometry of a flattened and inverted cone. Extending westward from within the massive replacement body into the vent proper is a large, well-developed system of subparallel steeply dipping veins. Activity in the early part of the century concentrated on underground mining of the vein systems, but since the late 1950's mining activity has involved both open pit and underground operations within the massive replacement body. The deepest underground activity extended down to the 2500 level. Level numbers designate approximate feet below the present topographic surface.

The most abundant minerals in the massive sulfide replacement body are pyrite and silica, the latter in the form of "chert," or chalcedony and quartz. Consequently this body has been referred to as the "pyrite-silica" body. In addition to its dominant minerals, it also contains large quantities of sphalerite, galena, and pyrrhotite, as well as a host of other minerals in minor quantities (Lacy, 1949). At the surface, this enormous pyrite-silica body is over 1500 meters long and attains a maximum width of over 300 meters. It shortens and narrows downward, being approximately 500 meters by 100 meters on the 2300 level. The pyrite in this body was the earliest major sulfide deposited in the district (Lacy, 1949). The dominant Pb-Zn mineralization occurs as pipe-like to tabular bodies

replacing the pyrite-silica body and the Pucara' Group limestone wallrock. Pyrrhotite also occurs in pipe-like bodies that pierce and replace the pyrite-silica body and are locally associated with economically important Pb-Zn bodies (Einaudi, 1977). The galena-sphalerite mineralization is, at least in part, of the same paragenetic stage as the pyrrhotite (Einaudi, 1977). The chimney-like pyrrhotite pipes attain maximum dimensions of approximately 60 meters by 175 meters in plan. The Pb-Zn bodies attain lengths and widths comparable to those of the pyrite-silica body, but they pinch out at shallower depths (Geological Staff, 1950; Einaudi, 1977).

The later enargite-tennantite veins strike dominantly east-west and extend from the pyrite-silica body into the vent itself where they cut conglomerate and quartz monzonite porphyry dikes (Figure 2). Veins extend along strike for as much as 500 meters from their terminus in the pyrite-silica body westwardly to their terminus in the vent. The southernmost vein system is somewhat anomalous, being up to one kilometer long and contained almost totally within Excelsior Group phyllite wallrocks. Veins range in width from a few centimeters to over 12 meters (Bowditch, 1935) and are commonly zones of closely spaced fractures. In general the veins are zoned. Enargite-pyrite in their central portions, along with trace amounts of tennantite and possibly hypogene covellite and bornite, passes gradually along strike into tennantite-pyrite-sphalerite with minor galena (Bowditch, 1935; Graton and Bowditch, 1936). Enargite-tennantite mineralization also occurs in steep pipe-like bodies within

the pyrite-silica body. Locally these pipe-like bodies occur at the splayed ends of the younger veins (Geological Staff of Cerro de Pasco Corporation, 1950).

The last reported stage of hydrothermal activity leached previously deposited sulfides and deposited a host of rare minerals in collapse breccias and other open spaces in the pyrite-silica body (Lacy and Hosmer, 1956). Minerals deposited include pyrite, hematite, and realgar associated with silver-rich minerals gratonite, baumhauerite, and aramayoite (Lacy and Hosmer, 1956). Alunite-sulfur vug fillings occur locally in the enargite-pyrite pipes (Geological Staff, 1950).

#### Surface Effects

The effects of oxidation at the pre-mining topographic surface were very extensive at Cerro de Pasco but most of the oxidized material has been mined away (Bowditch, 1935; Geological Staff, 1950). The oxidized zone is dominantly composed of red to brown porous material with a high silica content. The material, known locally as "pacos," is generally poorly indurated and locally contains pockets of laminated debris suggestive of fluvial reworking. Goethite and jarosite are abundant in the pacos. In the early part of this century, large amounts of this material were mined for the silver content of 200-400 ppm, or 6 to 12 ounces to the ton (Geological Staff, 1950). The effects of oxidation locally reach to the 300 level of the mine. Today, most of the oxidized material has been removed by modern open

pit operations. The Geological Staff (1950) reported that pacos reached down to the 300 level in the central and southern portions of the pyrite-silica body, but massive pyrite, polished and grooved with glacial striae, was exposed at the surface to the north. Glacial effects in the immediate vicinity of the district were minor. Surficial morainal material is present and although it is minor it has localized some of the small lakes that are found in the area.

Discontinuous zones of secondary enrichment of copper and silver underlie the oxidized zone. The enrichment chiefly occupied the zone between the 300 and 400 levels, though locally it reached downward to the 500 level (Geological Staff, 1950). Silver-bearing chalcocite together with covellite are the principal enrichment minerals reported.

#### Sedimentary Textures in Sulfide

In the course of the present study, several specimens were discovered as detached specimens in the McCune Pit and on leach dumps that display clearcut sedimentary textures in rocks composed dominantly of quartz and pyrite. Bedding is clearly defined by pyrite and quartz grains. Variation in grain size of pyrite between beds is common and is exhibited most clearly as conglomerate interbeds with clasts of pyrite in some samples (Figure 3). In thin section, pyrite appears to be infilling pore space between the quartz grains, possibly a diagenetic effect. Sedimentary textures observed in this "sedimentary" pyrite include ripple-marks, cross-bedding, and

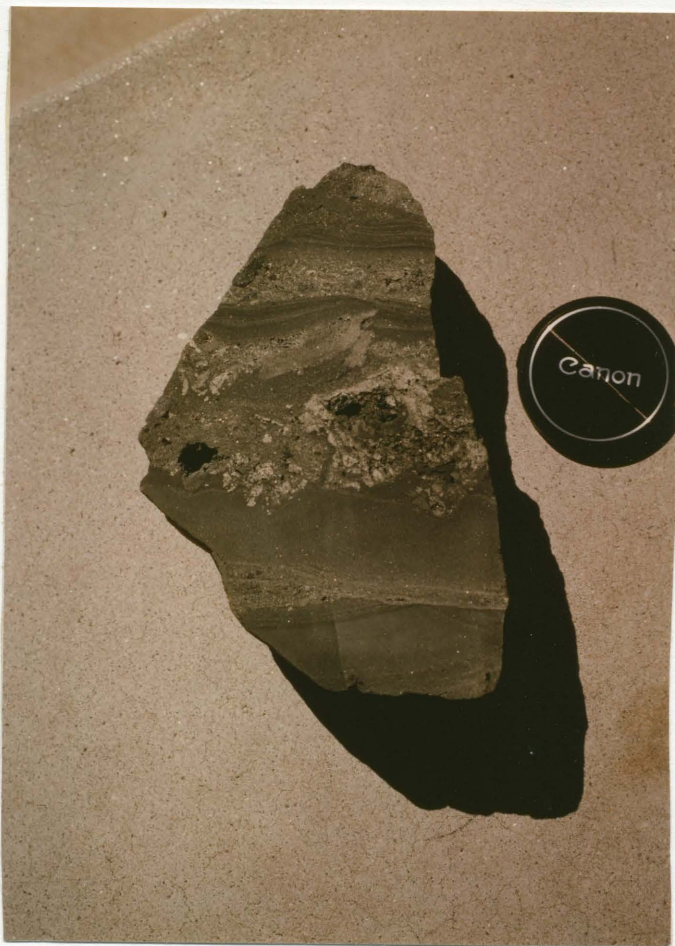


Figure 3. Slab A: "sedimentary pyrite" from Cerro de Pasco. -- Note conglomeratic bed and fold near the top of the picture.



soft-sediment deformation features. Ripple marks were found in only one specimen (Figure 4) where they were interlayered with planar bedded units, including conglomerate units. Soft sediment deformation features include penecontemporaneous folds and faults. Small faults have been found, the displacement of which varies from layer to layer. Isoclinal folds of individual pyrite layers have also been found, the isoclinal folds bounded by planar layers.

The significance of these rocks is not entirely clear. They suggest that the pyrite-silica body was exposed as a local source of sediment, probably shortly after it formed. The vent may well have contained isolated bodies of water in a lacustrine setting that could have preserved sedimentary pyrite from oxidation, so pyrite could have been locally shed from the pyrite-silica body into ponds or pockets in the vent and preserved. A major obstacle to understanding these rocks is the fact that none of them have been found in place, and none of the staff presently working at the mine knows where they can be found in place. Occurrences of laminated or bedded pyrite are noted on a few level maps of presently inaccessible parts of the mine. One occurrence is noted at the contact between the Excelsior Group and the Pucará Group. Other occurrences are noted in the upper portions of the pyrite-silica body. Replacement by pyrite in these rocks seems unlikely because no evidence of the original now-replaced mineral is found and the sedimentary textures are developed to such a remarkable degree. The total significance of these rocks remains to be determined.



Figure 4. Slab B: "sedimentary pyrite" from Cerro de Pasco. -- Note climbing ripples and conglomeratic beds.

## THE VOLCANIC SYSTEM

The igneous and volcanoclastic rocks at Cerro de Pasco outcrop in a roughly circular area approximately 2 km in diameter (Figure 2). The contacts between these rocks and the surrounding country rock are everywhere nearly vertical. The igneous and volcanoclastic rocks, therefore, fill a roughly cylindrical volcanic pipe-like structure, a structure identified as some type of volcanic vent by earlier studies (Bowditch, 1935). Within this structure are volcanoclastic agglomerates and tuff and intrusions of dacitic to quartz monzonitic composition. In addition, rootless blocks of sedimentary rocks are present.

### Ring Fault System

The vent margin (Figure 5) is observable at a number of locations, both in the mine and in the field. In the mine, the vent margin is defined by the contact between the Rumiallana Agglomerate and the pyrite-silica body. This boundary is somewhat arbitrary because the pyrite-silica body formed by replacement of part of the Rumiallana Agglomerate such that the contact is defined, in some places, by the last occurrence of remanent textures of the Rumiallana Agglomerate in the pyrite-silica body. At many localities in the mine, a fault is present near or at the contact that cuts the pyrite-silica body requiring that faulting occurred after mineralization.



Figure 5. The vent margin, looking west. -- The nearly vertical fault separating Rumiallana Agglomerate (light gray) to the south from Excelsior Group (dark gray) to the north slices through the center of the photo.



At every locality where the vent margin is observable in the field it is a fault. At some localities the physical expression of the fault is a single vertical polished surface. At other localities a zone, up to one meter wide, of closely spaced shear surfaces is observed. At still other localities, heterogeneous breccias containing fragments of rock from both within and outside the vent define the fault. Locally intense folding of the Excelsior Phyllite within one meter of the vent margin is observed.

#### Rootless Blocks

In the northwestern portion of the vent are two rootless blocks of older sedimentary rocks (Figure 2). These units are exposed in discontinuous outcrops. The units generally strike north-east and dip southeast. Within any given outcrop the strike and dip of bedding orientations is consistent, but between outcrops there are large differences. Between outcrops less than 100 meters apart, strikes can vary by 30° and dips by 20° (Figure 2). These variations must be due to faults between and within the blocks. Contacts between these blocks and other units can be located to within two to ten meters. Neither block shows any evidence of thermal metamorphism.

The northernmost and structurally lower of the two is composed of quartzite pebble conglomerate with clasts up to 10 centimeters across set in a quartz sand matrix which is locally hematite-stained and exhibits sparsely developed thin bedding. It was assigned to the Mitu Group by Bowditch et al. (1931). This assignment is highly

questionable, especially since the Mitu Group, exposed a little over a kilometer to the east, is composed of andesites and volcanic agglomerate. The unit could easily be part of the Mesozoic or Tertiary section. However, since there is no valid reason to assign it to any other particular formation, the Mitu Group (?) assignment is retained here.

The structurally higher block is composed of sandy limestone, micrite, and limestone pebble conglomerate, with minor interbeds of chert (Figure 6). It exhibits prominent well-developed thin to massive bedding defined by layers of chert and limestone-pebble conglomerate, and by partings in the limestone. The unit exhibits moderate topographic relief, outcropping as a ridge. In the eastern part of the block there are zones of abundant iron oxides on fractures (Kruger and Lacy, 1949). The unit is assigned to the Pucará Group on the basis of lithologic similarities.

In the southwestern portion of the vent there are two blocks of limestone pebble conglomerate. Bedding in the conglomerate is very rare; the three orientations that were measured strike north to northeast and dip southeast (Figure 2). No metamorphic effects are present in either block. The angular clasts of the conglomerate are pink and gray sandy limestone up to 25 centimeters across set in a matrix of similar composition. The blocks are part of the mid-Tertiary Shuco Conglomerate, which caps the hills to the south and west of the vent. Within the vent, the Shuco Conglomerate exhibits



Figure 6. Rootless block in the Cerro de Pasco vent. -- Massive white to light gray outcrops are Pucará Group within the vent, dipping below the tuffaceous sedimentary rocks (Tvt).

moderate relief, forming a ridge. The northernmost and largest of these blocks exhibits extensive gossan development, predominantly along fracture surfaces.

#### Volcaniclastic Rocks

The eastern half of the vent is dominated by a volcaniclastic agglomerate called the Rumiallana Agglomerate (Tr, Figure 2). The most abundant clast types in the Rumiallana Agglomerate are phyllite, limestone, and chert, together making up 90% or more of the clasts present. Five to ten percent of the clasts in many outcrops consist of a highly altered porphyritic igneous rock. Rare clasts of "quartz-eye porphyry" and sparse pieces of massive pyrite have also been observed. The relative abundance of clast types varies from locality to locality and the matrix commonly contains volcanic debris, including biotite and plagioclase, cemented by calcite. Clasts range up to 24 centimeters in longest dimension and are subangular to subrounded. The unit is locally thin-bedded (Figure 7) with some trough cross-bedding, but some portions are massive with no sign of bedding. Clasts are matrix-supported in every case observed and commonly accentuate bedding if it is present. The Rumiallana Agglomerate generally has a very subdued topographic expression, forming topographic lows. A minimum thickness of the Rumiallana Agglomerate can be obtained by measuring the elevation difference between its outcrops on the top of the hill northwest of the mine and





Figure 7. Outcrop expression of bedding in the Rumiallana Agglomerate. -- From the northeastern part of the Cerro de Pasco vent.

the lowest level reached by mining which also encountered the unit; vertical extent of over a kilometer is demonstrated.

The northwest and southwest portions of the vent are dominated by tuffaceous volcanic rocks (Tvt, Figure 2). Glass shards are present in thin section, but most show no evidence of deformation so most of the unit is best referred to as non-welded tuff (Smith, 1960). Some glass shards do show minor deformation suggesting incipient welding. Interbedded with these rocks are rare units exhibiting eutaxitic texture (Ross and Smith, 1966). The rocks are crystal-rich with crystals forming 50-80% of the rock. No systematic variations in welding were found either vertically or horizontally. The rocks are white to gray and commonly exhibit well-developed thin bedding. They are quartz- and feldspar-rich with variable amounts of biotite. Other minerals are rare although hornblende and epidote are locally present, and calcite is important as a cement for the rock. Bedding is clear in most outcrops but in some it is hard to identify. It is defined by variations in mineralogy emphasized by differential weathering characteristics between the beds.

A clear contact between the tuffaceous volcanic rock (Tvt) and the Rumiallana Agglomerate (Tr) was nowhere observed. On the contrary, in the area where the two units might be in contact, the limited outcrops that are available exhibit a lithology that is intermediate between the two units. The rocks that crop out are conglomeratic, with clasts similar to those found in the Rumiallana Agglomerate and with matrix material that is the same as that of the

tuffaceous volcanic rocks. The contact between the two units is, therefore, gradational.

### Intrusive Rocks

Earlier workers included all intrusive rocks in one unit, the Cerro Quartz monzonite. On figure 2, these rocks are divided into three units, including the Tvt unit discussed above and two units described in this section.

Extensive outcrops of porphyritic igneous rocks in the western portion of the vent are dacitic to rhyodacitic in composition. The phenocrysts to groundmass ratio varies greatly from 10:90 to 80:20; in general, phenocrysts comprise 30-50% of the rock. The mineralogy of the phenocrysts also varies from sample to sample. Quartz is present in nearly all samples but generally constitutes less than 10% of the phenocrysts. Mafic phenocrysts include biotite and hornblende and constitute 10-30% of the phenocrysts. Biotite is always much more abundant than hornblende; hornblende may indeed be absent. Feldspar constitutes the remaining phenocrysts, and locally exhibits marked compositional zoning. Feldspar phenocrysts are locally broken and quartz is locally highly embayed. The groundmass is aphanitic and purple to gray in color. Devitrification textures are common in thin section. Locally the rock exhibits a breccia texture, and the fragments and matrix appear in thin section to be of the same composition, indicating autobrecciation. The unit, shown as Tvd on Figure 2, will be referred to as 'the dacite unit.'

The dacites exhibit an obvious foliation in most outcrops, a lamination accentuated by differential weathering characteristics of the rock (Figure 8). Locally the outcrop expression of the foliation is obscure, especially where the rock has been hydrothermally altered. The foliation is planar to curvilinear, with minor undulations being common. These undulations have a "ropy" or "taffy" appearance similar to that of pahoehoe lava. In this section, the foliation is defined by the subparallel alignment of inequant mineral grains, especially plagioclase and biotite. In one locality in the field, the foliation was traced into a set of parallel closely spaced fractures.

Cutting the volcanic and volcanoclastic rocks are quartz monzonite porphyry dikes, Tqm on Figure 2, which contain sanidine phenocrysts up to 6 cm across making it a very distinctive rock in outcrop. Phenocrysts comprise 20-40% of the rock, of which approximately half are sanidine while the other half consist of quartz, biotite, and plagioclase in roughly equal amounts. Hornblende and tourmaline are locally present. The groundmass is gray and aphanitic. Evidence to determine the age relationship between the dikes and mineralization is conflicting. Altered fractures commonly cut the dikes, but unaltered dikes are found to cut altered rocks in places (Lacy, 1949). It appears, therefore, that emplacement of the dikes was contemporaneous with mineralization. The outcrop pattern of the quartz monzonite porphyry is very irregular. A narrow zone of east-west-trending dikes is defined in the west-central part of the vent. North of this zone is a northwest-trending group of outcrops, south





Figure 8. Outcrop expression of the foliation in the dacite unit (Tvd). -- From the western margin of the Cerro de Pasco vent.

of it is a northeast-trending array of outcrops. Quartz monzonite porphyry also crops out at scattered localities throughout the vent and three outcrops occur immediately to the north of the vent. No systematic trends were noted in these other areas.

#### Fractures and Hydrothermal Alteration

Mineralized fractures, and their accompanying alteration, occur at scattered localities throughout the vent. These fractures commonly have very small, 0-4 mm, apertures and are filled with iron oxides, hematite, jarosite, and goethite and quartz. The continuity of fractures varies from centimeters to meters, but the maximum length of fracture could not always be determined because of the discontinuity of outcrops. In most outcrops, the fractures have a very consistent trend within 10 degrees of east-west, with very few cross fractures. Locally, though, fracture orientations are much more random and some outcrops have almost a stockwork appearance. Hydrothermal effects associated with the fracturing vary in scale from individual selvages millimeters wide along fractures to 500-meter-square areas where the rock has undergone extensive chemical gains and losses. Detailed investigation of this alteration was not undertaken in this study; one of the areas has been reported upon in the literature by Kruger and Lacy (1949).

A large surficial exposure of hydrothermal alteration near the top of the hill northwest of the mine is associated with abundant east-west fractures. These fractures are commonly filled with

geothite and locally hematite and jarosite. The alteration is exposed in an approximately 500 meter square area. Most of the area is highly silicified, with silica being most abundant where the fracturing is most abundant. Alteration has completely changed the mineralogy of most of the rocks. Nevertheless, remnant textures allow the differentiation of quartz monzonite porphyry and Rumiallana Agglomerate in the field and make it possible to map the distribution of these units in the altered area. Alteration mineralogy is dominated by quartz and pyrophyllite. Lesser amounts of the calc-silicate minerals tremolite and wollastonite and the pyroxenes hedenbergite and aegirine-augite are present, though the systematics of their distribution is unknown. This alteration system is slightly north and west of the major vein system in the underground Lourdes mine workings. It represents the structurally highest part of the main vein system which has been preserved below the present erosion surface.

#### Summary

The interior of a volcanic neck has been exposed at Cerro de Pasco by erosion. Intrusive igneous rocks and volcanoclastic sedimentary rocks fill a nearly cylindrical structure, the conduit that localized volcanic activity 14 m.y. ago.

The oldest preserved rocks record pyroclastic activity and infilling of the vent structure. The tuffaceous rocks include welded-tuff and bedded non-welded-tuff. Parts of the Rumiallana Agglomerate show evidence of fluvial deposition, or at least reworking,

while other parts lack fluvial features. Later intrusions into this sedimentary fill were localized, for the most part, along the western margin of the vent. Dikes cross-cut the central part of the vent but they are volumetrically minor. The final stage of the evolution of the volcanic system involved extensive hydrothermal activity and alteration of the rocks within it. Small fumarolic systems were scattered throughout the vent area. A large hydrothermal system, affecting a cubic kilometer of rock, developed in the southeastern portion of the vent.



## STRUCTURAL GEOLOGY OF THE VOLCANIC SYSTEM

Sedimentary and volcanoclastic units within the vent are bedded, and the dacites exhibit a foliation. At the scale of Figure 2, these structural elements occur distributed throughout their respective rock units. Mineralized fractures are present, but their distribution is non-uniform, with the greatest concentrated in the southeastern portion of the vent. Each of these structural elements will be considered separately in the following sections.

### Bedding Orientations

The distribution of bedding orientation readings shown on Figure 2 is non-uniform. There are several reasons for this nonuniformity. In the western portion of the vent the bedded units have been displaced by the intrusive dacites. Outcrops are plentiful in the northern portion of the open pit mine and on the Pampa de San Andres, but in this area the Rumiallana Agglomerate is massive. There are other areas where the Rumiallana Agglomerate is massive, such as at the extreme northeast quadrant of the vent, but all of these areas are small. The scarcity of bedding orientation readings in the central part of the vent reflects the scarcity of outcrops in this area.

Examination of bedding orientations on Figure 2 reveals that they are not random, but vary systematically with their location within the vent. In general, the strike of bedding parallels the

trend of the vent margin. The strikes of all bedding orientations measured within the vent are plotted on Figure 9, which quantifies the relationship between bedding orientation and location in the vent. The vent was divided into sectors to organize the radial location of data points therein. This location was plotted as the abscissa of the graph. The angle that the strike of the bedding makes with north was plotted on the ordinate. If the vent were a perfect cylinder and bedding orientations conformed exactly to its geometry, then the plot would be a straight line. The distribution of data on Figure 9 shows scatter but approximates a straight line closely enough to demonstrate a correlation between bedding orientation and location in the vent.

The bedding consistently dips into the center of the vent. This consistent relationship in bedding orientations results in a small circle distribution of poles to the bedding planes on a lower hemisphere stereographic projection (Figure 10). The small circle distribution of poles to bedding planes describes a conical fold with a near vertical fold axis (Ramsay, 1967).

The scatter of data points on Figures 9 and 10 is reflected on Figure 2 as relatively large variations in strike and dip measurements over relatively small horizontal distances. A good example of how strike orientation can vary over short distances can be seen in the northern portion of the Tvt outcrops where strikes vary by more than  $50^{\circ}$  in less than 100 meters (Figure 2), and a good example of how dip orientations can similarly vary can be seen in the Tr outcrops just north of the Pampa de San Andres where dip readings vary by

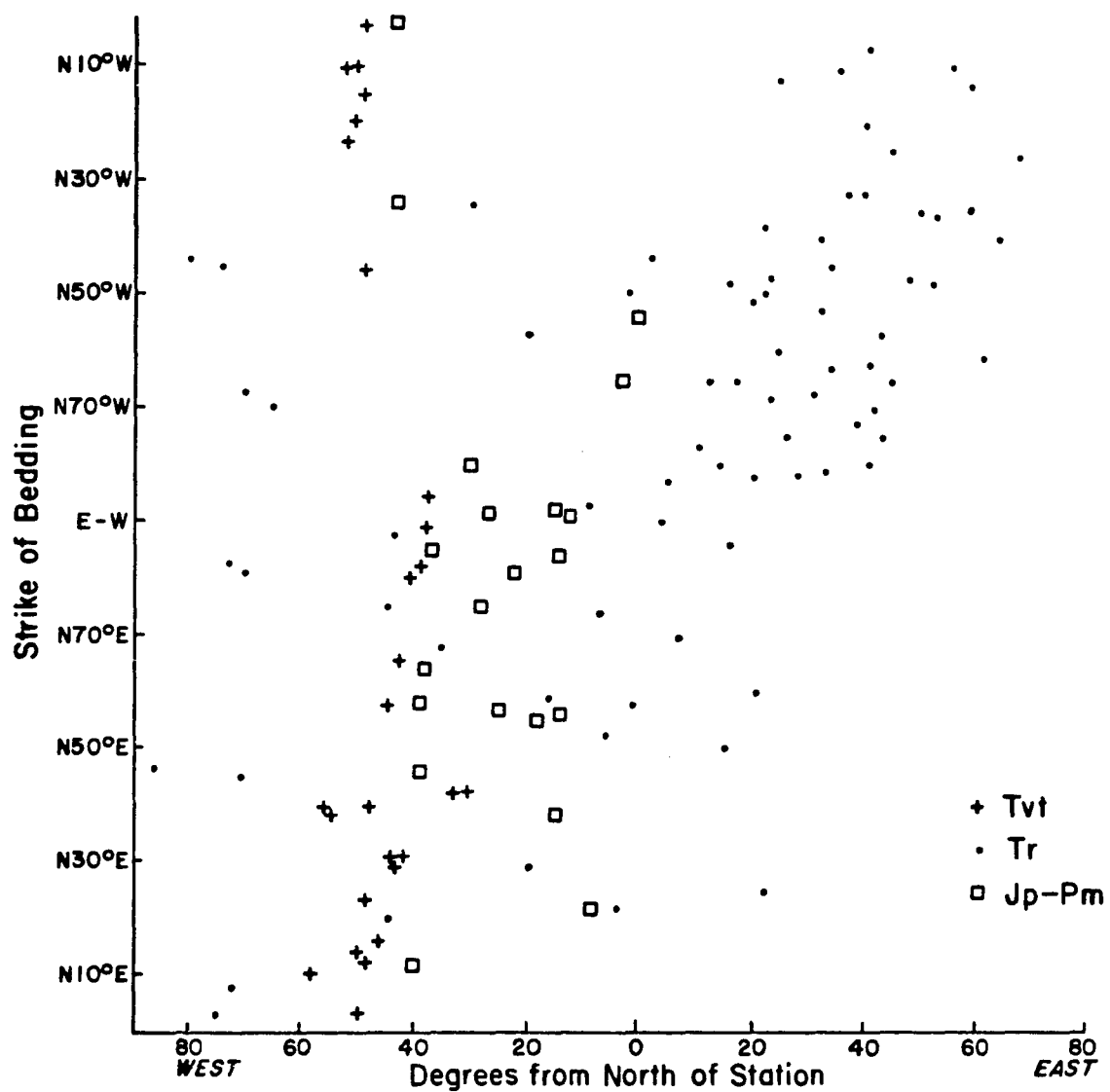


Figure 9. Relation of bedding orientations to spatial location within the vent at Cerro de Pasco. -- See text for explanation.

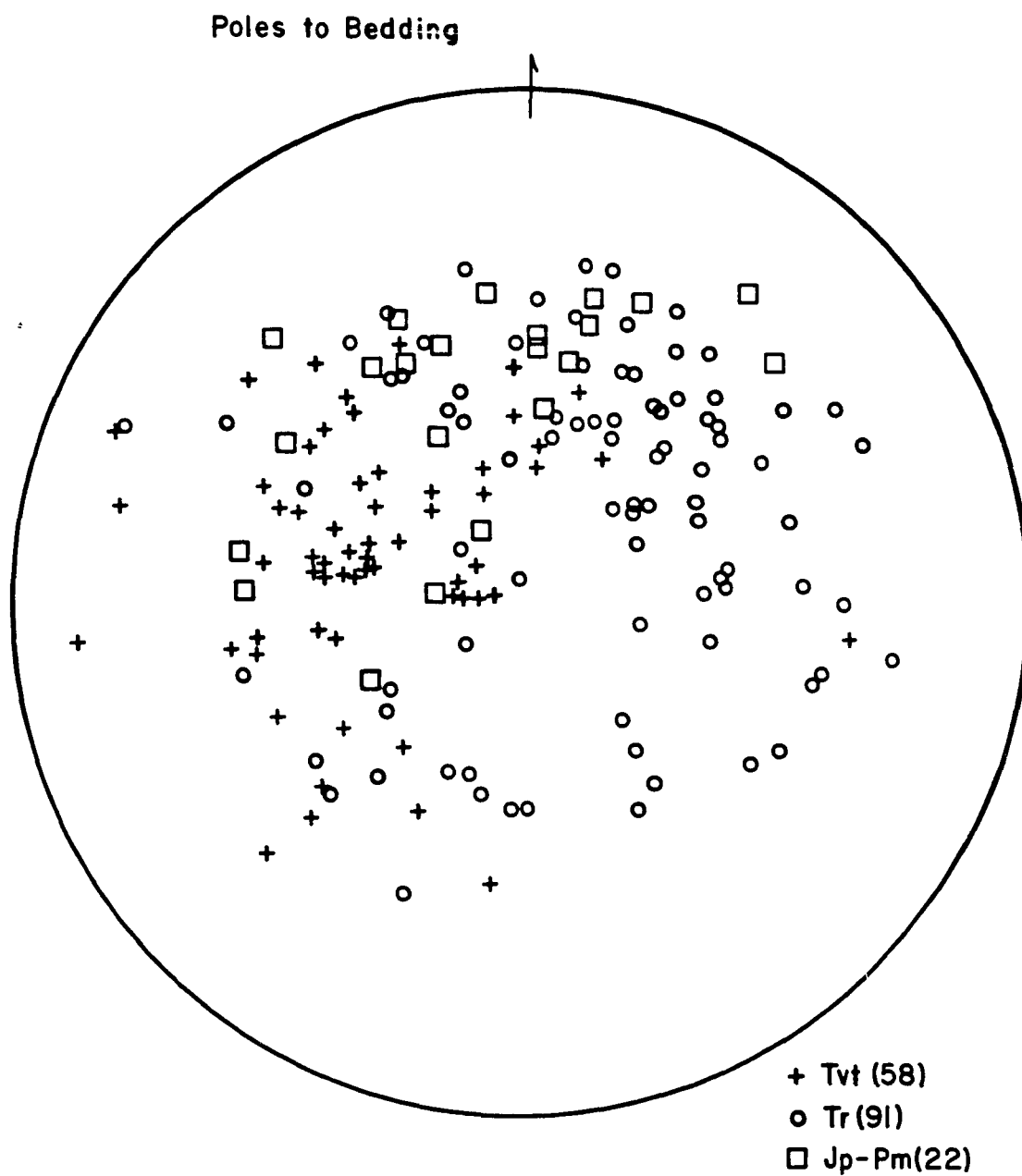


Figure 10. Lower hemisphere stereographic projection of poles to bedding orientations.

nearly  $40^\circ$  in less than 100 meters. These variations must reflect extensive and complicated faulting within the vent. The dikes that crop out to the north and south of the main east-west trending outcrops (Figure 2) have outcrop patterns that suggest possible en echelon offsets. These dike outcrop patterns may also reflect faulting within the vent. This myriad of faulting is exposed in the open pit mine and breaks the vent fill material into such a large number of blocks that they could not be shown at the scale of Figure 2. The scatter of data points on Figures 9 and 10 shows that these fault-bounded blocks have moved semi-independently during the evolution of the system.

An interesting deviation from the general pattern of inward-dipping bedding orientation is seen in the central part of the vent. In the central portion of the vent, immediately to the south of the main dike outcrops, bedding orientations define a small domal structure that can be seen well on section B-B' (Figure 2). Dips on the flanks vary from approximately  $20^\circ$  to  $60^\circ$ . The domal structure is 300-400 meters in diameter.

#### Foliation Orientation

Foliations in the dacite have been folded both at the map scale and at the outcrop scale (Figure 11). At the map scale, foliation orientations define a group of interpenetrating domes. The form lines on Figure 12 show the general morphology of one dome, as it is defined by trends of the foliation. In most places the



Figure 11. Fold in the dacite unit (Tvd). -- Located on the margin of the dome shown on Figure 12.

## VOLCANIC DOME

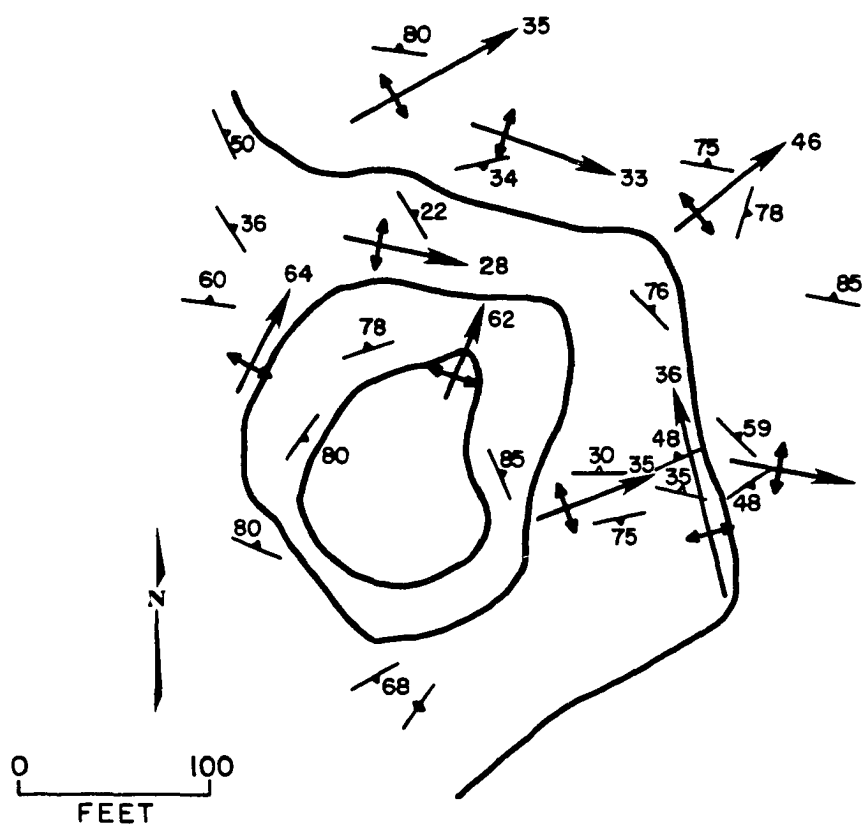


Figure 12. Foliation orientations, folds, and form lines defining the morphology of the southernmost "diapiric structure" shown on Figure 2.

foliation orientations are very steep as is common in volcanic and subvolcanic domes (Williams, 1932).

The orientations of the foliation readings reveal that the domes have, at least in part, a mushroom-cap geometry; consequently the term "dome" is not, strictly speaking, correct for these structures. In some localities the foliation of the volcanics dips inward toward the center of the "dome." The domes are therefore seen as having expanded in bulbous form like the caps of mushrooms at their culminations. The inward dipping foliation readings are interpreted as representing structurally lower portions of the domes (Figure 2). These difficulties have resulted in the use of the genetic term "diapiric structures" to identify these structures on Figure 2. The term "dome" will be used for these structures in the text. Irregularities in the orientation of the foliation are commonly observed even at the scale of an outcrop. These undulations account for as much as  $\pm 5$  to 10 degrees variance in foliation orientations and in general account for readings that appear anomalous.

Locally the foliation in the dacites has been deformed by passive flow to quasi-flexural flow folds (Donath and Parker, 1964). The folds are of low amplitude and commonly are present in only one or a few layers. The folded layers are generally bounded by planar layers, suggesting that the folded layers may be bounded by flow discontinuities. The overall distribution of the minor folds is hard to characterize. Locally they can be seen to conform to the geometry of the smaller domes (Figure 2).



Four of the domes are shown in Figure 2. The southernmost dome shown on Figure 2 is the one that is best exposed in the field. Figure 12 is a detailed 1:1200 map of this southernmost dome. In the northern part of Figure 12 are several antiforms with no intervening synforms. These antiforms are separated by ductile faults that formed flow discontinuities at the time of emplacement of the dome. In the southeastern part of Figure 12 is a refolded antiform. The dome immediately to the north of the one shown on Figure 12 is the one that is best defined by foliation readings on Figure 2; it is also the most cylindrical of the domes. The next dome to the north is the most poorly defined of the domes shown. The northernmost dome is entirely to the north of the east-west trending dike swarm. A small outcrop of Tvt overlies the southern part of this dome. All of the domes labeled on Figure 2 are less than 200 meters in diameter. Other small domes are certainly present, but limited outcrop data, do not allow them to be delineated. A possible example of an additional small dome can be seen in the southwestern part of the Tvd outcrops. In addition to the small domes, one large dome approximately 500 meters by 250 meters in horizontal section has been inferred from the orientation data. This larger dome is shown on sections B-B' and C-C' of Figure 2. Additional antiformal structures are inferred from the orientation data on Figure 2 and shown on sections B-B' and C-C' even though discontinuous outcrops make it impossible to delineate all of them in the field.

### Fracture and Vein Systems

Mineralized fractures, including ore-grade veins, strike dominantly east-west (Figure 13). Rose diagrams were constructed by grouping vein and fracture strike orientations in 10 degree intervals. Figure 13A represents strike orientations of fractures measured in the field. Figure 13B represents the strike orientations of veins measured from mine level maps. The veins are measured in 200-foot segments because visual inspection suggested that they were relatively consistent over this strike length, but not over longer strike lengths.

The vein systems exposed in the mine's underground workings strike dominantly east-west (Figure 13), but have variable dips (Figure 14). The vein systems can be divided into three general groups that are spatially separated, especially in the upper levels of the mine. The 28, 101, and associated veins form a group in the northern part of the mine. The 43 and associated veins form a group in the central part of the mine. The Cleopatra and associated veins form a group in the southern part of the mine. The northern group of veins dips to the south; and the central and southern groups dip to the north (Figure 14). The northern and central vein systems converge at depth at a position just to the north of the new Lourdes shaft. The pyrrhotite pipes are located to the east of nearly all of the vein mineralization, but converge at approximately the same north-south position as the fracture systems (Einaudi, 1977). On the deepest level reached by mining operations, the pyrite-silica body is

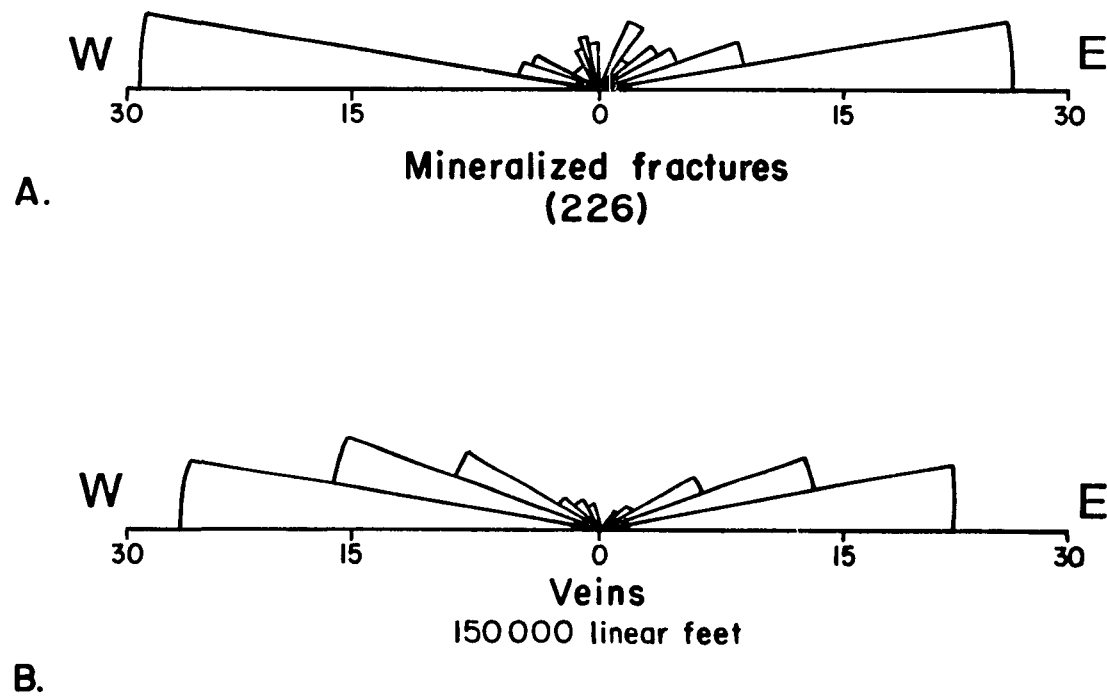


Figure 13. Rose diagrams showing the orientation of mineralized fractures measured in the field (A) and the orientation of vein segments measured from mine level maps (B). -- Scale shows percentage of readings. Number in parenthesis indicates the number of readings.

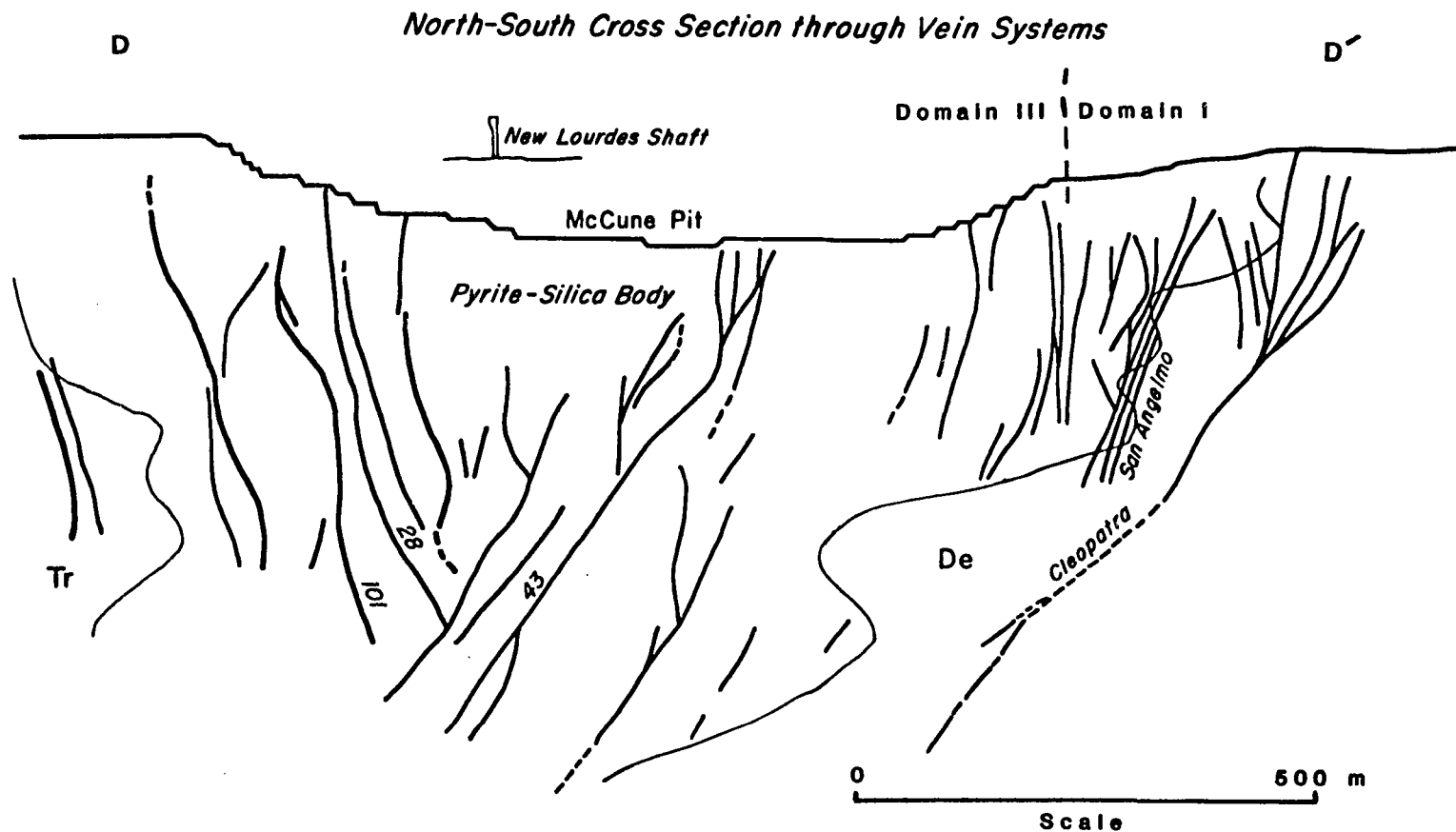


Figure 14. North-south cross-section, looking east, through the vein system at Cerro de Pasco. -- Modified from Rivera (1970). For location see Figures 2 and 15. Numbers represent vein designations used in the district.

reduced to a small tabular body centered on approximately the same position, with the veins restricted to the pyrite-silica body at this level.

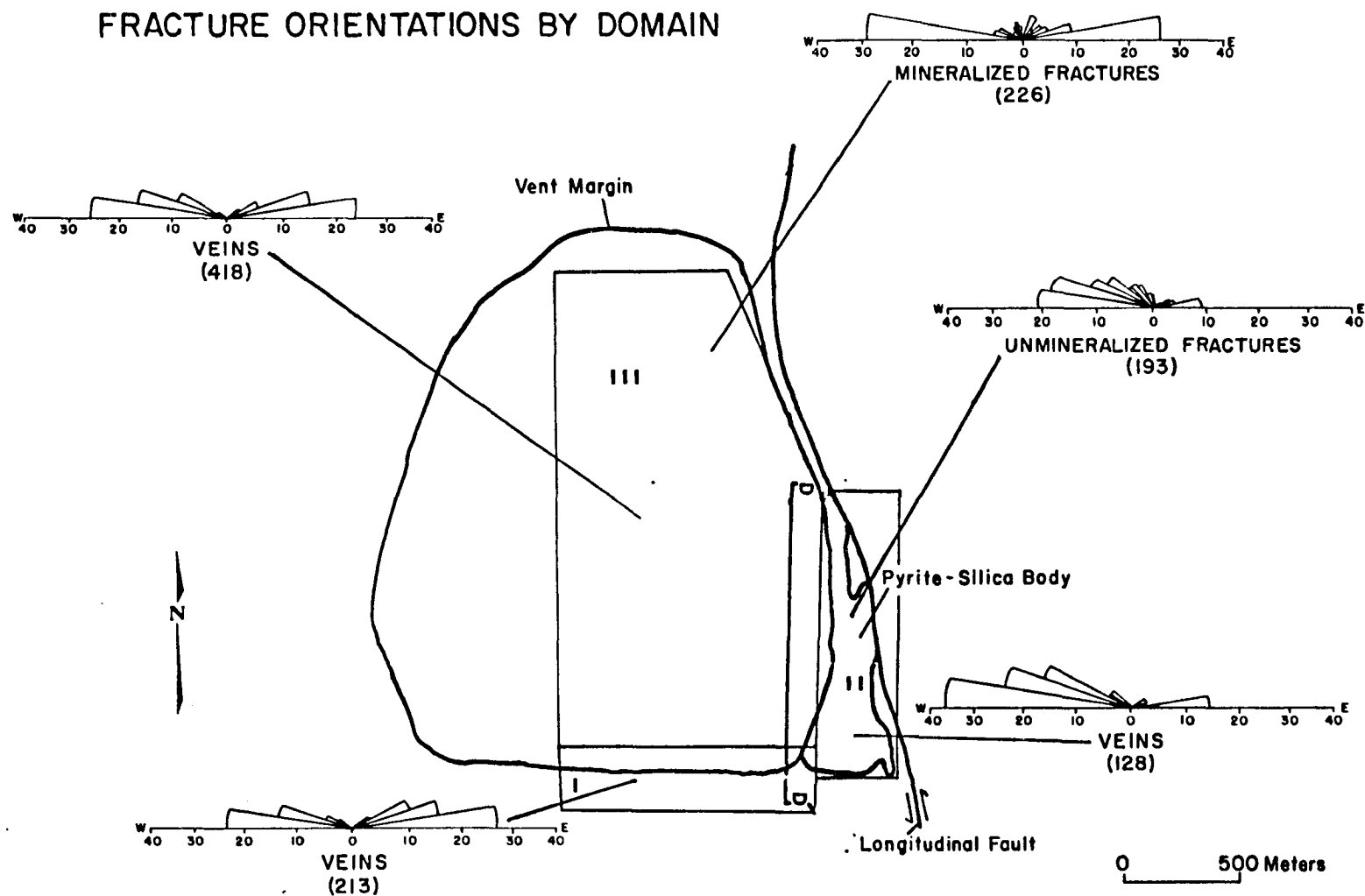
The southernmost vein system dips to the north, but it does not converge with the other sets. The Cleopatra is the largest vein in the district, up to 12 meters wide (Bowditch, 1935) and almost a kilometer long. Nearly all of the southernmost vein system is contained within the Excelsior Group south of the southern margin of the vent. Part of the system intersects the southernmost portion of the pyrite-silica body in the upper levels of the mine. The San Anselmo vein occurs at the contact between altered Rumiallana Agglomerate and Excelsior Group phyllite, a contact which marks the southern margin of the vent.

In order to investigate possible relations between fractures and other structural elements, the area can be divided into three domains (Figure 15). Domain I is located along the vent margin, Domain II is between the vent margin and the Longitudinal Fault, and Domain III lies within the vent. There are important lithologic difference between the domains. Domain I consists dominantly of Excelsior Group with some Rumiallana Agglomerate, Domain II of the pyrite-silica body and Domain III of Rumiallana Agglomerate and quartz monzonite porphyry.

Fracture orientations from Domain I are almost exclusively from presently inaccessible portions of the underground mine; the

Figure 15. Rose diagrams showing orientations of mineralized fractures and vein segments by domain as described in the text. -- Numbers in parenthesis show total number of readings. Scale shows percentage of total readings.

# FRACTURE ORIENTATIONS BY DOMAIN



orientations reported were measured from mine level maps. The veins trend generally east-west with a slight northeast bias. The dip of this group of veins is consistently steep and to the north (Figure 12). The Geological Staff (1950) report that offsets have been observed across some of these fractures. In all cases reported offsets indicated normal fault displacements on the fractures.

Fracture orientations in Domain II include measurements from the McCune open pit mine bench maps and underground level maps and those measured by the author. The unmineralized fracture orientations come from bench maps of the open pit mine. All of the fractures show a dominant west-northwest trend, with most fracture orientations between N60W and E-W.

Fracture orientations in Domain III include mineralized fractures measured in the field and vein segments from the underground mine. Fifty percent of these orientations strike within 10 degrees of east-west. The vein structures of the underground mine in Domain III are the converging set discussed earlier. The veins form a general V pattern that opens upward and converges downward (Figure 14). The mineralized fractures measured in the field dip steeply, generally greater than  $80^{\circ}$ , and no systematic variations were observed.

#### Summary

Bedding orientations of sedimentary and volcanoclastic units within the vent define a conical structure with a near vertical axis



(Figure 9). Analysis of the orientation data include significant deviations from the simple pattern, reflecting extensive faulting within the vent. Foliation orientations from the dacites define several interpenetrating domes (Figure 2) ranging from 100 m to 500 m in maximum diameter. In vertical section the domes have a mushroom-cap geometry. The domes are restricted to the western portion of the vent and localized near the ring fault.

Fracture orientations strike generally east-west (Figure 13), but with significant deviations. The fracture orientations were analyzed in terms of domains that were defined in reference to the major structures in the district. Domain I is located along the vent margin, Domain II is between the vent margin and the Longitudinal Fault, and Domain III lies within the vent. Fracture orientations are consistent within domains, but vary between domains, suggesting that these groupings will be important for interpretation.

## ALTERATION

An extensive hydrothermal system developed during the waning stages of the development of the volcanic system at Cerro de Pasco, contemporaneous with intrusion of quartz monzonite porphyry dikes. Extensive alteration assemblages developed as parts of the hydrothermal system, principally in Rumiallana Agglomerate. These alteration assemblages will be described in detail for two reasons, first to complete the description of the evolution of the volcanic system, and second to provide a basis for theoretical analysis to constrain physicochemical conditions at the time of mineralization.

Analyses of lateral and vertical variation in the distribution and characteristics of alteration minerals allow the delineation of alteration zones developed parallel to the fracture-controlled flow channels discussed earlier. The initial work to define these zones was done by Bowditch (1935). Alteration at Cerro de Pasco is most conveniently divided into three zones developed in envelopes subparallel to the veins; an inner quartz-alunite-kaolinite zone, an intermediate quartz-phylllosilicate zone and an outer calcite-chlorite-epidote zone. The inner zone thickness varies from 2-3 cm, where best developed, to a vanishingly thin selvage in areas where the intermediate zone is developed immediately adjacent to the fracture wall. The intermediate zone thickness ranges up to 1 to 2 meters. Identification of these zones for this study is based on the

study of 95 thin sections with extensive supplementary x-ray diffraction data. Boundaries between zones are gradational, and sulfides, dominantly pyrite, are present in all zones. Details of the alteration zonation will be described for later use to constrain values of intensive variables at the time of mineralization.

#### Distribution

The alteration zones form planar envelopes to the veins. The physical expression of the veins varies from one of tabular slabs of sulfide minerals commonly up to 25 cm wide, and locally more, to zones of closely spaced fractures with apertures of 1-5 mm filled with sulfides. In either case, the fractures were the flow channels for hydrothermal fluids. The quartz-alunite-kaolinite zone formed along the fracture wall and grades into the quartz-phyllosilicate zone as one traverses into the wallrock away from the vein. Similarly, the quartz-phyllosilicate zone grades into the calcite-chlorite-epidote zone further into the wallrock. The same zonation occurs laterally along the strike of the vein. Quartz phyllosilicate zone assemblages occur along the margin of the massive sulfide body, where they attain a maximum thickness of several meters, in addition to their development along the veins. The quartz-alunite-kaolinite assemblage is found in hydrothermally altered remnants of sedimentary rock in the massive sulfide body.

The alteration mineralogy is surprisingly simple considering the heterogeneity of the chemistry of the wallrocks on a small scale

and the complexity of the ore mineralogy. The Rumiallana Agglomerate contains abundant calcite, both as limestone clasts and as cement. It also contains potassium-bearing phases in the form of biotite and muscovite in the phyllite clasts. The mineralogic composition of the unit changes drastically between individual beds or groups of beds centimeters thick. In spite of these variations, essentially identical alteration assemblages are developed in all of the rocks.

#### Quartz-Alunite-Kaolinite Zone

Quartz is the most abundant mineral in this zone, constituting 60-90% of the zone, with alunite, kaolinite, and pyrite constituting the remainder. The maximum thickness of this zone is 2-3 cm. Along the fracture wall the altered wallrock may contain nothing but quartz and pyrite. Even at this advanced stage of alteration the original texture of the rock is still discernible, being manifested by subtle color differences in the quartz. Alunite occurs as acicular to tabular grains with a variety of habits. Alunite, and locally zunyite, occurs replacing muscovite in what were phyllite clasts (Figure 16) in the Rumiallana and in the matrix of altered Rumiallana. Kaolinite occurs as fine-grained matted aggregates scattered through the rock. Locally kaolinite, alunite, and quartz (Figure 17) occur as fine-grained aggregates intergrown to give a matted appearance. Several minor phases are present. A titanium oxide phase which occurs as stubby crystals suggesting anatase is locally present in this zone.

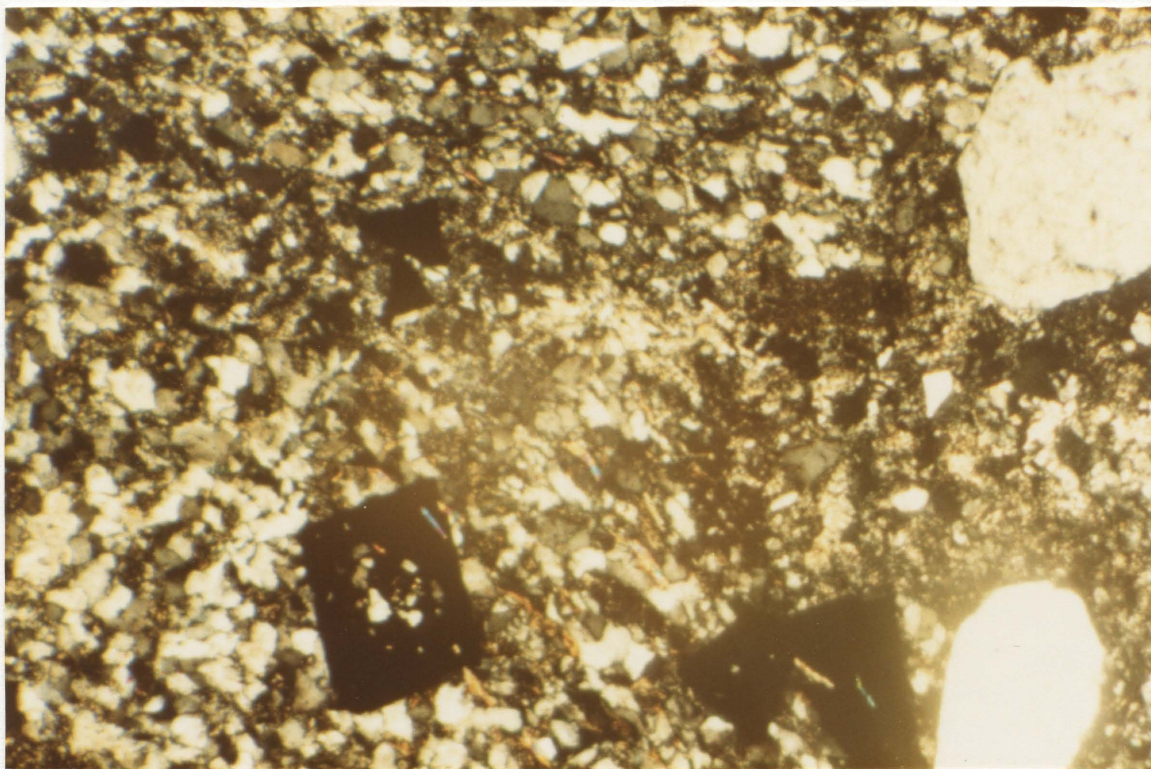


Figure 16. Quartz-alunite-kaolinite alteration zone, altered Rumiallana Agglomerate (100x). -- Note alunite (relatively high birefringence) in the "clast" near the center of the photo. Opaque cube-form mineral is pyrite.



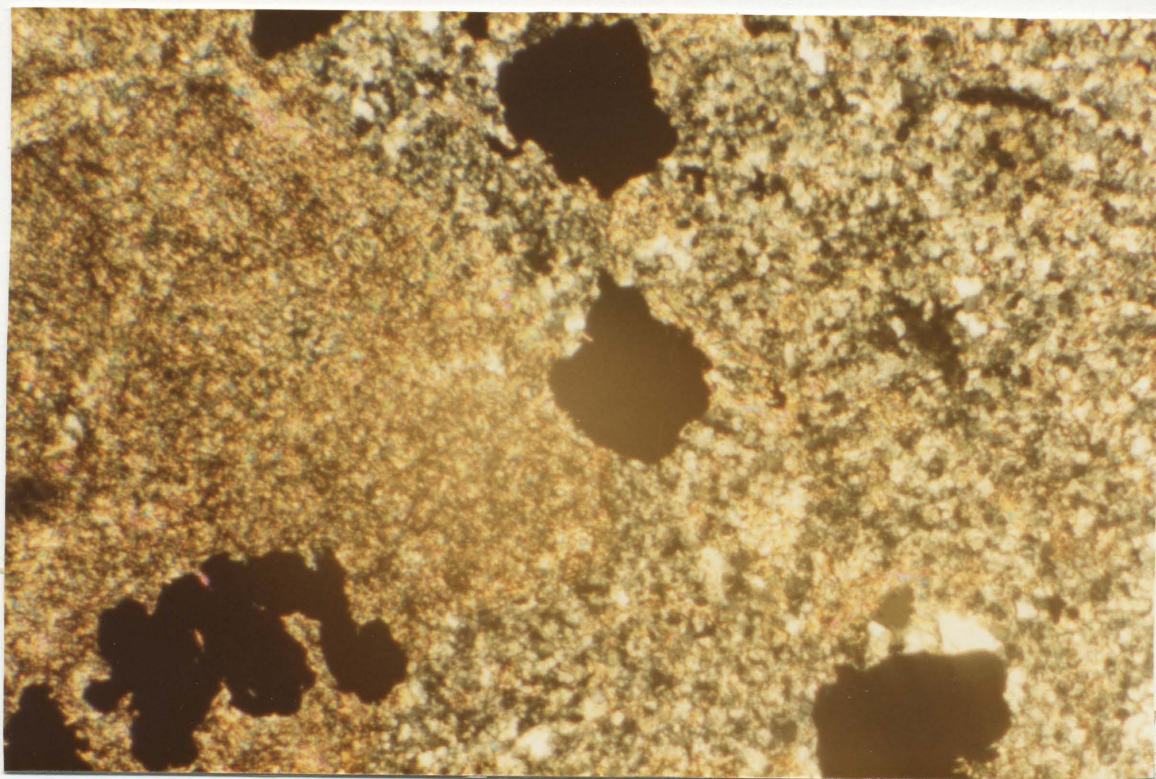


Figure 17. Part of the gradational boundary between the quartz-alunite-kaolinite zone and the quartz-pyrophyllite-kaolinite zone, altered Rumiallana Agglomerate (100x). -- Note fine-grained aggregate of kaolinite, alunite, and quartz on the left side of the photo. Opaque is pyrite.

Calc-silicate minerals include wollastonite, tremolite, and aegerine. They are rare and no systematic distribution was noted.

#### Quartz-Phyllosilicate Zone

The quartz-phyllosilicate zone is characterized by sericite, kaolinite, pyrophyllite, and pyrite, with quartz and pyrite making up 30-60% of the zone. The contact with the quartz-alunite-kaolinite zone is gradational, with layer-silicate minerals becoming more abundant and alunite becoming less abundant away from the flow channels. Quartz and phyllosilicate minerals commonly occur as fine-grained matted aggregates, though the layer-silicate minerals (Figure 18) are locally coarse grained. A titanium oxide phase is locally present in this zone, also, and is most commonly found as inclusions in the phyllosilicate minerals. Calc-silicate minerals, including tremolite, hedenbergite, wollastonite, and aegerine, are present but not common. Acicular grains of green tourmaline that are so small that are only visible at the highest point of the microscope are locally present along the margin of the pyrite-silica body.

#### Calcite-Chlorite-Epidote Zone

The quartz-phyllosilicate zone grades into calcite-chlorite-epidote alteration. Calcite commonly has replaced plagioclase and less frequently biotite. Biotite also alters to chlorite. Minor sericite may develop in the feldspars. Epidote locally replaces biotite and is present in the groundmass or matrix material. Calcite



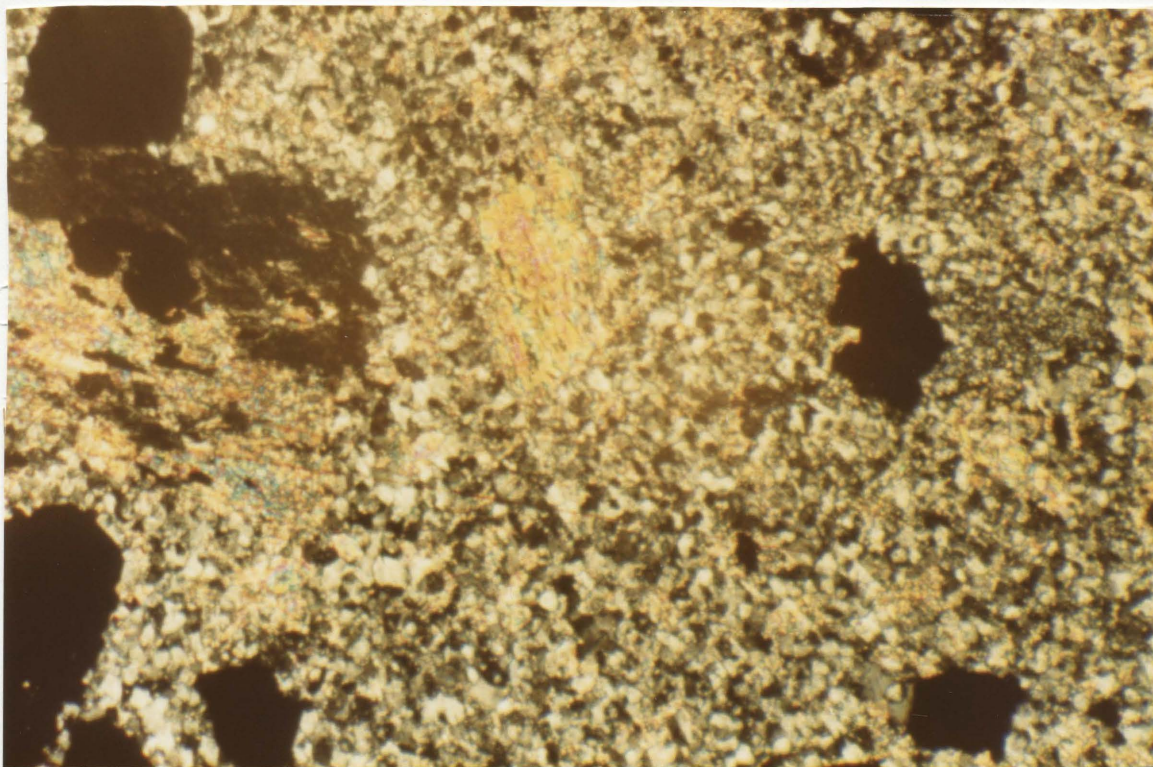


Figure 18. Quartz-muscovite-kaolinite zone, altered Rumiallana Agglomerate (100x). -- Note coarse- and fine-grained muscovite. Opaque is pyrite.



occurs in the groundmass as replacement in the igneous rocks and as cement in the Rumiallana Agglomerate, commonly forming 5-15% of these rocks.

#### Alteration marginal to the Pyrite-Silica Body

Alteration of the Rumiallana Agglomerate along the western margin of the pyrite-silica body is characterized by sericite, kaolinite, quartz and pyrite. No pyrophyllite was found. This zone varies in width from 1-5 meters. To the west it grades in to the calcite-chlorite-epidote zone. On the east it is bounded by the pyrite-silica replacement body.

#### Alteration in Limestone

The development of alteration minerals in the Pucar Group limestones is spotty and inconspicuous and even where present they occur at low abundance levels, seldom being more than 10% of the rock. The veins do not cut the Pucar, but most of the eastern contact of the massive sulfide body is against Pucar Group rocks. Purple, gray, or black jasperoid is common, but its development is discontinuous. Dolomite is also common, and siderite is locally present. These effects are normally present only within one or two meters of the contact. Carbonate-filled fractures are locally abundant and form zones that may extend for tens of meters away from the contact.

### X-ray and Microprobe Studies

Petrographic studies were found to be inadequate definitively to characterize the fine-grained minerals in the phyllosilicate zone, largely because differentiation between muscovite and pyrophyllite was impossible in thin section, the reason that Bowditch (1935) did not report pyrophyllite. The presence of mixed layer clays in addition to kaolinite was suspected.

Problems of identification required X-ray diffraction studies, and minerals with  $7\text{\AA}$ ,  $9.4\text{\AA}$  and  $10\text{\AA}$  d-spacings were found. Clay separates from 18 samples of the quartz-phyllosilicate zone were studied. The  $9.4\text{\AA}$  and  $10\text{\AA}$  minerals were identified as pyrophyllite and muscovite respectively. The samples containing the  $7\text{\AA}$  minerals were heated for one hour at  $600^\circ\text{C}$  (Carroll, 1967) to differentiate kaolinite from chlorite. All 18 samples were found to be kaolinitic. No smectites were found.

Microprobe analyses indicated that the  $9.4\text{\AA}$  and  $10\text{\AA}$  minerals can be characterized as ternary mixtures of muscovite, pyrophyllite, and celadonite components. Ideal muscovite ( $\text{KAl}_2^{\text{VI}}\text{Al}^{\text{IV}}\text{Si}_3\text{O}_{10}(\text{OH})_2$ ) is an end member component of compositions that are actually found in nature. Introduction of  $\text{Fe}^{++}$  or  $\text{Mg}^{++}$  in the octahedral site with  $\text{Si}^{+4}$  in the tetrahedral site, accompanied by removal of  $\text{Al}^{+3}$  from both the octahedral and tetrahedral sites, can be described in terms of solid solution between muscovite and celadonite ( $\text{KAl}^{\text{VI}}(\text{Fe}^{++}, \text{Mg}^{++})^{\text{VI}}\text{Si}_4^{\text{IV}}\text{O}_{10}(\text{OH})_2$ ). A second substitution involving the introduction of interlayer vacancies and  $\text{Si}^{+4}$  in the tetrahedral

site accompanied by removal of interlayer  $K^+$  and  $Al^{+3}$  from the tetrahedral site can be described in terms of solid solution between muscovite and pyrophyllite ( $Al_2^{VI}Si_4O_{10}(OH)_2$ ). The mole fraction of these components in natural layer silicate minerals can be calculated from microprobe data.

Original microprobe analyses were recalculated using two methods suggested by McDowell and Elders (1980). Values in the upper half of Table 1 are calculated assuming cations (Na, K, Ca) = 6.00, which assumes filled octahedral sites. No assumption is made as to ferric/ferrous iron ratios or total charge. The lower portion of the table was calculated assuming  $Fe^{+3}/Fe_{Tot} = 0.865$ , an average value given by Weaver and Pollard (1973). The calculation also requires that the  $\Sigma + \text{charge} = 22.00$ . N. in table 1, indicates the number of analyses of each sample. The two methods yield essentially the same results (Table 1).

#### Variations within the Phyllosilicate Zone

Muscovite, celadonite, and pyrophyllite components were calculated for each analysis based on layer charge deficiencies from ideal stoichiometry (Weaver and Pollard, 1973). These calculations include negligible margarite and paragonite components with muscovite. It is clear from the microprobe analyses that celadonite and pyrophyllite components are present in the "muscovites." Two of the samples are essentially stoichiometric pyrophyllite. Figure 19 shows the pyrophyllite, celadonite, and muscovite components calculated

Table 1. Microprobe Analyses.

		922	118	165	1660	160	948	1654	813
A) $\Sigma$ of Cations = Six	Al $\emptyset$	1.234	1.694	1.795	1.924	1.732	1.716	1.993	1.995
	MG	0.143	0.232	0.176	0.064	0.205	0.146	0.002	0.001
	FE	0.114	0.069	0.019	0.009	0.032	0.129	0.005	0.003
	TI	0.009	0.005	0.010	0.003	0.032	0.009	0.001	0.001
	ALT	0.709	0.738	0.619	0.617	0.613	0.728	0.331	0.030
	SI	3.291	3.262	3.381	3.383	3.387	3.272	3.669	3.970
	K	0.713	0.732	0.665	0.578	0.701	0.784	0.007	0.004
	NA	0.009	0.011	0.038	0.011	0.008	0.006	0.014	0.012
	CA	0.005	0.016	0.020	0.003	0.006	0.003	0.016	0.002
	N	20	19	19	15	16	20	16	8
B) $\Sigma$ Charges = 22.00	Al $\emptyset$	1.793	1.762	1.811	1.949	1.757	1.768	2.073	1.989
	MG	0.145	0.235	0.176	0.064	0.206	0.148	0.002	0.001
	FE	0.029	0.017	0.005	0.002	0.008	0.032	0.001	0.001
	TI	0.009	0.005	0.010	0.003	0.032	0.009	0.001	0.001
	ALT	0.675	0.699	0.610	0.603	0.598	0.698	0.290	0.028
	SI	3.325	3.301	3.390	3.397	3.402	3.302	3.710	3.972
	K	0.719	0.741	0.667	0.581	0.704	0.791	0.007	0.004
	NA	0.009	0.011	0.038	0.011	0.008	0.006	0.014	0.012
	CA	0.005	0.017	0.020	0.003	0.006	0.003	0.016	0.002
	N	20	19	19	15	16	20	16	8

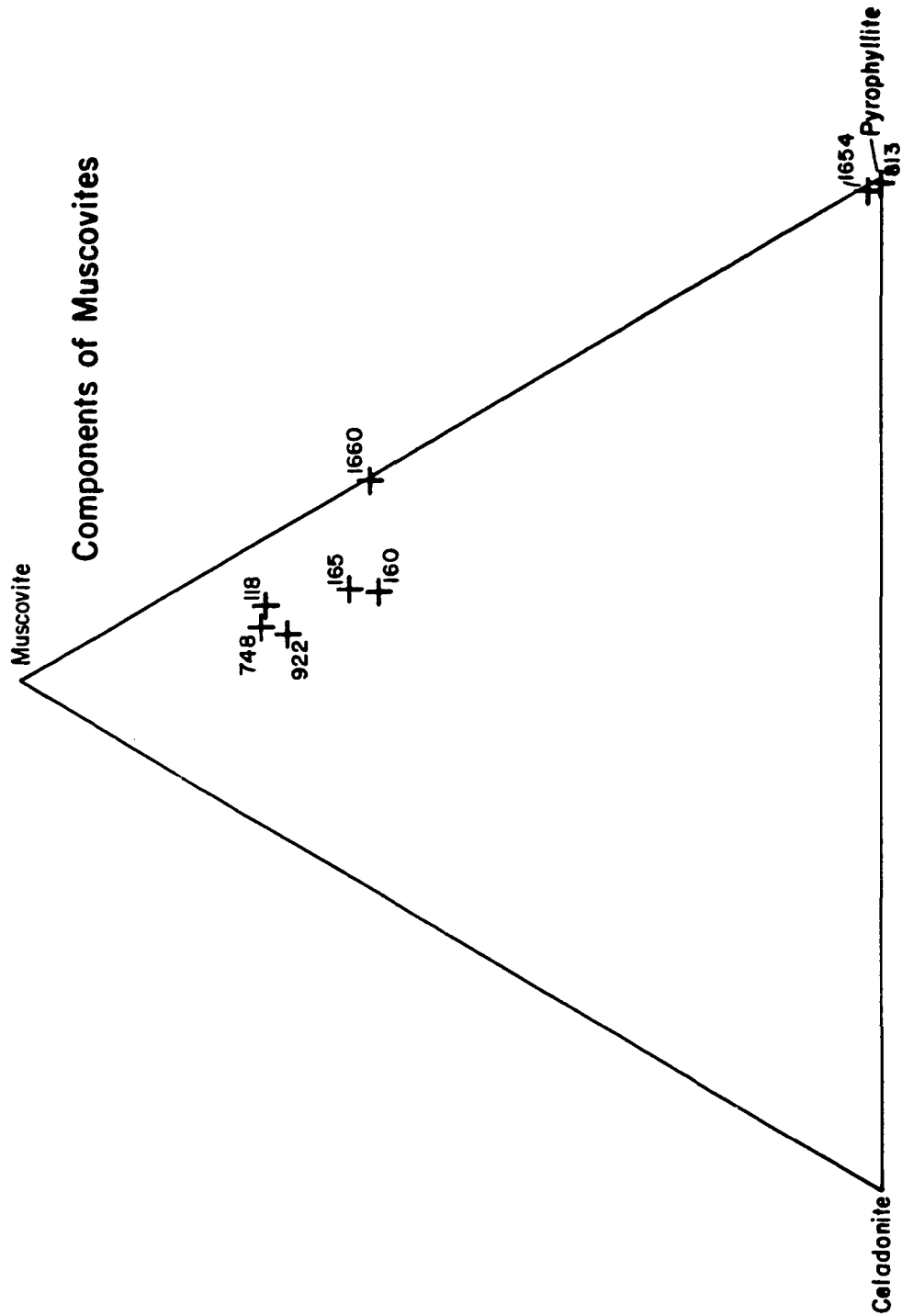


Figure 19. Components of fine-grained white micas calculated from microprobe analyses.

from the data shown in Table 1. The spatial relations of these samples are shown on Figure 20. All samples have low celadonite components at less than 15%. Samples 118, 922, and 948 are all from the margin of the pyrite-silica body and have low pyrophyllite components at approximately 20%. Samples 160 and 165 are from a weakly mineralized vein system exposed in the open pit, probably the distal portions of the 101 and associated veins. The muscovite component has dropped to approximately 60% relative to 70% for samples adjacent to the pyrite-silica body, and the pyrophyllite component is up to approximately 30%. Samples 1660 and 1654 are from the 44 vein on the 1600 level and show lateral zoning along the vein. Sample 1654 is closer to the central, highly mineralized portion of the vein and 1660 is from the barren distal portion of the vein. Sample 1654 is essentially stoichiometric pyrophyllite and 1660 exhibits approximately a 40% pyrophyllite component, showing an increasing pyrophyllite toward the central mineralized portions of the veins. Sample 813 is from the hill northwest of the mine, and thus represents the highest part of the mineralized system presently preserved. The microprobe analyses show essentially stoichiometric pyrophyllite. Several X-ray diffraction samples from this area also reveal pyrophyllite as the sole layer silicate mineral present.

Microprobe analyses and X-ray diffraction studies suggest zoning within the Phyllosilicate Zone in terms of the pyrophyllite component of the layer lattice phases. The general trend of the horizontal variations can be seen on a "reconstructed vein"

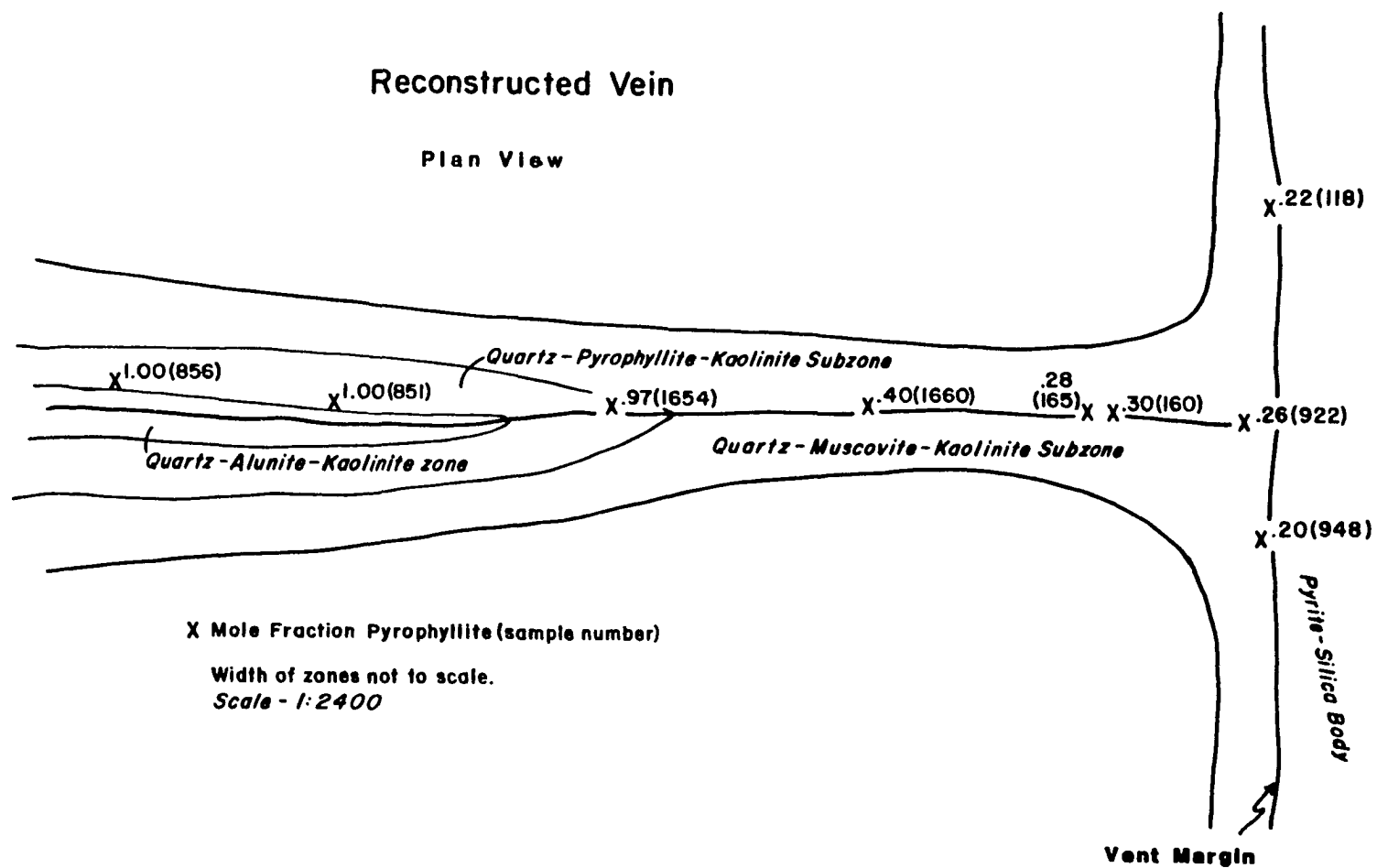


Figure 20. Schematic diagram of alteration zonation. -- The innermost zone of approximately 100 times its actual width and the other zones are approximately 10 times their actual widths. See text for locations of individual samples.

(Figure 20). X-ray diffraction samples from the margin of the pyrite-silica body reveal the presence of muscovite and muscovite-kaolinite, but not pyrophyllite. Microprobe analyses of Samples 118, 922, and 948 exhibit no vertical zoning amongst the samples, all of which are from the margin of the pyrite-silica body. Microprobe analyses of samples from the vein alteration assemblages 160, 165, 1660, and 1654 suggest a zoning of the pyrophyllite component of the sample from low values in samples from the outer portions of the veins to pure pyrophyllite in the central portions. X-ray diffraction studies of samples from the highly mineralized section of the 43 vein on the 800 level of the mine reveal pyrophyllite-kaolinite assemblages, supporting the findings of the microprobe studies. Microprobe and X-ray diffraction studies of the highest portions of the vein system preserved, the outcrops on the hill to the northwest of the mine, reveal pyrophyllite as the sole phyllosilicate mineral present. The pyrophyllite is part of the primary hypogene alteration assemblage, rather than supergene, as indicated by its association with pyroxenes such as hedenbergite and aegerine and calc-silicate minerals such as tremolite, which clearly represent a moderate to high temperature assemblage. Therefore it appears that the phyllosilicate minerals zone to pyrophyllite vertically upward.

The horizontal trend from high muscovite component to high pyrophyllite component is summarized in Figure 20 and relates to similar zoning patterns reported in the sulfide mineralogy of the veins by Bowditch (1935). No vertical zoning was observed along the



margins of the pyrite-silica body. However, vertical zoning from muscovite-kaolinite or pyrophyllite-kaolinite to pyrophyllite is evident within the vein system.

#### Geometry of Alteration Zones

The simplest case of alteration zoning is rarely observed because of overprinting of alteration assemblages and structural complications. It is common for fracture spacing to be less than the 10 cm to 2 meter width of the phyllosilicate alteration zone. The phyllosilicate zone is also developed along the western margin of the pyrite-silica body. Locally the earlier phyllosilicate zone associated with the pyrite-silica body is overprinted by alteration zones associated with the younger veins, resulting in a complex distribution of alteration minerals. Locally, post-mineral faulting has disrupted and displaced the alteration assemblages.

The distribution of the alteration assemblages defines fracture bounded matrix blocks, with the vent margin fault defining the eastern limit of the blocks. Partially replaced sedimentary rocks within the pyrite-silica body exhibit a mineralogy characteristic of the quartz-alunite-kaolinite zone. The quartz-phyllosilicate zone is developed marginal to the pyrite-silica body and provides the clearest definition of the eastern boundary of the matrix blocks. The northern and southern boundaries of individual blocks are defined by vein systems. The western boundary of the matrix blocks is nowhere observable. The fractures which bound the matrix blocks are the

channels which have localized the flow of hydrothermal solutions and the deposition of minerals.

#### Disruption of the Alteration Patterns

Veins that have cut the pyrite-silica body have disrupted alteration patterns. Part of the disruption results from the fact that the pyrite-silica body itself is not amenable to the development of silicate alteration minerals. As a result, alteration patterns terminate at the margin of the pyrite-silica body whether or not the vein does. Where the veins cut the margin of the pyrite-silica body, the quartz-muscovite-kaolinite alteration associated with the vein merges with the similar assemblages associated with the pyrite-silica body, resulting in a complicated geometry at the junction. The overall distribution of alteration assemblages is complicated by this overlapping and by disruption caused by post-mineral faulting.

Locally, alteration assemblages have been completely removed from the margin of the massive sulfide body by late fault movements. The quartz-phyllsilicate alteration produces a distinctive rock, which can be and has been used as a mappable unit within the mine. As a result, when this zone is missing from a mineralized area, it is obvious; faulting and internal adjustments within the vent clearly continued after mineralization.

#### Lourdes Fragmental

A minor debate has flurried for years through the Cerro de Pasco literature over a unit known as the "Lourdes Fragmental." The

"Lourdes fragmental" is a light gray to white rock containing silicified fragments of Excelsior Group and quartz monzonite in a fine grained matrix which resembles an igneous rock. The rock locally exhibits flow structures and commonly is intensely altered (Lacy, 1949; Einaudi, 1968). This rock has been mapped as a separate unit on the mine level plans since mining operations started. It is named for the Lourdes shaft which cut extensive intervals of the unit in its upper portions (Boutwell, 1920).

Interpretations of the origin of the rock have been varied. Boutwell (1920) and Bowditch (1935) interpreted it as an intrusive fragmental phase of the "Cerro Quartz Monzonite." McLaughlin (1924) interpreted it as a tuff at the base of the Rumiallana Agglomerate. Lacy (1949) distinguished two types of Lourdes Fragmental. One type is a mechanical mixture of Rumiallana Agglomerate and Cerro Quartz Monzonite at the contact between the two. The second and more extensive type of 'Lourdes Fragmental' is simply Rumiallana Agglomerate that has been altered in the vicinity of the Cerro Quartz Monzonite. This second type is essentially the same material as the Quartz-Phyllosilicate alteration zone of this study and is related both to intrusion of the quartz monzonite porphyry and mineralization in the veins.

#### Summary

Three alteration assemblages based on mineralogy (Bowditch, 1935) have been delineated. The assemblages have gradational

boundaries with one another and can be used to define alteration zones which are parallel to fracture-controlled flow channels. In the simplest case, the zones are sequentially arranged outward from and parallel to a fracture filled with vein material (Figure 20). The 2-3 cm thick quartz-alunite-kaolinite zone is closest to the vein. The quartz-phyllosilicate-kaolinite zone, 10 cm to 2 meters thick, is next removed, with the quartz-pyrophyllite-kaolinite subzone toward the vein and the quartz-muscovite-kaolinite subzone away from the vein. In addition to this gross zoning within the quartz-phyllosilicate-kaolinite zone, microprobe analyses indicate that the pyrophyllite component of the muscovite increases toward the vein within the quartz-muscovite-kaolinite subzone. The outermost calcite-chlorite-epidote zone is poorly defined. The most common wallrock in the area that is presently accessible for study is the Rumiallana Agglomerate. The Rumiallana Agglomerate is everywhere characterized by a sufficiently diverse mineralogy so that the outer boundary of the calcite-chlorite-epidote zone is difficult to define.

## GEOCHEMISTRY

In recent years considerable effort has gone into applying basic chemistry and physics to geologic systems and, in particular, hydrothermal systems (Helgeson, 1979; Norton, 1981; and references therein). These studies suggest that the evolution of hydrothermal systems leads to the development of a characteristic set of observable features which can be used to interpret the history of the system. These features include ore and alteration mineral assemblages (Helgeson, 1979; Hemley and Jones, 1964; Meyer and Hemley, 1967; and many others) as well as fractures (Koide and Bhattacharji, 1975; Knapp and Norton, 1981).

Equilibrium mineral assemblages, as well as numerical models of hydrothermal systems, can be used to constrain temperatures, pressures, and fluid compositions associated with hydrothermal systems. At Cerro de Pasco, vein mineralization is dominated by pyrite-enargite with lesser tennantite and rare chalcopyrite, the latter being restricted to the lower portion of the Cleopatra vein system and the lower portion of the massive sulfide body. Alteration assemblages include alunite, pyrophyllite, muscovite, kaolinite, quartz and lesser quantities of other minerals as discussed in the last section. Phase relations for these minerals will be reviewed, as well as numerical models for this type of system.

### General Conditions

The complexity of the hydrothermal system at Cerro de Pasco has made quantitative analysis difficult. In particular, the complex mineralogy defies analysis in terms of simple geochemical models. The writer knows of no location where enough mineral phases coexist to define an equilibrium assemblage that could be used to constrain all of the intensive thermodynamic variables of the system. Consequently subsystems must be used to study systematic variations in mineralogy that are observed.

Geothermometry has been difficult, but several factors suggest that much of the mineral deposition occurred at approximately 300°C. In general, the sulfide assemblages discussed by Einaudi (1977) are compatible with temperatures around 300°C, though the late stage mineralization may have been significantly lower. An extensive search for samples of quartz suitable for measurement of fluid inclusion filling temperatures yielded only a few samples. The sparse filling temperatures measured clustered around 300°C (Table 2). The assemblage pyrophyllite-kaolinite-quartz, found marginal to the vein systems, is only stable between 300°C and 350°C if the activity of aqueous silica in the coexisting hydrothermal solution is at quartz saturation.

Additional support for temperatures of approximately 300°C comes from numerical models of hydrothermal systems. Detailed models have been developed to predict temperatures and pressures in hydrothermal systems associated with cooling intrusions. These numerical models predict maximum temperatures in the range of 200-400°C above cooling intrusions emplaced at shallow levels of the crust, depths of

Table 2. Fluid Inclusion Filling Temperatures

---



---

Sample #153									
Filling Temperature (°C)									
201	201	214	212	218	227	229	212	215	205
214	221	225	230	239	242	245	256	254	242
235	238	229	197	202	186	243	242	243	
Sample #856									
Filling Temperature (°C)									
333	334	325	317	311	321	313	327	328	319
318	329	331	352	345	345	349	346	375	394
384	381	384	375	397	395	404	405	406	374
376	377	324	318	310	319				

---

1-2 km and pressures of 200-500 bars (Norton, 1981; Norton and Knight, 1977; Cathles, 1977). Temperature variation in the lithocaps of these intrusions is characterized by an initial increase followed by a period of on the order of several tens of thousands of years of relatively constant temperature followed by a return to ambient conditions. The magnitude of temperature increase at any point is a function of several factors. Among the most important factors controlling temperature distributions in hydrothermal systems are properties of the fluid phase (Norton and Knight, 1977). Viscosity, heat capacity, and the coefficient of thermal expansion are fluid properties which exert an important influence on the evolution of hydrothermal systems. Heat capacity and the coefficient of thermal expansion are maximized in the 300-400°C temperature range, at 200-600 bars, and the viscosity is minimized in approximately the same range. This coincidence of extrema in the values of these fluid properties results in maximum heat and mass transport in this temperature range, such that large volumes of rock in the lithocap of an intrusion can be heated to temperatures on the order of 300°C. The source of the hydrothermal solutions at Cerro de Pasco is uncertain. However, conditions predicted by these models are compatible with the geologic setting at Cerro de Pasco.

Constraining geochemical conditions at the time of mineralization has also been difficult. In particular the massive sulfide replacement body contains a diverse and complex mineralogy, exhibiting complex textural relations (Lacy, 1949). In addition, Einaudi (1977) has suggested that some of the sulfide assemblages in



the massive sulfide body may represent nonequilibrium assemblages, making analysis even more difficult. However, consistent mineral zonations found associated with the vein systems allow important constraints to be placed on fluid compositions associated with mineralization.

To aid in analysis, phase diagrams were constructed at a variety of temperatures and pressures. Diagrams were constructed at temperatures ranging from 25°C to 400°C, though only a few are reported below. Diagrams for the system  $K_2O-Al_2O_3-SiO_2-SO_3-H_2O-HCl$  were constructed for pressures of 100 bars, 300 bars and 500 bars. These variations in pressure result in minor variations in the location of phase boundaries but do not affect the general trends. The diagrams reported below are constructed at 500 bars for convenience in comparisons with other literature. The data base used for constructing diagrams in the system  $Fe_2O_3-FeO-Cu_2O-As_2O_3-H_2S-SO_3-H_2O$  does not account for the pressure dependence of phase relations in the system.

Some chemical conditions must also be specified for the phase diagrams. The  $\text{Log } a^2(H^+) \cdot a(SO_4^{=})$  was set at -12.0 for most diagrams because this is just below that needed to stabilize alunite, at quartz saturation, at 300°C. These conditions require that the  $\text{Log } a H_2S = -3$ , if oxidation conditions were near the hematite-magnetite oxidation buffer as is common in many hydrothermal systems and as suggested for the vein systems at Cerro de Pasco by Einaudi (1977). The  $\text{Log } a(As(OH)_4^-) \cdot a(H^+)$  was set at -12, an intermediate value reported by Knight (1977).

### Geochemical Systems

A complex multicomponent geochemical system would be needed to characterize the hydrothermal system at Cerro de Pasco completely. Sulfide and sulfosalt minerals are abundant, a wide variety of ore minerals is present in minor quantities (Lacy, 1949), and alteration minerals include a wide variety of silicates. Jasperoid and various carbonates are common alteration products in the Pucará Group. Although minor phases do occur, the most important aspects of the alteration mineralogy, in terms of mass abundance, can be described in the system  $K_2O-Al_2O_3-SiO_2-SO_3-H_2O-HCl$ . The innermost and intermediate alteration assemblages are dominated by the phyllosilicate minerals, quartz, and alunite. Pyrite is the only abundant mineral which cannot be described in this system. Equilibrium among mineral phases and an aqueous solution is discussed by Helgeson et al. (1978) and can be written as (Bird and Norton, 1981; Eq. 1):

$$0 = \sum_i^{\hat{i}} n_{i,r} \phi_i + \sum_j^{\hat{j}} n_{j,r} \lambda_j \quad (1)$$

where  $i$  ( $i=1, 2, \dots, \hat{i}$ ) and  $j$  ( $j=1, 2, \dots, \hat{j}$ ) respectively denote the mineral phases ( $\phi$ ) and the species in the coexisting fluid ( $\lambda$ ). The stoichiometric reaction coefficient,  $n$ , for the  $r$ th reaction is positive for products and negative for reactants.

Composition-concentration relations among mineral phases and an aqueous solution are defined by the Law of Mass Action (Bird and Norton, 1981; Eq. 2):

$$\sum_{l=1}^{\hat{1}} n_{l,r} \log \left( \frac{a_{\lambda l}}{Z a_{H^+}} \right) = \log K_r - \sum_{i=1}^{\hat{1}} n_{i,r} \log a_{\phi i} \quad (2)$$

where  $K_r$  is the equilibrium constant for the  $r$ th reaction and  $Z$  is the charge of the  $l$ th aqueous species.  $a_{\phi i}$  is the activity of the mineral phase, which equals 1 for stoichiometric minerals. Phase stabilities, thus defined, can be depicted on activity-activity diagrams calculated for specified temperatures, pressures, and compositions.

Thermodynamic data reported by Helgeson et al. (1978) were used to construct such phase diagrams. These diagrams depict the stability of mineral phases as functions of temperature, pressure, and the composition of the coexisting aqueous phase. Equilibrium mineral assemblages were used, in conjunction with these diagrams, to characterize fluid compositions, to the extent possible, at the time the minerals formed.

Alteration minerals record physical-chemical conditions related to the hydrothermal system. Caution must be exercised in evaluating the significance of alteration minerals because local variations in the chemistry of the wallrocks can buffer the solution and affect the mineralogy which forms. Consistent mineral zonation in large volumes of variable wallrock composition is more likely related to conditions imposed by the hydrothermal system. Consequently, alteration minerals and their zonation can be used to constrain the values of temperature, pressure, and fluid composition at the time of alteration and mineralization.

### Phase Relations

Pyrophyllite-kaolinite-quartz and andalusite-pyrophyllite-quartz provide unvariant reactions which are useful in determining P-T conditions of alteration-mineralization assemblages containing these phases (Helgeson et al., 1978). Phase relations for the system  $\text{Al}_2\text{O}_3\text{-SiO}_2\text{-H}_2\text{O}$  (Figure 21) show that below  $300^\circ\text{C}$ , solutions must be supersaturated with respect to quartz to be in equilibrium with pyrophyllite. Above approximately  $350^\circ\text{C}$ , pyrophyllite may be in equilibrium with diaspore and quartz or andalusite. Jasperoid and chert are abundant in the pyrite-silica body, indicating the precipitation of amorphous silica from the hydrothermal solutions which deposited these minerals. However, x-ray analyses of the alteration assemblages associated with the veins and marginal to the pyrite-silica body all revealed sharp quartz peaks and no evidence of diffuse x-ray patterns was found, indicating that the hydrothermal solutions associated with these assemblages were at quartz saturation (Carroll, 1967). Also, quartz equilibrium is maintained in modern hydrothermal systems above approximately  $200^\circ\text{C}$  (Arnorsson, 1975), suggesting that silica activity was at quartz saturation during the formation of most hydrothermal ore deposits, including the vein systems at Cerro de Pasco. Clearly the following analysis cannot be applied directly to the pyrite-silica body and included alteration assemblages, because quartz saturation will be assumed.

Phase relations among alunite, andalusite, microcline, phyllosilicates, silica phases, and an aqueous solution can be shown

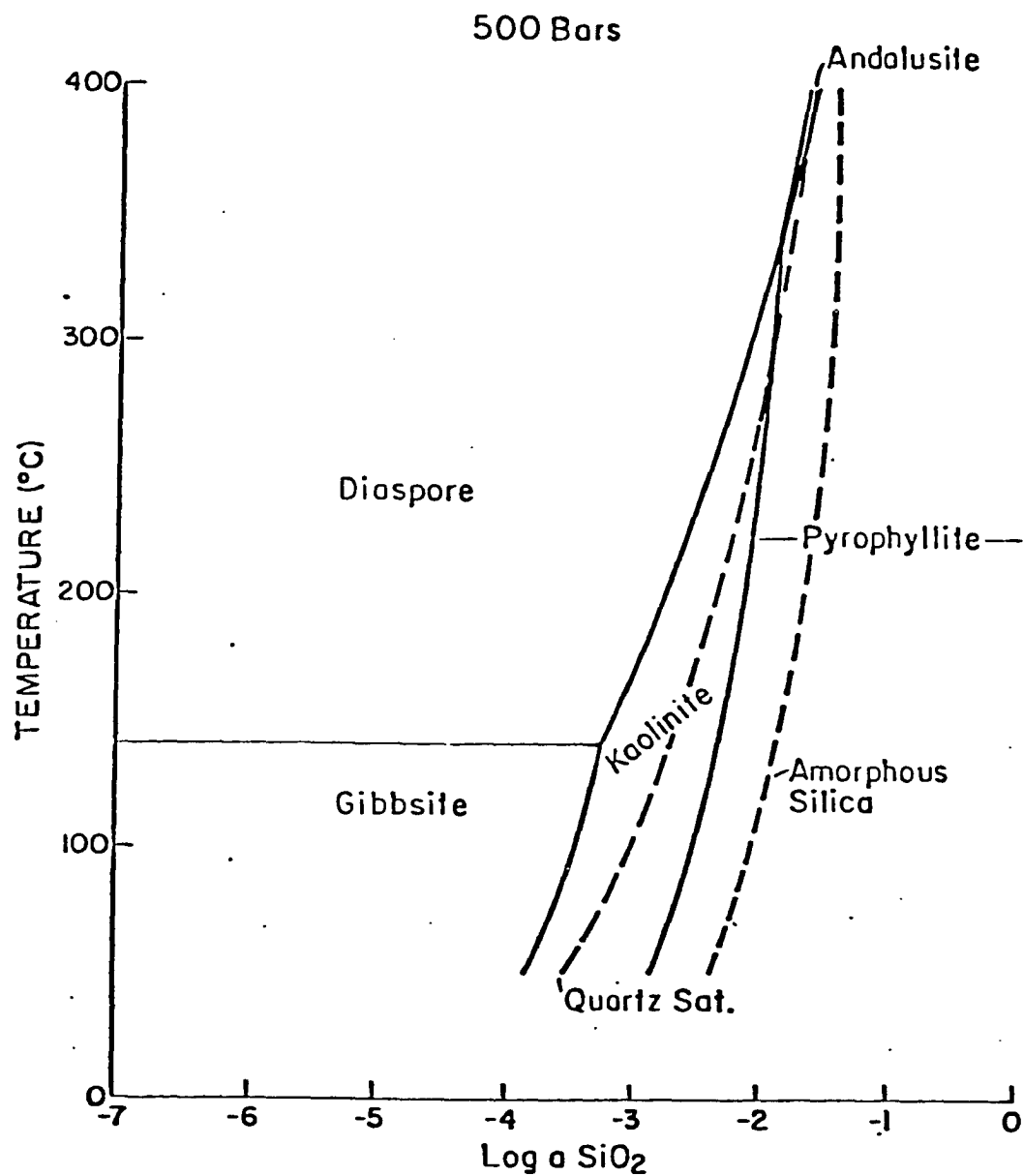


Figure 21. Activity-temperature diagram for the system  $\text{Al}_2\text{O}_3$ - $\text{SiO}_2$ - $\text{H}_2\text{O}$ . -- Solid lines represent phase boundaries. Dashed lines represent saturation surfaces. Above 300°C, the quartz saturation surface continues along the koolinite-pyrophyllite and andalusite-pyrophyllite boundaries. Data for the diagram from Helgeson et al. (1978).

on activity-activity diagrams of the system  $K_2O-Al_2O_3-SiO_2-SO_3-H_2O-HCl$  (Figures 22 and 23). Alunite and muscovite are stable at higher values of  $\log a(K^+)/a(H^+)$  than are kaolinite, pyrophyllite, and gibbsite or diaspore. At a given value of  $\log a(SiO_2)$ , microcline requires a larger value of  $\log a(K^+)/a(H^+)$  than muscovite. With increasing temperature, the kaolinite stability field decreases in size. The muscovite field expands and then contracts with increasing temperature at constant  $\log a^2(H^+) \cdot a(SO_4^{=})$  and expands with decreasing  $\log a^2(H^+) \cdot a(SO_4^{=})$ . At quartz saturation, and below  $300^\circ C$ , kaolinite, muscovite, and microcline are the equilibrium phases at increasing  $\log(a(K^+)/a(H^+))$  values. At amorphous silica saturation, pyrophyllite will be the low potassium-low sulfate equilibrium phase.

The alunite stability field increases with increasing  $\log a^2(H^+) \cdot a(SO_4^{=})$  and increasing temperature. At constant  $\log a^2(H^+) \cdot a(SO_4^{=}) = -12.00$ , alunite replaces muscovite as the stable phase in equilibrium with quartz at  $300^\circ C$  and higher temperatures. At higher values of the activity product  $(H^+)^2 \cdot (SO_4^{=})$ , alunite replaces muscovite as the equilibrium phase with quartz at lower temperatures. The formation of alunite requires acid-sulfate rich solutions. Formation of aluminous alteration assemblages from rock forming silicate minerals requires the consumption of hydrogen ions. At Cerro de Pasco alunite commonly forms after muscovite in altered clasts of Excelsior Group phyllite. Formation of one mole of alunite from muscovite requires

Figure 22. Activity-activity diagrams for the system  $K_2O-Al_2O_3-SiO_2-SO_3-HCl-H_2O$ . -- Solid lines represent phase boundaries. Dashed lines represent saturation surfaces.  $\log (a^2_H + aSO_4^{2-}) = -12.0$ . Data for diagrams from Helgeson et al. (1978).

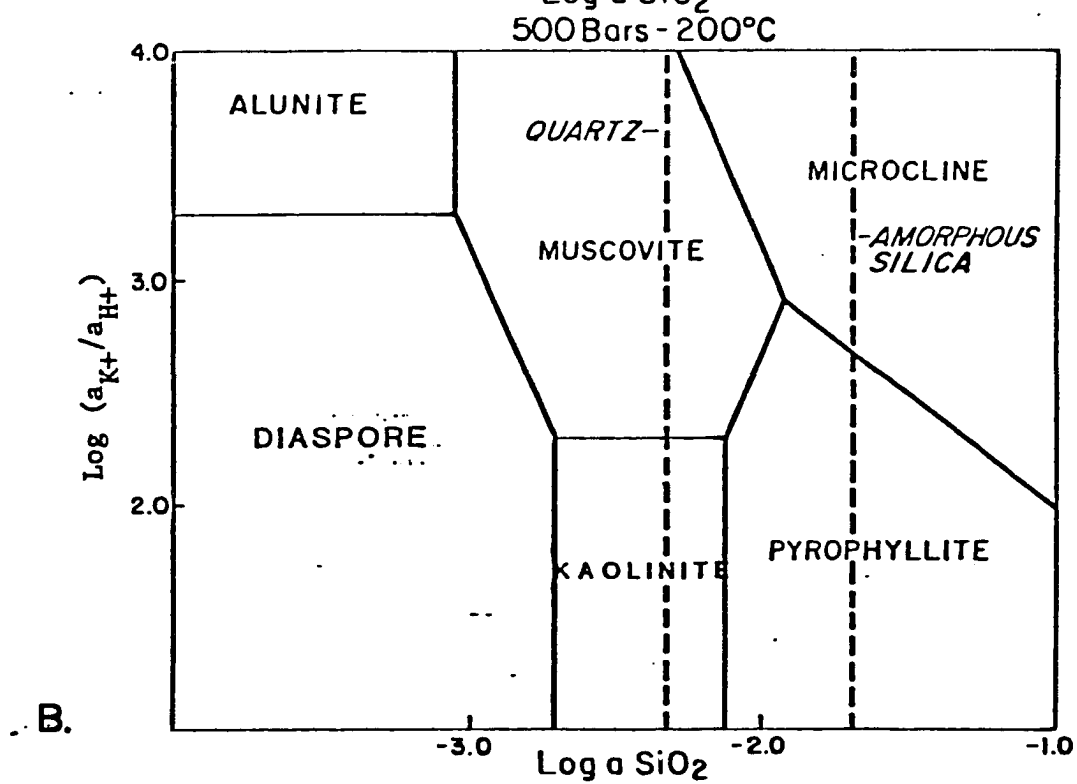
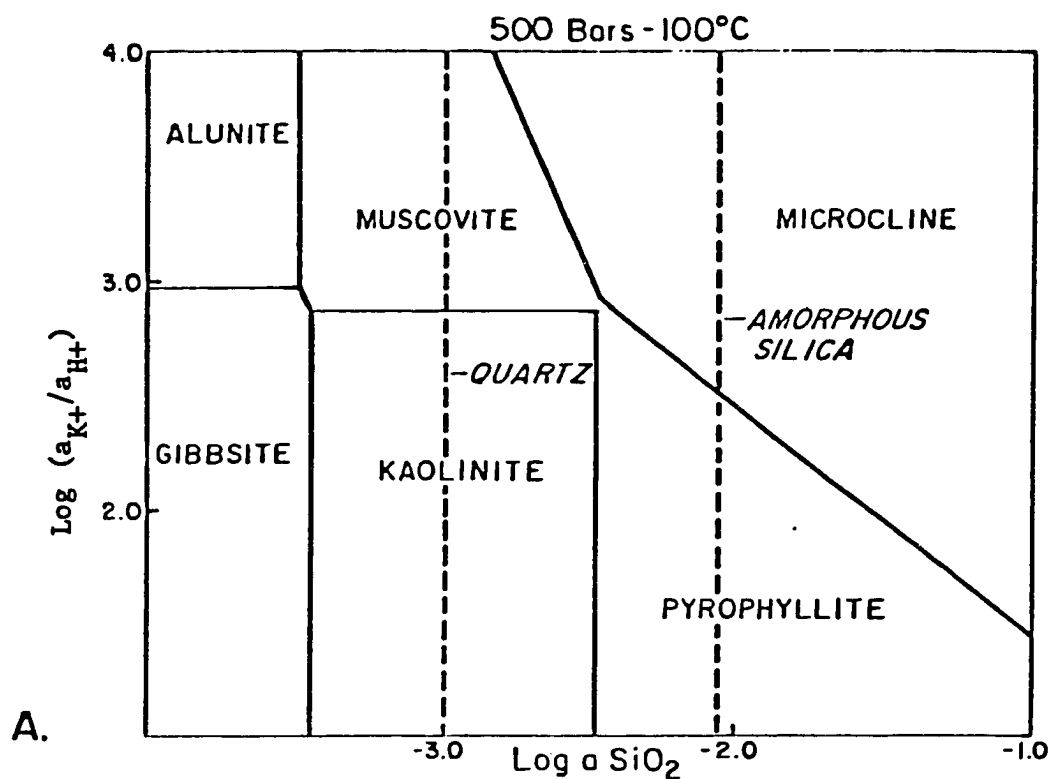
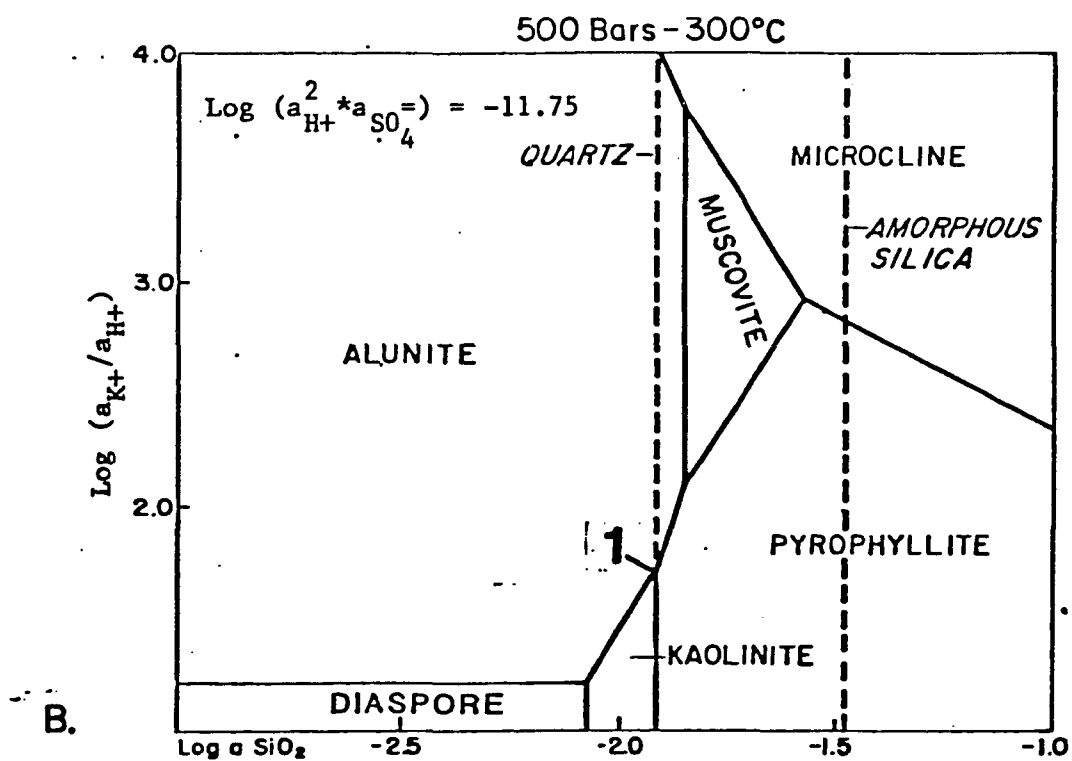
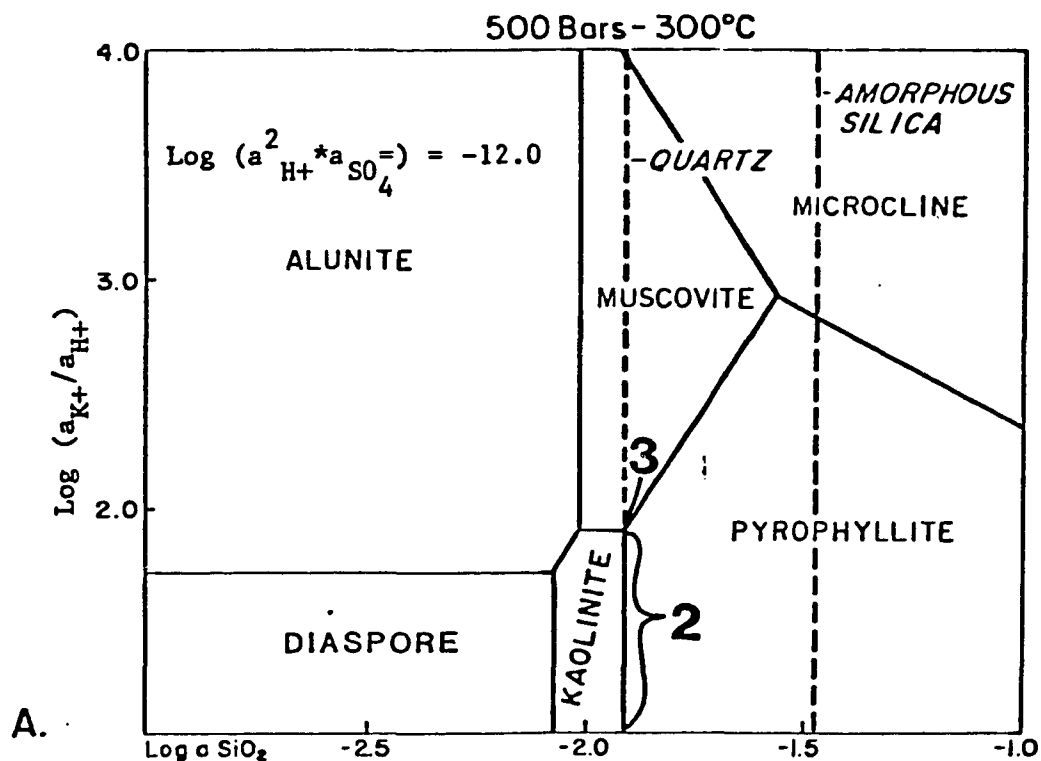
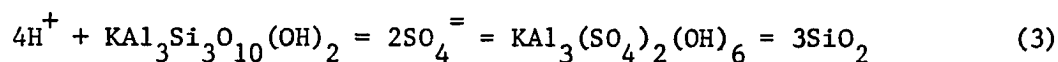




Figure 23. Activity-activity diagrams for the system  $K_2O-Al_2O_3-SiO_2-SO_3-HCl-H_2O$ . -- Solid lines represent phase boundaries. Dashed lines represent saturation surfaces. Numbers indicate conditions compatible with alteration assemblages as discussed in the text. Data for diagrams from Helgeson et al. (1978).



the consumption of four moles of  $H^+$  (Knight, 1977; Hemley et al., 1962), Eq. 3.



The general conditions associated with the alteration zones delineated above can be seen on Figure 23. Point 1 shows the conditions in the system for the quartz-alunite-kaolinite-pyrophyllite assemblage. Point 2 shows the conditions for the quartz-pyrophyllite-kaolinite zone. Point 3 shows the conditions for the quartz-muscovite-kaolinite zone. The activity diagrams show the chemistry of aqueous solutions in equilibrium with these assemblages at the specified conditions. As is normal, the general trend is for the  $\log a(K^+)/a(H^+)$  in solution to increase with increasing distance from the vein. This analysis assumes that the activity of muscovite is unity. However, the microprobe analysis presented on Figure 19 and Table 1 indicate that this is not correct. The assumption is made because no adequate thermodynamic model is available to characterize solid solution between muscovite and pyrophyllite. This simplification will affect the absolute magnitudes calculated, but shouldn't change the overall trends.

#### Cu-Fe Sulfides and Cu-As Sulfosalts

Helgeson et al. (1978) did not include Cu-As sulfosalt minerals in the compilation of their thermodynamic data base. However, phase relations for these minerals below 300°C have been discussed by Gustafson (1963) and Knight (1977). It is not certain that the data from these studies are completely consistent with the newer

data base of Helgeson et al. (1978). However, Knight (1977) provides an internally consistent data base including Cu-Fe sulfide and Cu-As sulfosalt minerals.

Phase relations for the system  $\text{Fe}_2\text{O}_3\text{-FeO-Cu}_2\text{O-As}_2\text{O}_3\text{-H}_2\text{S-SO}_3\text{-H}_2\text{O}$  are shown on Figure 24. Enargite and tennantite are stable at lower values of  $\text{Log } a(\text{Fe}^{++})/a^2(\text{H}^+)$  than the copper-iron sulfides. Tennantite is stable at higher values of  $\text{Log } a(\text{Cu}^+)/a(\text{H}^+)$ . With decreasing temperature the stability fields of enargite and tennantite expand dramatically. Consequently, decreasing temperature and increasing acidity of the hydrothermal solutions would both favor the formation of the sulfosalt minerals. However, the value of the activity product  $(\text{H}^+)(\text{As}(\text{OH})^-)$  value must be higher than  $10^{-14}$  in order to stabilize the sulfosalt minerals (Knight, 1977). Figure 24 shows the general conditions associated with massive sulfide mineralization where pyrite, pyrrhotite and locally chalcopyrite coexist (A) and vein mineralization where pyrite and enargite coexist (B). At all temperatures investigated, the vein assemblage requires a lower activity ratio of  $(\text{Fe}^{++})/(\text{H}^+)^2$  and a higher activity ratio of  $(\text{Cu}^+)/(\text{H}^+)$ . The chalcopyrite in the massive sulfide body occurs as exsolution blebs in sphalerite of the same paragenetic age as the pyrite and pyrrhotite. If this can be considered an equilibrium assemblage in the thermodynamic sense, then the assemblage constrains the value of  $\text{Log } a \text{H}_2\text{S}$  in the coexisting solution. The  $\text{Log } a \text{H}_2\text{S}$  must be greater than -2 at  $300^\circ\text{C}$  and -4 at  $200^\circ\text{C}$  for this assemblage to coexist. Increasing the activity of  $\text{H}_2\text{S}$

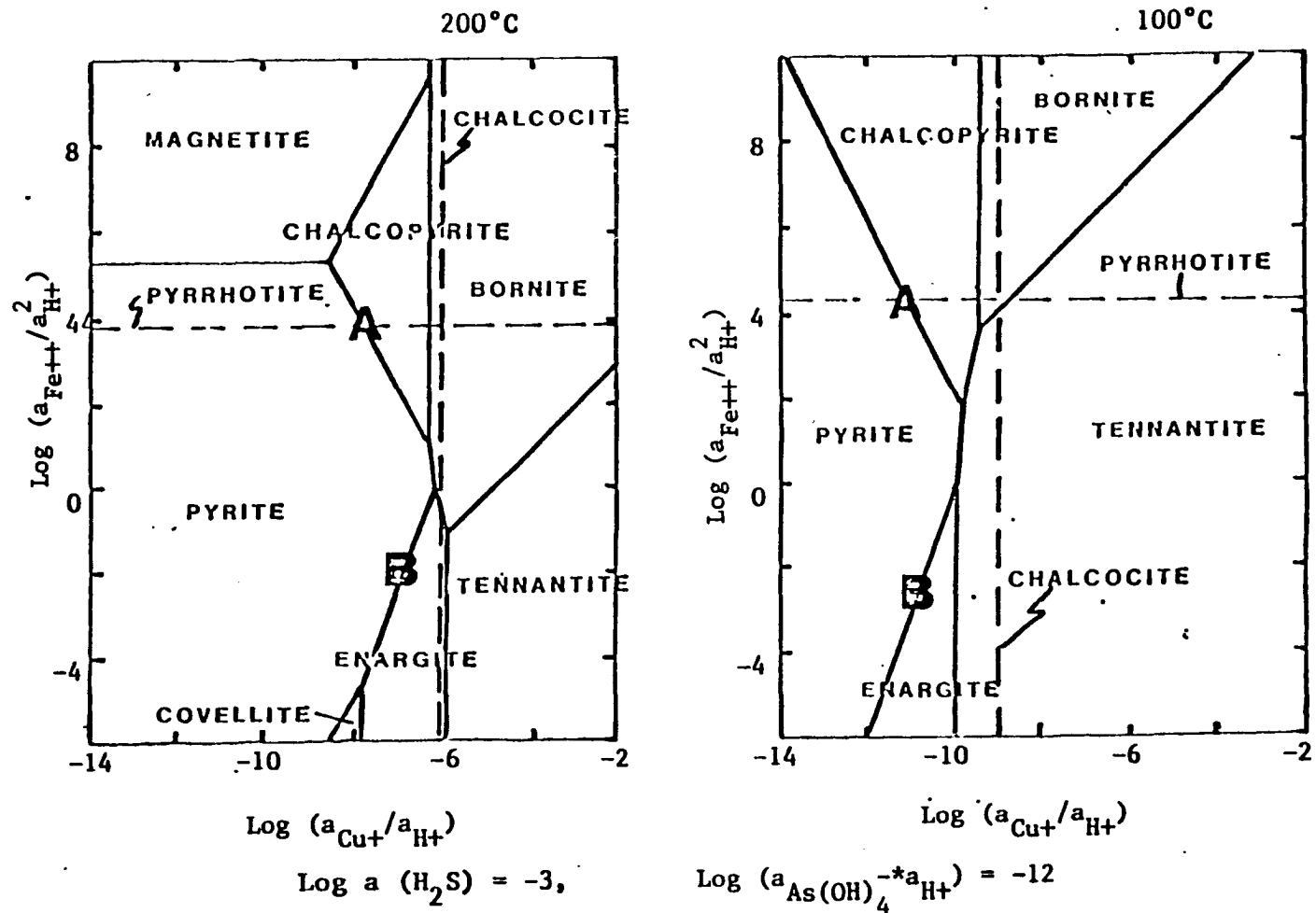


Figure 24. Activity-activity diagrams for the system  $\text{Fe}_2\text{O}_3\text{-FeO-Cu}_2\text{O-As}_2\text{O}_3\text{-H}_2\text{S-SO}_3\text{-H}_2\text{O}$ . -- Solid lines represent phase boundaries. Dashed lines represent saturation surfaces. Letters indicate conditions compatible with mineralization, see text for further discussion. Diagrams from Norton (1981).

results in the assemblage being stable at lower values of  $\text{Log } a(\text{Fe}^{++})/a^2(\text{H}^+)$  and  $\text{Log } a(\text{Cu}^+)/a(\text{H}^+)$ .

## OTHER FELSIC VOLCANIC SYSTEMS

High levels of felsic volcanic systems have been described from numerous places (Smith and Bailey, 1968; Williams and McBirney, 1979). In some instances, volcanic cones have been developed that are reminiscent of the popular image of volcanoes. In other cases, volcanic activity has resulted in the accumulation of material within volcanic vents and in larger surficial depressions referred to as calderas (Williams, 1942). The fill material commonly includes welded and water-lain tuff as well as lacustrine sediments which have filled topographic depressions. Volcanic domes of dacite to rhyolite composition commonly intrude this fill. Megabreccias composed of rocks from the vent walls are abundant in some systems.

Modern calderas are often the sites of lakes, such as Crater Lake, Oregon (Williams, 1942). In older calderas the former presence of lakes may be documented by lacustrine sedimentary rocks, often interbedded with volcanic and volcanoclastic rocks (Francis, Baker and Halls, 1981). In Pleistocene time, a lake filled the Long Valley caldera (Bailey, Dalrymple and Lamphere, 1976). The topographic depression associated with caldera subsidence results from downdropping within the vent and inward lateral movement of material from the vent margin into the vent. At the Valles caldera, 700 meters of sedimentary fill accumulated from erosion and slumping of the caldera walls (Doell et al., 1968). At Long Valley, subsidence dropped the vent floor

at least a kilometer, and perhaps as much as three kilometers (Bailey et al., 1976).

The material that cascades into the vent as rock slides and rock falls varies in clast size from pieces the size of hand samples to blocks tens of meters across. The resulting formations have been referred to as megabreccia (Lipman, 1976; Lambert, 1974). The lithology and quantity of matrix material in megabreccias is variable. In the calderas of the San Juan volcanic field, the breccia blocks are enclosed by ash-flow material of rhyolitic composition (Lipman, 1976). In other cases the blocks are enclosed in a volcanoclastic matrix. These differences may represent the level of exposure within the system with the amount of igneous material increasing at greater depths. Intrusive ring complexes probably represent the lowest part of this progression toward greater quantities of igneous material in deeper parts of caldera systems (Smith and Bailey, 1968).

Caldera formation requires subsidence and structural adjustments within the volcanic vent of the system. The structural boundary of the system is defined by a ring fault system that bounds a central cauldron block. In large systems, such as the Valles caldera (Smith, Bailey and Ross, 1961) and the Long Valley caldera (Bailey et al., 1976), the cauldron block has subsided as a relatively intact cylinder. In some cases this central cylinder is elevated after subsidence by resurgent igneous activity (Smith and Bailey, 1968). In smaller calderas such as Krakatoa (Williams, 1941), the cauldron block appears



to break up as it subsides resulting in a highly fractured and chaotically jumbled floor.

After collapse, subsequent igneous activity is localized along the ring-fault zones of many calderas. This igneous activity includes pyroclastic eruptions which contribute to the infilling of the subsidence structure and volcanic domes which were another manifestation of this activity in the Long Valley, Valles, and Island Park calderas (Smith et al., 1961; Hamilton, 1965; Bailey et al., 1976). The volcanic domes are of dacitic to rhyolitic composition and often form exogenous domes (Williams, 1932).

Hydrothermal activity is characteristic of the last stage of many caldera systems; in recent caldera systems, this activity is manifested by hot springs. In some ancient systems hydrothermal ore deposits record this activity. Base and precious metal vein deposits are associated with calderas in the Creede (Steven and Ratte, 1965) and Lake City (Slack, 1980) districts of Colorado. Vein and massive sulfide mineralization is associated with caldera formation in Japan (Kouda and Koide, 1978; Ohmoto, 1978). A wide variety of other metals are enriched in many calderas in the western United States (Rytuba, 1981).

## DISCUSSION

In spite of extensive earlier research on the ore deposit at Cerro de Pasco, very little has been said about the spatially and temporally associated volcanic system. Early workers suggested that a large volcanic cone once stood above the present level of exposure (Bowditch, 1935). However, the sedimentary and volcanoclastic fill within the vent, with subhorizontal bedding, cast serious doubt on this idea. Lacy (1953), based on the volcanoclastic nature of the Rumiallana Agglomerate, has suggested that explosive volcanism characterized the early stages of igneous activity, while others have suggested analogies with a diatreme model (Geological Staff of Cerro de Pasco Corporation, 1950; Silberman and Noble, 1977). The purpose of this section is to draw upon the lithologic, structural and geochemical relationships presented to develop a detailed model for the evolution of the volcanic system at Cerro de Pasco.

### Initial Phases

The initial phases of development of the volcanic system at Cerro de Pasco are obscure. At present, a ring fault system bounds a cylindrical structure approximately 2 km in diameter. Silberman and Noble (1977) have suggested an analogy to diatreme formation to explain the structure. Alternatively the ring fault system may bound a subsided block as depicted in the classic model of caldera formation

(Smith and Bailey, 1968), or it could be a simple volcanic throat that has served as a structural conduit to localize the intrusion of magmas.

The structure is clearly more than a simple volcanic throat that has localized intrusive activity. The structure has been infilled by volcanoclastic sediments and rootless slide blocks. It has, in part, localized intrusive activity, but has a more complex history.

The analogy to a diatreme is interesting. Williams and McBirney define diatremes as:

. . . steep-sided, more or less cylindrical or funnel-shaped breccia pipes that have penetrated the crust, apparently as a moderately low-temperature gas-rich intrusion.

The Rumiallana Agglomerate could have been such a gas-entrained breccia, though it would have to have been reworked in its highest levels to account for fluvial structures. Silberman and Noble (1977) appeal to the diatreme model to explain sedimentary structures in the Rumiallana Agglomerate that they interpret as resulting from base surge. Base surge deposits normally form from flat turbulent clouds of material that move horizontally from the base of an erupted column of material (Moore, 1967). In this case, though, those sedimentary structures may have formed as a result of explosive movement of material within the vent (Noble, personal communication, 1982). The model is also appealing because it would explain the presence of clasts in the Rumiallana Agglomerate that must have been derived from greater depths, such as the clasts of altered porphyritic igneous rocks. However, the diatreme model does not explain the tuffaceous sedimentary

rocks in the western portion of the vent. The location of these rocks within the vent requires that they resulted from pyroclastic activity on the floor of the vent, an activity inconsistent with diatreme characteristics. These rocks have a gradational contact with the Rumiallana Agglomerate indicating that, at least in part, the deposition of the latter unit was contemporaneous with pyroclastic activity. Sedimentary features indicative of explosive volcanism in the Rumiallana Agglomerate could have resulted from this pyroclastic activity on the vent floor.

At the present level of exposure, the ring fault system bounds material that has infilled the vent. The infilling material includes tuffaceous sedimentary rocks, rootless blocks and volcaniclastic agglomerate. This material has been intruded by felsic domes and dikes. At the present level of exposure the vent is not a breccia pipe.

In order to form a cavity for the vent fill, the central block bounded by the ring fault system must either have been downdropped or moved up and out of the way. The second alternative requires an explosive mechanism to "blow out" the hole bounded by the ring fault system. This might have been accomplished by a phreatic explosion or a "gas-rich intrusion" as envisioned for the diatreme model. The only evidence for such upward vertical movement is in the form of small clasts in the Rumiallana. The largest of these clasts is approximately 50 cm in longest dimension and most are much smaller. These clasts could easily have been brought to the surface in

conjunction with the pyroclastic activity. All other evidence for vertical movement within the vent indicates downdropping. This evidence includes the disposition of rootless blocks, the nature of the volcanoclastic sediments, and the folding and attitudes of these units. This type of downdropping (Figure 25) within a volcanic vent can have led to the development of a caldera (Williams, 1942; Smith and Bailey, 1968).

#### Infilling of the Vent

Because of subsidence the vent was a topographic low through all but its earliest history, perhaps with isolated bodies of water which could serve as local depositional basins. The vent margin probably served as a buttressed unconformity where sediments accumulated against the exposed vent wall. Inspection of section B-B' on Figure 2 shows that the Rumiallana Agglomerate and the tuffaceous sedimentary rocks infilled the vent up to and against the vent margin. It is not known how much of the vent wall was exposed at any one time. It may be that the volcanoclastic units infilled the vent at approximately the same rate that the floor subsided or that the floor subsided in large increments. At some point in its early history, the vent margin had enough topographic relief for blocks up to 1 km long to slide into the vent from the walls.

Infilling of the vent was accomplished by a variety of volcanic and sedimentary processes. The non-welded nature of most of the tuffaceous sedimentary rocks indicates that they are primarily

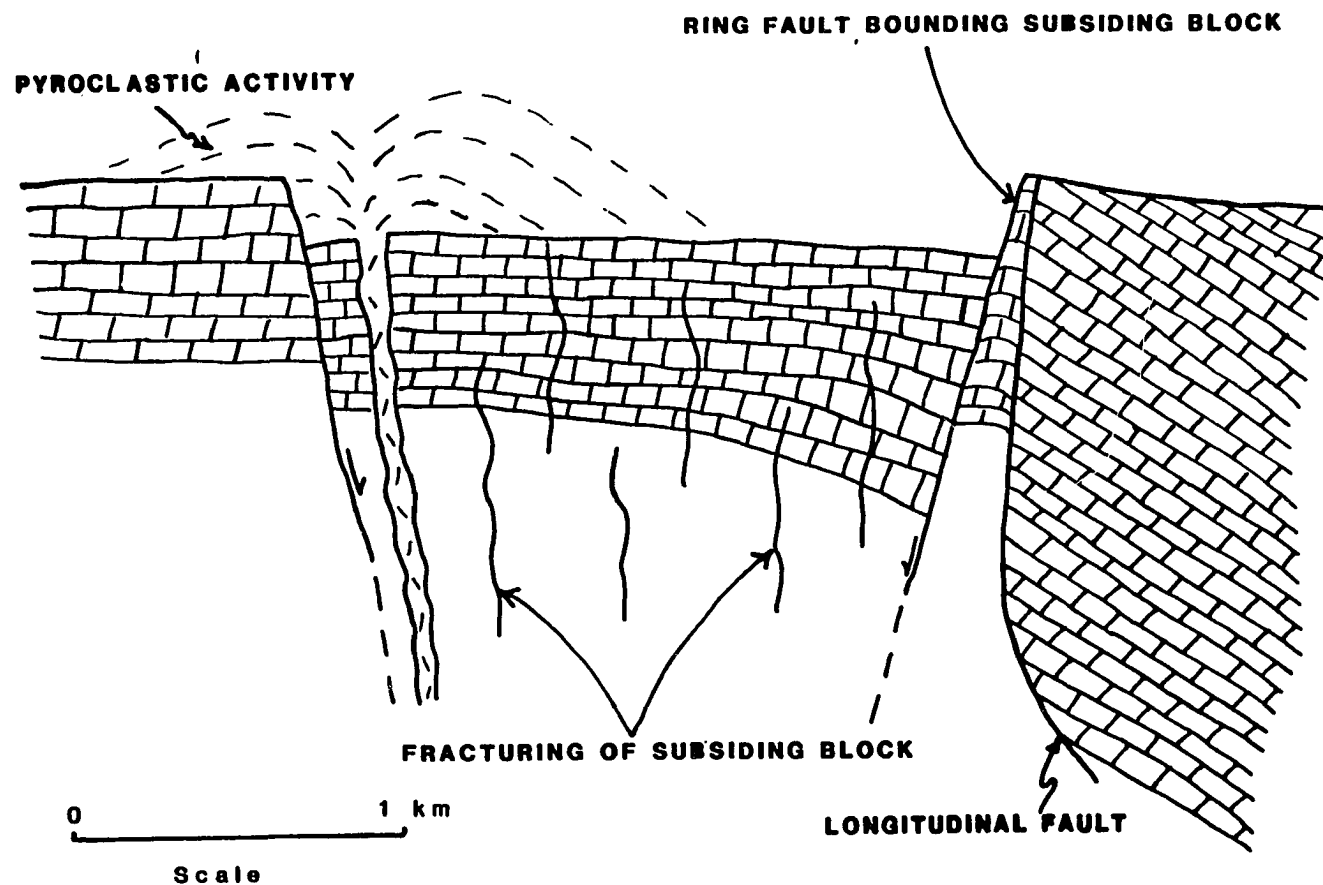


Figure 25. Initial phase of vent development as seen in a schematic east-west section. -- The cauldron block may have broken up and rotated during subsidence. Surface evidence indicates that pyroclastic activity was dominantly in the western half of the vent. Limestone shown thickening based on the data of Szekeley and Grose (1972). No vertical exaggeration.

air-fall deposits. Their close association with the dacite domes suggests that they may have formed by a series of Pelean type eruptions (Figure 26). Dacite diapiric-domes were emplaced on the floor of the vent, or perhaps immediately below the floor. Eruptions from these domes could have thrown material into the air which fell back to form the tuffaceous sedimentary rocks. Locally within this sequence, the rocks exhibit incipient welding and rarely dense welding; indicating that some of the pyroclastic material moved close to the ground and retained its heat after deposition. Infilling by the Rumiallana Agglomerate was contemporaneous with this volcanic activity as indicated by volcaniclastic material in the matrix of the Rumiallana Agglomerate and the gradational contact between the two units. The Rumiallana Agglomerate is in part fluvial, but probably also includes lahars and lacustrine deposits (Figure 26). An attempt was made to find a consistent relationship between the dip of the strata and the distance from the vent margin, as this might relate to the mechanism of folding or initial sedimentary dips. No systematic relationships were found.

The foliation in the dacites is interpreted as a flow foliation formed by differential slip across foliation planes. This mechanism results in the formation of ductile faults that locally bound rootless folds (Figure 12). The geometry of the folds shows that they are passive to quasiflexural folds, indicating conditions of high mean ductility and moderate to high ductility contrast at the time of formation (Donath and Parker, 1964).

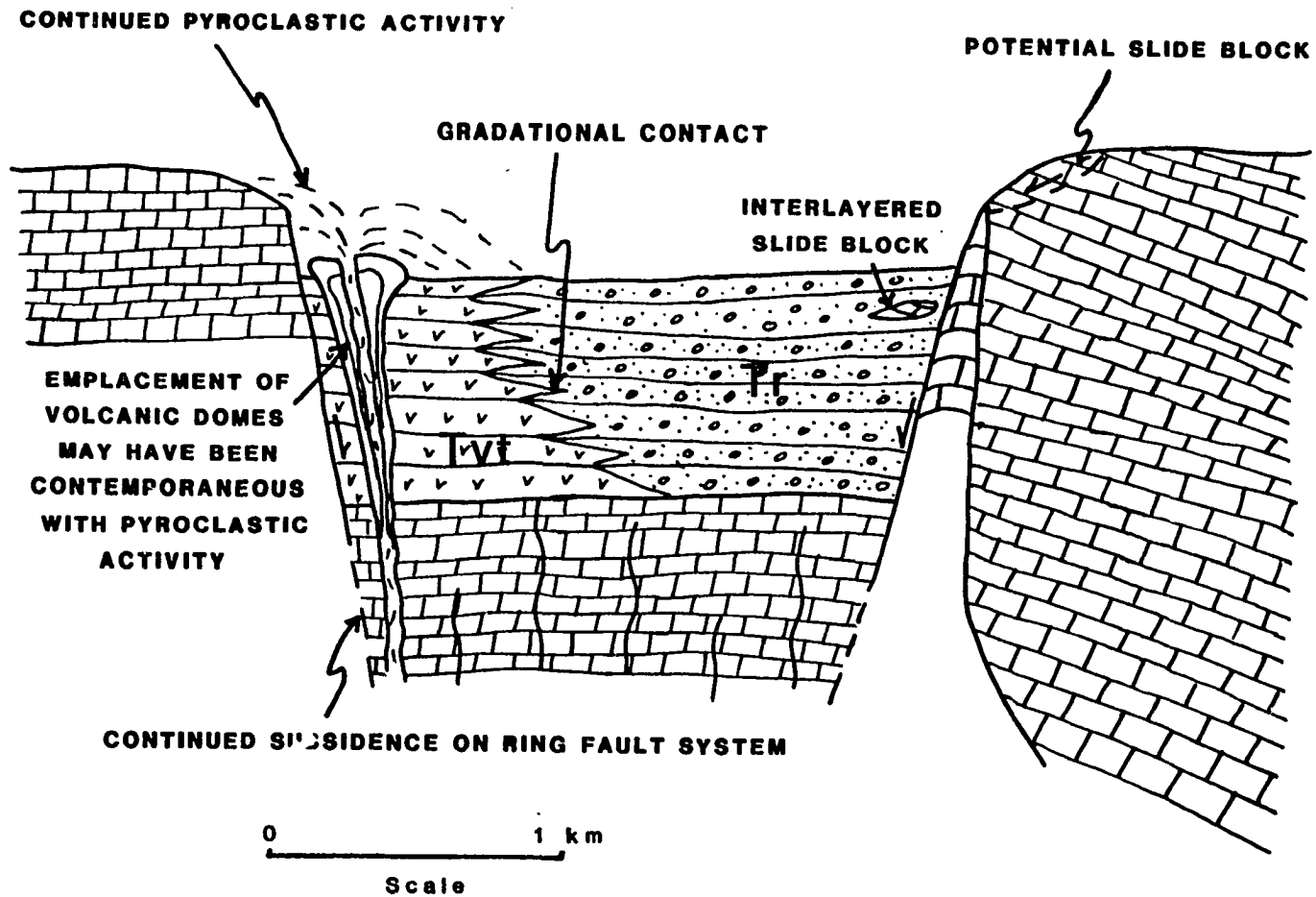


Figure 26. Infilling of the vent structure. -- Pyroclastic activity may have included Pelean type eruptions on the floor of the vent. Rumiallana Agglomerate (Tr) contains some pyroclastic material. No vertical exaggeration.



At the present level of exposure, the dacites are intrusive into the surrounding rocks. This intrusive relationship is shown by foliation orientations and bedding orientations in the surrounding rocks. The generally steep foliation orientations are characteristic of diapiric structures such as volcanic and subvolcanic domes (Williams, 1942) and salt domes (Balk, 1947). The mushroom-cap geometry of the domes indicates a very shallow level of emplacement. Models of intrusion based on gravity instabilities (Ramberg, 1981) exhibit this type of geometry near or at a free surface.

#### Structural Collapse and Fracturing

The conical fold defined by the data on Figures 9 and 10 records the downdropping and collapse of the sedimentary units into the vent (Figure 27). The scatter in the data suggests that the units were broken into blocks that moved semi-independently during the collapse. The subsidence of the floor was nonuniform, with the greatest subsidence in the center of the vent. It is important to observe that the bedding orientations from the Pucará Group block and Mitu (?) Group block (Figure 2) fall on the small circle which defines the conical fold (Figure 10). The orientations demonstrate that these blocks are floored by rocks within the vent, rather than by Excelsior Group. The blocks have thus moved into the vent from its margin and subsided with the contemporaneously emplaced vent contents. This subsidence could have been imposed upon a diatrema but is more reasonable as the last event associated with caldera subsidence.

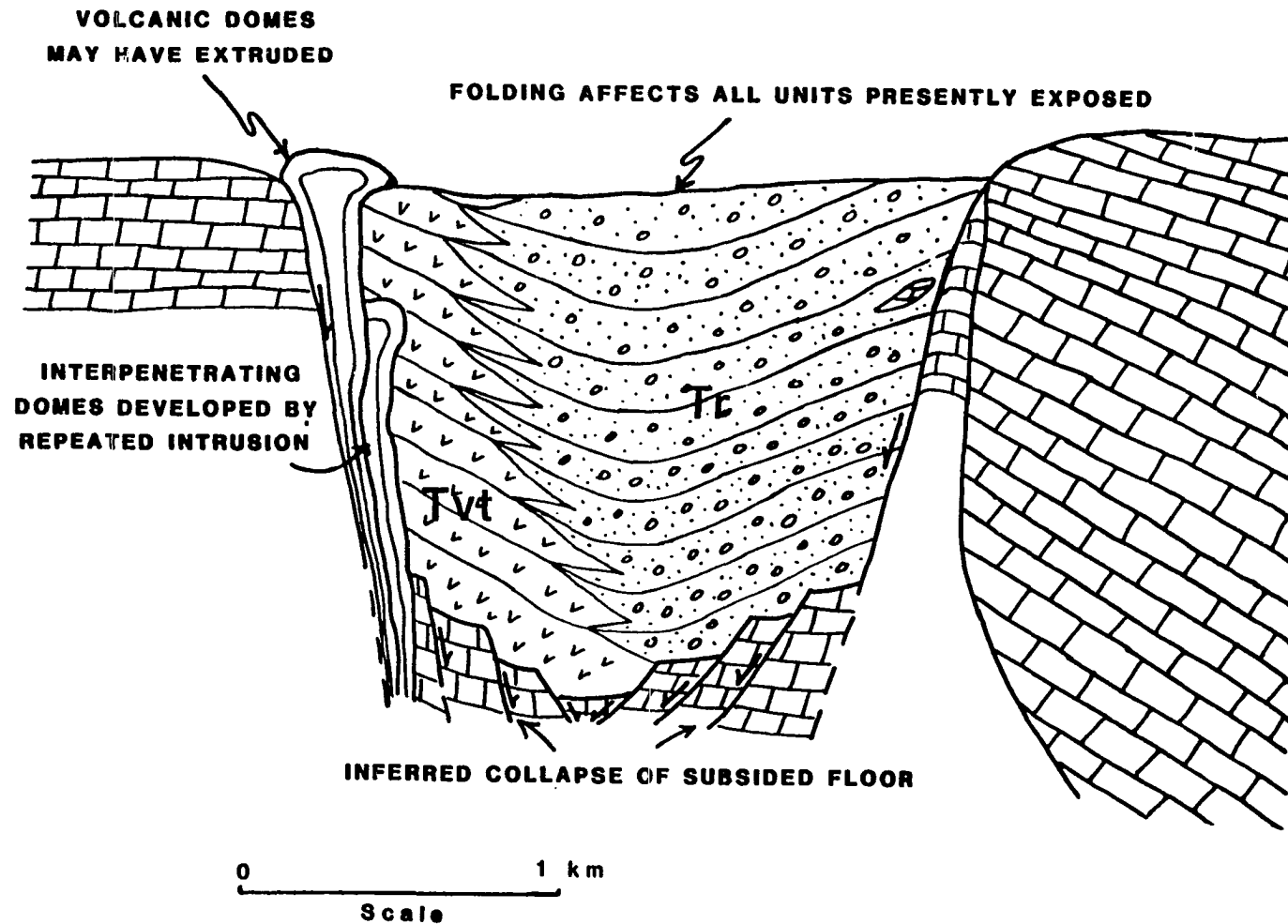


Figure 27. Structural collapse of the system. -- The "floor" of the vent may have broken into blocks that moved differentially early in the history of the system. Vent fill material has also been broken into blocks (not shown on figure because of scale) that moved differentially during the folding. No vertical exaggeration.

Slumping near the ring faults which form the structural margins of calderas is common (Williams and McBirney, 1979). Much of this slumping probably takes place at the same time as the caldera collapse, when fractures and other slump features form in response to the removal of lateral support. Fractures in Domain I (Figure 15), near the vent margin, are approximately parallel to the strike and dip of the margin and formed in response to slumping along the margin.

Sinistral strike-slip motion along the Longitudinal Fault would cause northwest-trending tension fractures to form, a type of fracture that has been referred to as feather joints by Cloos (1932), or more generally as pinnate fractures (Hobbs, Means and Williams, 1976). Pinnate fractures generally exhibit orientations 40 to 60 degrees divergent from the larger strike-slip fault they are associated with. They have been observed at all scales from thin section (Dunn, Fountain and Jackson, 1973) to regional faults (Tchalenko and Ambraseys, 1970). Fractures in Domain II strike N60W to E-W, 45 to 75 degrees divergent from the N15W striking Longitudinal Fault (Figure 15) and are therefore consistent with strike-slip motion on the fault.

Fractures in Domain III (Figure 15), those within the vent, have a consistent east-west strike and those filled with ore grade vein minerals converge at depth. The orientation of these fractures does not suggest an obvious relationship to the vent or the Longitudinal Fault; they are spatially related to part of the quartz monzonite

porphyry dike swarm. These dikes thicken with depth suggesting that they may be the apophyses of a larger intrusive body.

Several workers have used elastic theory to investigate stress distributions and fracture orientations in the vicinity of fluid-filled cavities, such as magma chambers (Roberts, 1970; Pollard, 1973; Koide and Bhattacharji, 1975; Knapp and Norton, 1981). Roberts (1970) and Pollard (1973) present two-dimensional analysis of stress distributions around elliptical cavities and evaluate failure conditions at the cavity walls. Koide and Battacharji (1975) present a three-dimensional analysis of stress distributions around ellipsoidal cavities and evaluate failure conditions in the medium surrounding the cavity; Knapp and Norton(1981) present a two-dimensional analysis, employing finite elements, of stress distributions around a cooling pluton, and evaluate the evolution of stresses due to heat transfer away from the magma chamber.

The analysis of Koide and Battacharji (1975) and Knapp and Norton (1981) both predict fracture sets in the host rocks above the magma chamber that dip steeply and converge to a point above the chamber. The geometry of the fracture sets is controlled by the shape of the magma chamber. The lithocap of an ellipsoidal magma chamber would be expected to exhibit concentric, inward-dipping, "funnel-shaped," fracture sets, with the center of the funnel above the magma chamber.

The studies by Koide and Battacharji (1975) and Knapp and Norton (1981) have suggested three principal causes for the fracturing in the lithocaps of the intrusions. The first is the

redistribution of stresses induced by the presence of the magma chamber itself. The second is the stress variations induced by the transfer of thermal energy away from the cooling pluton. And the third is stresses induced by changes in magma pressure within the magma chamber.

The converging downward geometry of the fractures in Domain III (Figure 14) and their spatial association with diking suggests that these theoretical studies may be applicable to this fracture set. Some fractures in this set cut dikes and others are cut by dikes, suggesting that fracturing was temporally as well as spatially related to the diking. These relationships suggest that the fractures formed in conjunction with dike emplacement. In the uppermost levels of the mine the minor dikes that are present are off-center with respect to the converging fracture sets. However, deeper in the mine, on the 1000 level and below, the fractures do converge on a 100 m wide dike. This dike is larger in the deeper levels of the mine. Consequently, the fractures in Domain III are interpreted as having formed in the litho-cap of the intrusion that fed the dikes present in the underground mine.

The model studies predict concentric and radial fracture sets above magma chambers. The fractures in Domain III strike consistently east-west. This discrepancy could be due to the shape of the subjacent magma chamber. Concentric and radial fracture sets are predicted for magma chambers of ellipsoidal or cylindrical shapes. The dike swarm exposed at the surface, in the central part of the vent

(Figure 2), is distinctly elongate in the east-west direction. If an east-west elongate magma chamber is present below the fractures in Domain III, its shape would explain the lack of concentric and radial fracture sets.

Ward (1961) has interpreted the vein structures as forming in association with wrench tectonics of external, regional origin; the fractures interpreted as local features formed as part of the large-scale folding and thrusting in the area. If this tectonism was going on during the evolution of the volcanic system, then it should be reflected in the geometry of the deformed rocks within the vent. However, the conical fold shown on Figure 10 shows no evidence of post-collapse deformation. Consequently the volcanic activity and mineralization appear to post-date regional compressional deformation, which Megard (1979) and others have assigned to the early to middle Tertiary.

#### Hydrothermal System

The general characteristics of the ore deposit at Cerro de Pasco, and the hydrothermal system that formed it were recognized early (Bowditch, 1935; Lacy, 1949). Subsequent studies have aimed at elucidating details of the evolution of the hydrothermal system (Lacy and Hosmer, 1956) or using the mineralogical characteristics of the deposit to constrain conditions of formation (Einaudi, 1977). The mineralogical characteristics of the alteration assemblages, together

with the general characteristics of the deposits, can also be used to help constrain conditions of formation.

The fracture permeability which formed by a variety of processes, as discussed above, localized the flow of hydrothermal solutions. Initially, solution flow was localized by the permeable zone defined by the vent margin and mineralization formed when these solutions encountered chemically reactive limestone. This flow pattern is shown by the restriction of mineralization in the lowest levels of the mine to the ring-fault zone of the vent margin and the occurrence of the earliest-formed pyrite in this zone (Lacy, 1949). These early solutions deposited large quantities of quartz and pyrite to form the pyrite-silica body (Lacy, 1949). Pyrrhotite and galena-sphalerite pipes replaced parts of the pyrite-silica body (Einaudi, 1977). Later solutions deposited pyrite-enargite in the veins.

Phase relations for stable mineral assemblages in the vein and massive sulfide settings indicate different conditions during mineral deposition. Einaudi's (1977) data on the iron content of sphalerites together with mineral stability relations place constraints on these conditions. Einaudi (1977) concluded that  $f_{O_2}$  and  $f_{S_2}$  of the solutions associated with vein mineralization were 4 to 5 orders of magnitude higher than those associated with the massive sulfide mineralization.

Solutions in equilibrium with the massive sulfide mineral assemblage, including pyrite, pyrrhotite and locally exsolution blebs of chalcopyrite in sphalerite (Einaudi, 1977), are represented by

point A on Figure 24 and solutions in equilibrium with the vein mineral assemblage, dominated by pyrite and enargite, are represented by point B. Several factors could contribute to this apparent variance in composition. Decreasing temperature must result in the stability of enargite and tennantite at lower values of  $\log a(\text{Cu}^+)/a(\text{H}^+)$ . Knight (1977) and Brimhall and Ghiorso (1983) have presented thermodynamic calculations for the oxidation of reduced, sulfur-rich solutions. For their calculations oxidation increases the  $\text{H}^+$  ion concentration of the solution. The activity ratios for  $(\text{Fe}^{++}/(\text{H}^+)^2)$  and  $(\text{Cu}^+)/(\text{H}^+)$  are decreased. In order to stabilize enargite the activity ratio for reduced copper must decrease at a slower rate than the activity ratio for reduced iron. These variations are compatible with oxidation of an initially reduced solution as it rose into the vent. Rising late solutions equilibrating with the massive sulfide body and moving upward into what would later be the main ore zone of the vein system, would undergo oxidation and temperature decrease. The deposition of pyrite could further reduce the activity ratio for  $(\text{Fe}^{++})/(\text{H}^+)^2$  in the solution. These combined effects brought enargite, and locally tennantite, into equilibrium.

In addition to depositing sulfide and sulfosalt minerals in the veins, these solution altered the adjacent wallrocks. As discussed above, these solutions had high activity products of  $\text{H}^+$  and  $\text{SO}_4^{=}$ , conditions which resulted in the formation of alunite in the alteration zone adjacent to the vein mineralization (Figure 23).



Point A on Figure 28, constructed at quartz saturation, represents a solution in equilibrium with alunite. Progressive depletion of hydrogen ion in the intergranular solutions outward from the vein leads to the mineral zoning indicated by the arrow A-B on Figure 28. This reproduces the zoning observed lateral to the veins and suggests that hydrogen ion metasomatism is the dominant process that is responsible for the alteration assemblages observed. Thus the alteration zones parallel to the veins indicate that intergranular solutions were progressively depleted in hydrogen ion relative to potassium ion away from the vein wall (Figure 28). This depletion was probably accomplished by cation exchange between the solution and the wallrocks coupled with diffusion within the aqueous solution. The exchange was accomplished by adding hydrogen ions to the rocks to generate the alteration minerals, while cations present in the original rock, principally  $\text{Ca}^{++}$ ,  $\text{Mg}^{++}$ , and perhaps  $\text{K}^+$ , were leached and carried away by the solution. The method of transport from the wallrock to the flow channel was probably also by ionic diffusion through the intergranular solution.

The mineral phase diagrams allow constraints to be placed on compositions of hydrothermal solutions associated with mineralization. Values of  $\log a(\text{K}^+)/a(\text{H}^+)$  ranged from approximately 1.0 to 2.0 (Figure 23) for the solutions coexisting with alteration assemblages marginal to the veins. The compositions of the solutions in equilibrium with the sulfide and sulfosalt minerals is more difficult to constrain. The activity ratios of  $(\text{Fe}^{++})/(\text{H}^+)$  and  $(\text{Cu}^+)/(\text{H}^+)$  were probably lower

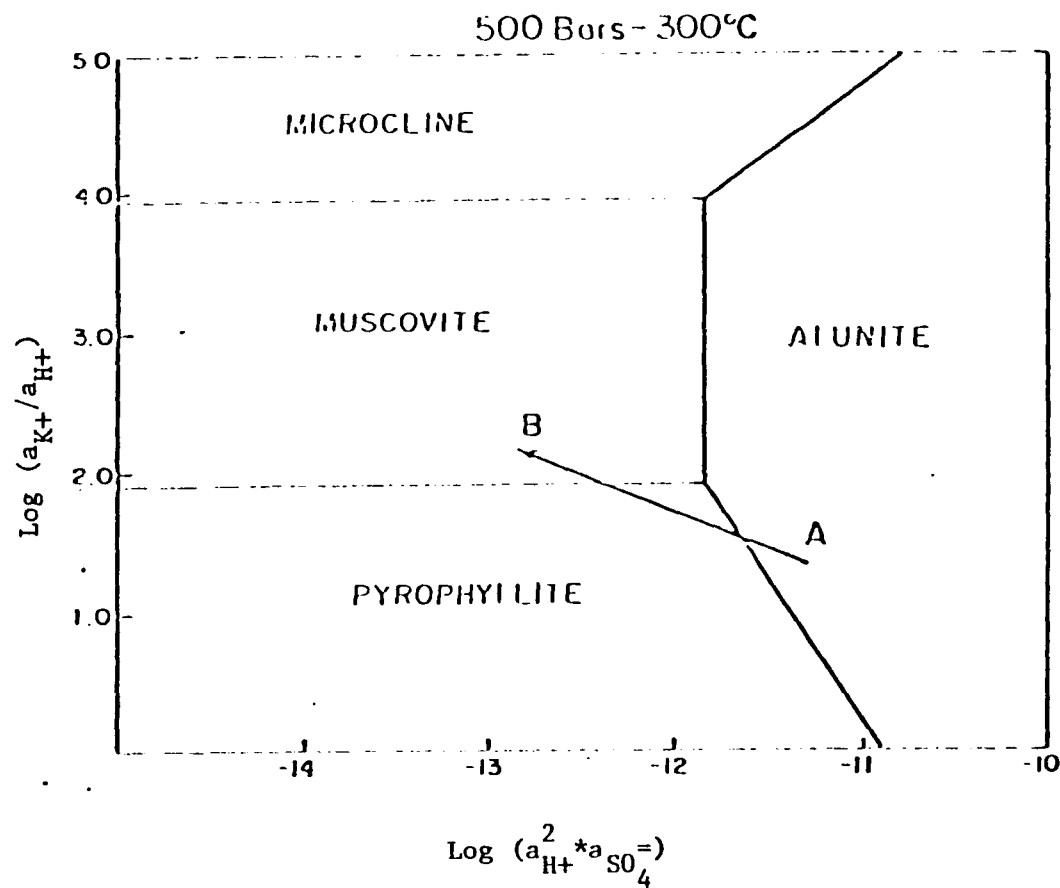


Figure 28. Activity-activity diagram for the system  $K_2O-Al_2O_3-SiO_2-HCl-H_2O$ . -- Activity  $SiO_2$  set at quartz saturation. Point A indicates conditions compatible with alteration immediately adjacent to the vein. The arrow indicates the variation in activity ratios away from the vein margin. Data for diagram from Helgeson et al. (1978).

for solutions in equilibrium with the vein mineral assemblage than for the massive sulfide mineral assemblage. For the conditions specified in the construction of the activity-activity diagrams on Figure 24, the activity ratio of  $(\text{Fe}^{++})/(\text{H}^+)^2$  is 4 to 6 orders of magnitude lower and the activity ratio of  $(\text{Cu}^+)/(\text{H}^+)$  is the same or slightly lower. These conclusions are not significantly changed unless the activity of  $\text{H}_2\text{S}$  varied by more than 2 orders of magnitude from that specified on Figure 24.

The lack of Ca-Mg silicates in the alteration assemblages allows upper limits to be placed on additional activity ratios in the solution. Figure 29 shows phase relations in the system  $\text{MgO-Al}_2\text{O}_3\text{-SO}_3$ . The general lack of Ca-Mg minerals indicates that  $\log a(\text{Ca}^{++})/a^2(\text{H}^+)$  values were less than approximately 5.0 (point A). Isolated occurrences of Ca-Mg silicates indicate that locally these activity ratios were greater.

Temperature is constrained by the assemblage pyrophyllite-kaolinite-quartz, which is stable only above 300°C. In addition, sparse fluid inclusion filling temperatures measured in quartz range from 250°C to 400°C, uncorrected for pressure. Above 350°C, andalusite is the stable alumino-silicate phase. Andalusite has not been reported from Cerro de Pasco, nor was it found in thin section in this study. The assemblage muscovite-kaolinite-quartz indicates temperatures below 300°C. The transition from pyrophyllite requires a decrease in temperature at quartz saturation. Even if  $\log a(\text{K}^+)/a(\text{H}^+)$  were high enough to equilibrate muscovite, pyrophyllite should still

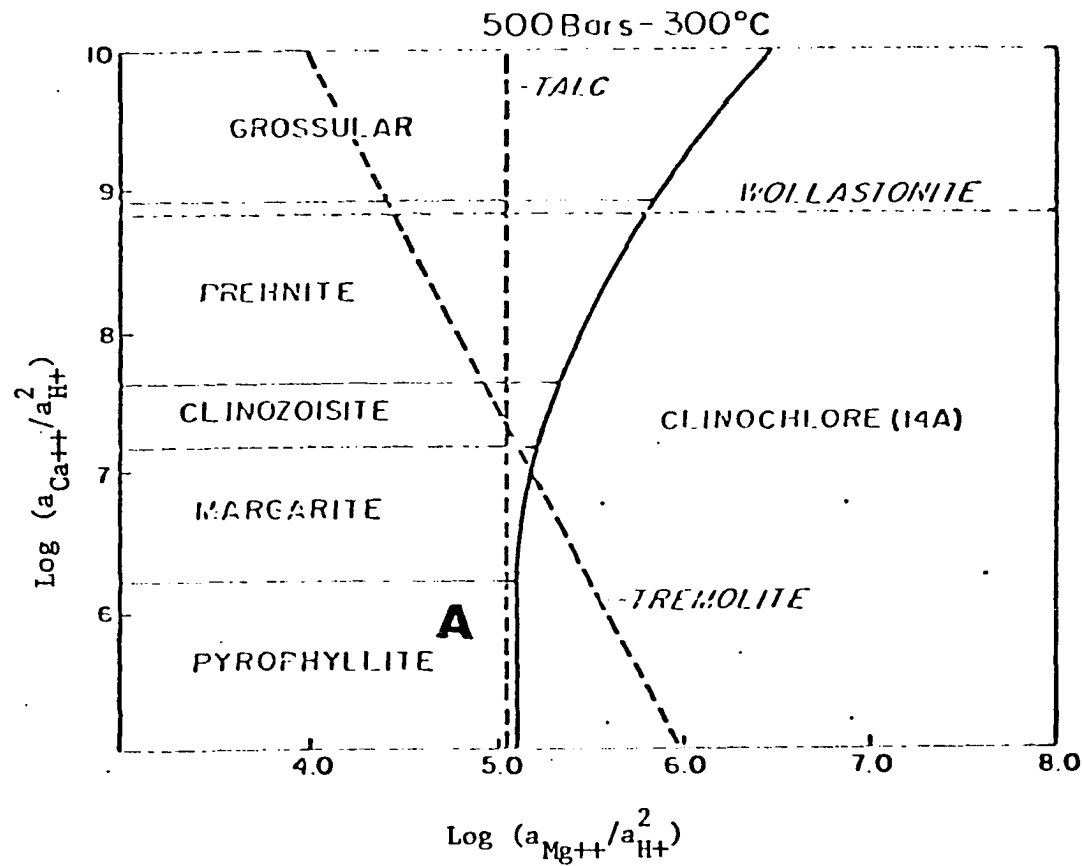


Figure 29. Activity-activity diagrams for the system  $\text{CaO-MgO-Al}_2\text{O}_3\text{-SiO}_2\text{-H}_2\text{O}$ . -- Activity of  $\text{SiO}_2$  set at quartz saturation. Solid lines represent phase boundaries. Dashed lines represent saturation surfaces. Point A indicates conditions compatible with all alteration assemblages. Data for the diagram from Helgeson et al. (1978).

be present in the assemblage if kaolinite is. Below 300°C, the activity of  $\text{SiO}_2$  must be above quartz saturation for pyrophyllite and kaolinite to coexist. At quartz saturation and below 300°C, kaolinite-muscovite is the equilibrium assemblage.

#### Level of Exposure

Several factors suggest that a very shallow level of the system is exposed at Cerro de Pasco, possibly 1 km deep or less (Figure 30). The aphanitic matrix of the Quartz Monzonite Porphyry dikes and dacite domes suggest shallow levels of emplacement, as does the mushroom-cap geometry of the domes. The non-welded nature of most of the tuffaceous volcanic rocks indicates formation at the surface and burial controlled by downdropping of the floor of the vent. The total lack of thermal metamorphic effects on the rootless blocks also suggest shallow burial.

Several lines of evidence indicate that there may be a pluton below the present level of exposure. The dikes exposed in the underground mine become larger in the deepest levels. Approximately a cubic kilometer of rock has been hydrothermally altered and mineralized. A subjacent pluton is the most likely source of thermal energy to drive this system. The alteration assemblages suggest temperatures of approximately 300°C, similar to those predicted by numerical models of the lithocaps of cooling intrusives (Norton, 1979). Finally, in the shallowest levels of the underground mine the alteration assemblages are clearly restricted to the margins of the fracture bounded matrix

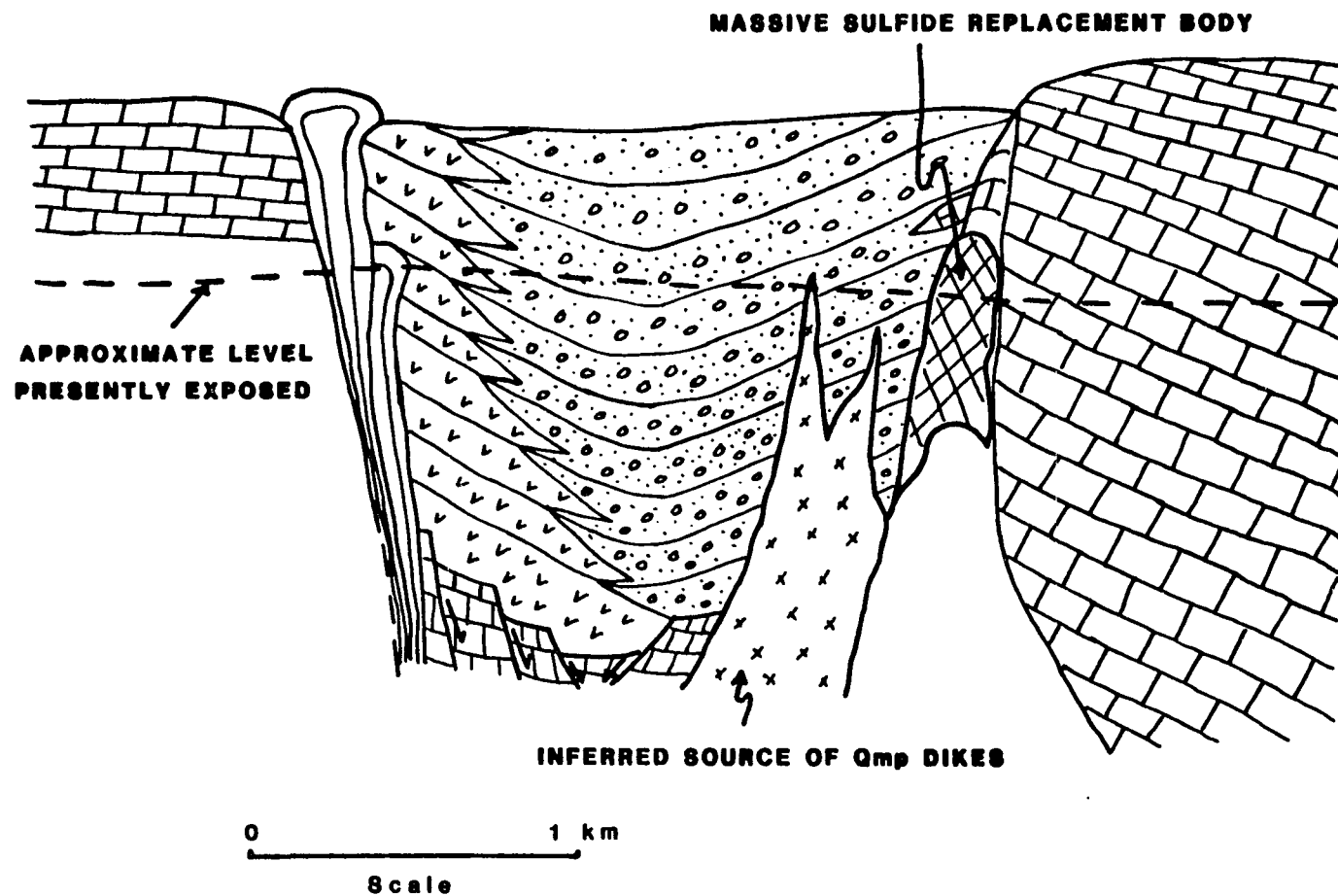


Figure 30. Late stage hydrothermal activity resulted in ore deposition. -- No vertical exaggeration.

blocks. In the deeper levels of the mine the alteration assemblages are more pervasive between the fracture bounded flow channels, suggesting closer proximity to an igneous thermal source.

## CONCLUSIONS

Four principal conclusions have come from this study.

First, the volcanic system at Cerro de Pasco is best characterized as an intermediate depth exposure of a caldera system which has experienced resurgent igneous activity. A roughly cylindrical ring fault system approximately 2 km in diameter defines a volcanic vent that bounds the felsic volcanic system. The vent was filled by volcanoclastic agglomerate, bedded and welded tuff, and slide blocks from the vent walls. Structural collapse within the vent deformed this material into a conical fold with a near vertical fold axis. Resurgent igneous activity included volcanic domes localized along the western margin of the vent and dikes intruded at scattered localities throughout the vent. Resurgence of the central caldera block as described by Smith and Bailey (1968) is not observed. Hydrothermal ore deposition occurred during the final stage in the evolution of this caldera system. Of course, the term caldera as used by Williams (1941) or Williams and McBirney (1979) refers to a topographic form. The topographic surface at the time of volcanism, at Cerro de Pasco, has been removed by erosion and consequently the term caldera cannot be applied precisely. However, the structural evolution of the system reflects processes similar to those inferred for caldera formation (Smith and Bailey, 1968).



Second, the fracture permeability that localized the ore deposit had several origins, in part associated with the evolution of the volcanic system and in part related to regional structures. The ring fault system localized the solutions that deposited the earliest mineralization, the pyrite-silica body. The southern part of the vein system fills fractures formed by slumping along the vent margin, possibly during caldera collapse. The vein structures between the Longitudinal Fault and the vent margin formed in response to sinistral strike-slip motion along the Longitudinal Fault. The vein structures within the vent formed in response to resurgent igneous activity which is manifested by quartz monzonite porphyry dikes.

Third, zoned alteration assemblages and hydrothermal ore mineralization formed as hydrothermal solutions rose into the oxidized environment of the volcanic vent. Early deposited pyrite and pyrrhotite buffered later solutions as they rose through the system. As these later solutions rose into what would be the main ore zone of the vein system, they followed a path of decreasing temperature and increasing oxidation. Oxidation of the solution led to the generation of  $H^+$  and  $SO_4^{=}$  ions. As the solution rose from the massive sulfide body into the vein system the activity ratio of  $(Fe^{++})/(H^+)^2$  probably decreased 4 to 6 orders of magnitude and the activity ratio of  $(Cu^+)/ (H^+)$  probably decreased 1 to 2 orders of magnitude. Hydrogen ions generated by oxidation of the solution altered the wallrocks adjacent to the vein. The activity ratio for  $(K^+)/ (H^+)$  probably increased by 1 to 2 orders of magnitude from the solutions in fracture

controlled flow channels to the solutions in the central portion of matrix blocks.

Fourth, mineralization at Cerro de Pasco represents a classic example of ore deposition at an intermediate depth in a volcanic system. The deposit has classically been related to plutonism, by Lacy (1953) for instance, and the significance of the associated volcanic system has been minimized. However, it is very misleading and, in the end, probably impossible to separate the effects of volcanism and the effects of plutonism on the development of the ore deposit. Volcanism and plutonism have interacted during the evolution of this igneous system in a complex way to generate a structural framework to host ore deposition and generate a hydrothermal system to transport ore forming constituents into the structures. Thus, the ore deposition is best seen as a late stage, intermediate level manifestation of the evolution of this volcanic/plutonic system.

## LIST OF REFERENCES

- Arnorsson, S., 1975, Application of the silica geothermometer in low temperature hydrothermal areas in Iceland, *Am. J. Sci.*, v. 275, p. 763-784.
- Bailey, R. A., Dalrymple, G. E., and Lamphere, M. A., 1976, Volcanism, structure and geochronology of Long Valley Caldera, Mono County, California: *Jour. Geoph. Res.*, v. 81, p. 725-744.
- Balk, 1947, Salt-dome structure: *Am. Assoc. Petroleum Geologists Bull.*, v. 31, p. 1295-1299.
- Bird, D. K. and Norton, D. L., 1981, Theoretical prediction of phase relations among aqueous solutions and minerals: Salton Sea geothermal system: *Geochimica et Cosmochimica Acta*, v. 45, p. 1479-1493.
- Boutwell, J. M., 1920, Geology, ore deposits, and prospects of the property of the Cerro de Pasco Copper Corporation, Cerro de Pasco, Peru: Private Report, 179 p.
- Boutwell, J. M., McLaughlin, D. H., and Walker, W. F., 1920, Mining geology of the properties of the Cerro de Pasco Corporation, Cerro de Pasco, Peru: Scale 1:5000.
- Bowditch, S. I., 1935, The geology and ore deposits of Cerro de Pasco, Peru: Unpublished Ph.D. thesis, Harvard University, 160 p.
- Bowditch, S. I., Boutwell, J. M., McLaughlin, D. H., Walker, W. S., and Noble, J. A., 1931, Geologic map of the Cerro de Pasco District, Scale 1:10,000.
- Brimhall, Jr., George H. and Ghiorso, Mark S., 1983, Origin and ore-forming consequences of the advanced argillic alteration process in hypogene environments by magmatic gas contamination of meteoric fluids: *Econ. Geol.*, v. 78, p. 73-90.
- Carroll, D., 1967, Clay Minerals: A guide to their X-ray identification: *Geol. soc. America, Sp. Paper 126*, 80 p.
- Cathles, L. M., 1977, An analysis of the cooling intrusives by groundwater convection which includes boiling: *Econ. Geol.*, v. 72, p. 804-826.

- Cloos, E., 1932, "Feather joints" as indicators of the direction of movements on faults, thrusts joints and magmatic contacts: Natl. Acad. Sci. Proc., v. 18, p. 387-395.
- Cobbing, E. S., Pitcher, W. S., Wilson, J. J., Caldock, J. W., Taylor, W. P., Mc Court, W., and Snelling, N. S., 1981, The geology of the western Cordillera of northern Peru: Overseas Memoir 5, Institute of Geological Sciences, London, 143 p.
- Doe, B. R., Steven, T. A., Delevaux, M. H., Stacey, S. S., Lipman, P. W., and Fisher, F.S., 1979, Genesis of ore deposits in the Sandman volcanic field, southwestern Colorado; lead isotope evidence: Econ. Geol., v. 74, p. 1-26.
- Doell, R. R., Dalrymple, G. B., Smith, R. L., and Bailey, R. A., 1968, Paleomagnetism, potassium-argon ages, and geology of rhyolites and associated rocks of the Valles Caldera, New Mexico: Geol. Soc. Am. Mem. 116, p. 211-248.
- Donath, F. A. and Parker, R. B., 1964, Folds and Folding: Geol. Soc. America Bull., v. 75, p. 45-62.
- Dunn, D. E., Lafountain, L. S., and Jackson, R.e., 1973, Porosity dependence and mechanism of brittle failure in sandstones: Jour. Geoph. Res., v. 78, p. 2403-2417.
- Einaudi, M. T., 1968, Pyrrhotite-pyrite-sphalerite relations at Cerro de Pasco, Peru: Unpublished Ph.D. thesis, Harvard University, 381 p.
- Einaudi, M. T., 1977, Environment of ore deposition at Cerro de Pasco, Peru: Econ. Geol., v. 72, p. 893-924.
- Francis, P. W., Baker, M. C. W., and Halls, C., 1981, The Kari Kari Caldera, Bolivia, and the Cerro Rico stock: Jour. volc. Geothem. Res., v. 10, p. 113-124.
- Geological Staff of Cerro de Pasco Corporation, 1950, Lead and zinc deposits of the Cerro de Pasco Corporation in central Peru: Internat. Geol. Cong., 18th, Great Britain, 1948, Part VII, p. 54-186.
- Graton, L. C. and Bowditch, S. I., 1936, Alkaline and acid solutions in hypogene zoning at Cerro de Pasco: Econ. Geol., v. 31, p. 651-698.
- Gustafson, L. B., 1963, Phase equilibria in the system Cu-Fe-As-S: Econ. Geol., v. 58, p. 667-701.

- Hamilton, W., 1965, Geology and Petrogenesis of the Island Park Caldera of rhyolite and basalt, eastern Idaho: U.S. Geol. Survey, Prof. Paper 501-C, 37 p.
- Helgeson, H. C., 1979, Mass transfer among minerals and hydrothermal systems: In, Barnes, H. L., ed., Geochemistry of hydrothermal ore deposits: John Wiley, New York, p. 568-610.
- Helgeson, H. C., Delany, J. M., Nesbitt, H. W., and Bird, D. K., 1978, Summary and critique of the thermodynamic properties of rock forming minerals: Am. Jour. Sci., v. 278A, 229 p.
- Hemley, J. S., Hostetler, P. B., Gude, A. S., and Montjoy, W. T., 1969, Some stability relations of alunite: Econ. Geol., v. 64, p. 599-612.
- Hemley, J. S., and Jones, W. R., 1964, Chemical aspects of hydrothermal alteration with emphasis on hydrogen metasomatism: Econ. Geol., v. 59, p. 538-569.
- Hobbs, B. E., Means, W. D., and Williams, P. F., 1976, An outline of structural geology: John Wiley and Sons, New York, 571 p.
- Jenks, W. F., 1951, Triassic to Tertiary stratigraphy near Cerro de Pasco, Peru: Geol. Soc. America Bull., v. 62, p. 203-220.
- Knapp, R. B. and Norton, D., 1981, Preliminary numerical analysis of processes related to magma crystallization and stress evolution, in cooling pluton environments: Am. Jour. Sci., v. 281, p. 35-68.
- Knight, J. E., 1977, A thermochemical study of alunite, enargite, luzonite and tennantite deposits: Econ. Geol., v. 72, p. 1321-1336.
- Koide, H. and Bhattacharji, S., 1975, Formation of fractures around magmatic intrusions and their role in ore localization: Econ. Geol., v. 70, p. 781-799.
- Kouda, R. and Koide, H., 1978, Ring structures, resurgent cauldron, and ore deposits in the Hokuroka Volcanic field, northern Akita, Japan: Mining Geology, v. 28, p. 233-244.
- Kruger, F. C. and Lacy, W. C., 1949, Geological explanation of geophysical anomalies near Cerro de Pasco, Peru: Econ. Geol., v. 44, p. 485-491.

- Lacy, W. C., 1949, Types of pyrite and their relations to mineralization at Cerro de Pasco, Peru: Unpublished Ph.D. thesis, Harvard University, 193 p.
- Lacy, W. C., 1953, Differentiation of igneous rocks and its relation to ore deposition in central Peru: Soc. Geol. Peru Bol., v. 26, p. 121-138.
- Lacy, W. C. and Hosmer, H. L., 1956, Hydrothermal leaching in central Peru: Econ. Geol., v. 51, p. 69-79.
- Lambert, I. B. and Sato, T., 1974, The Kuroko and associated ore deposits of Japan: A review of their features and metallogenesis: Econ. Geol., v. 69, p. 1215-1236.
- Lambert, M. B., 1974, The Bennett Lake cauldron subsidence complex, British Colombia and Yukon Territory: Canada Geol. Survey Bull., v. 227, 213 p.
- Lipman, P. W., 1976, Caldera-collapse breccias in the western San Juan Mountains, Colorado: Geol. Soc. America Bull., v. 87, p. 1397-1410.
- Lipman, P. W., Fisher, F. S., Mehuert, H. H., Naeser, C. W., Luedke, R. G., and Steven, T. A., 1976, Multiple ages of mid-Tertiary mineralization and alteration in the western San Juan Mountains, Colorado: Econ. Geol., v. 71, p. 571-588.
- McDowell, D. and Elders, W. A., 1980, Layer silicate minerals in borehole Elmore No. 1, Salton Sea geothermal field, California, U.S.A.: Contrib. Mineral. Petrol., v. 74, p. 293-310.
- McLaughlin, D. H., 1924, Geology and physiography of the Peruvian Cordillera, Departments of Junin and Lima: Geol. Soc. America Bull., v. 35- p. 591-632.
- McLaughlin, D. H., Graton, L. C. et al., 1933, Copper in the Cerro de Pasco and Morococha districts, Department of Junin, Peru: Copper Resources of the World, 16th Inter. Geol. Cong., Washington, p. 513-544.
- Megard, F., 1979, Estudio geologico de los Andes del Peru Central: Inst. Geol. Minero y Metal., Bol. No. 8, 220 p.
- Meyer, C., and Hemley, J. S., 1967, Wall rock alteration: In Geochemistry of Hydrothermal Ore Deposits, H. L. Barnes, ed., New York: Holt, Rinehart and Winston, p. 166-235.

- Moore, J. G., 1967, Base surge in recent volcanic eruptions: *Bull. Volc.*, v. 30, p. 337-363.
- Newell, N. D., Chronic, J., and Roberts, T. G., 1953, Upper Paleozoic of Peru: *Geol. Soc. America Mem.* 58, 276 p.
- Noble, D. C., 1982, Personal communication, Professor of Geology, University of Nevada at Reno, Reno, Nevada.
- Noble, D. C., McKee, E. H., and Megard, F., 1979, Early Tertiary "Incaic" tectonism, uplift and volcanic activity, Andes of central Peru: *Geol. Soc. America Bull.*, v. 90, p. 903-907.
- Norton, D., 1979, Transport phenomena in hydrothermal systems: The redistribution of chemical components around cooling magmas: Centieme anniversaire de la Societe Francaise de Mineralogie, Nancy, *Bull. Mineral.*, v. 102, p. 471-486.
- Norton, D., 1981, Personal communication, Professor of Geology, University of Arizona, Tucson, Arizona 85721.
- Norton, D., and Knight, J. E., 1977, Transport phenomena in hydrothermal systems: Cooling plutons: *Am. Jour. Sci.*, v. 277, p. 937-981.
- Ohmoto, H., 1978, Submarine Calderas: A key to the formation of volcanogenic massive sulfide deposits: *Mining Geology*, v. 28, p. 219-231.
- Peterson, U., 1965, Regional geology and major ore deposits of central Peru: *Econ. Geol.*, v. 60, p. 407-476.
- Pollard, D. D., 1973, Derivation and evaluation of a mechanical model for sheet intrusions: *Tectonophysics*, v. 19, p. 233-269.
- Ramberg, H., 1981, Gravity deformation and the earth's crust as studied by centrifuged models: Academic Press, London and New York, 2nd Ed., 452 p.
- Ramsay, J. G., 1967, Folding and fracturing of rocks: McGraw-Hill, New York, 568 p.
- Rivera, N., 1970, Mina Cerro de Pasco, in Departamento de Geologia de la Cerro de Pasco Corporation (Seccion Minas), Geologia de los yacimientos minerales operandos per la Cerro de Pasco Corporationi La Oroya, Peru, Cerro de Pasco Corporation, p. 12-40.

- Roberts, J. L., 1970, The intrusion of magma into brittle rocks: In, Newall, G. and Rost, N., Eds., Mechanism of Igneous Intrusion, Gallery Press, Liverpool, p. 287-338.
- Rogers, R. D., 1982, Evolution of fracture permeability during caldera collapse and resurgence at Cerro de Pasco, Peru: Geol. Soc. America Abstracts with Programs, v. 14, no. 7, p. 601-602.
- Ross, C. S., and Smith, R. L., 1960, Ashflow Tuffs: Their origin, geological relation and identification: U.S. Geological Survey Professional Paper 366, 81 p.
- Rytuba, J. J., 1981, Relation of calderas to ore deposits in the western United States: Arizona Geol. Soc. Digest, v. 14, p. 227-236.
- Silberman, M. L. and Noble, D. C., 1977, Age of igneous activity and mineralization, Cerro de Pasco, central Peru: Econ. Geol., v. 72, p. 925-930.
- Slack, J. F., 1980, Multistage vein ores of the Lake City District, western San Juan Mountains, Colorado: Econ. Geol., v. 75, p. 963-991.
- Smith, R. L., 1960, Ashflows: Geological Society Bulletin, vol. 71, p. 795-842.
- Smith, R. L. and Bailey, R. A., 1968, Resurgent cauldrons: In Studies in Volcanology: Geol. Soc. America Mem. 116, p. 613-662.
- Smith, R. L., Bailey, R. A., and Ross, C. S., 1961, Structural evolution of the Valles caldera, New Mexico, and its bearing on the emplacement of ring dikes: U. S. Geol. Survey, Prof. Paper 424-D, p. D145-D149.
- Steven, T. A. and Lipman, P. W., 1976, Calderas of the San Juan volcanic field, southwestern Colorado: U.S. Geol. Survey, Prof. Paper 958, 35 p.
- Steven, T. A., Luedke, R. G., and Lipman, P. W., 1974, Relation of mineralization to calderas in the San Juan volcanic field, southwestern Colorado: U.S. Geol. Survey Jour. of Research, v. 2, no. 4, p. 405-409.



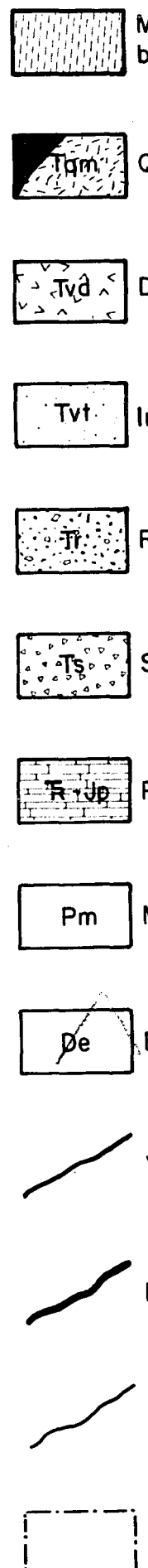
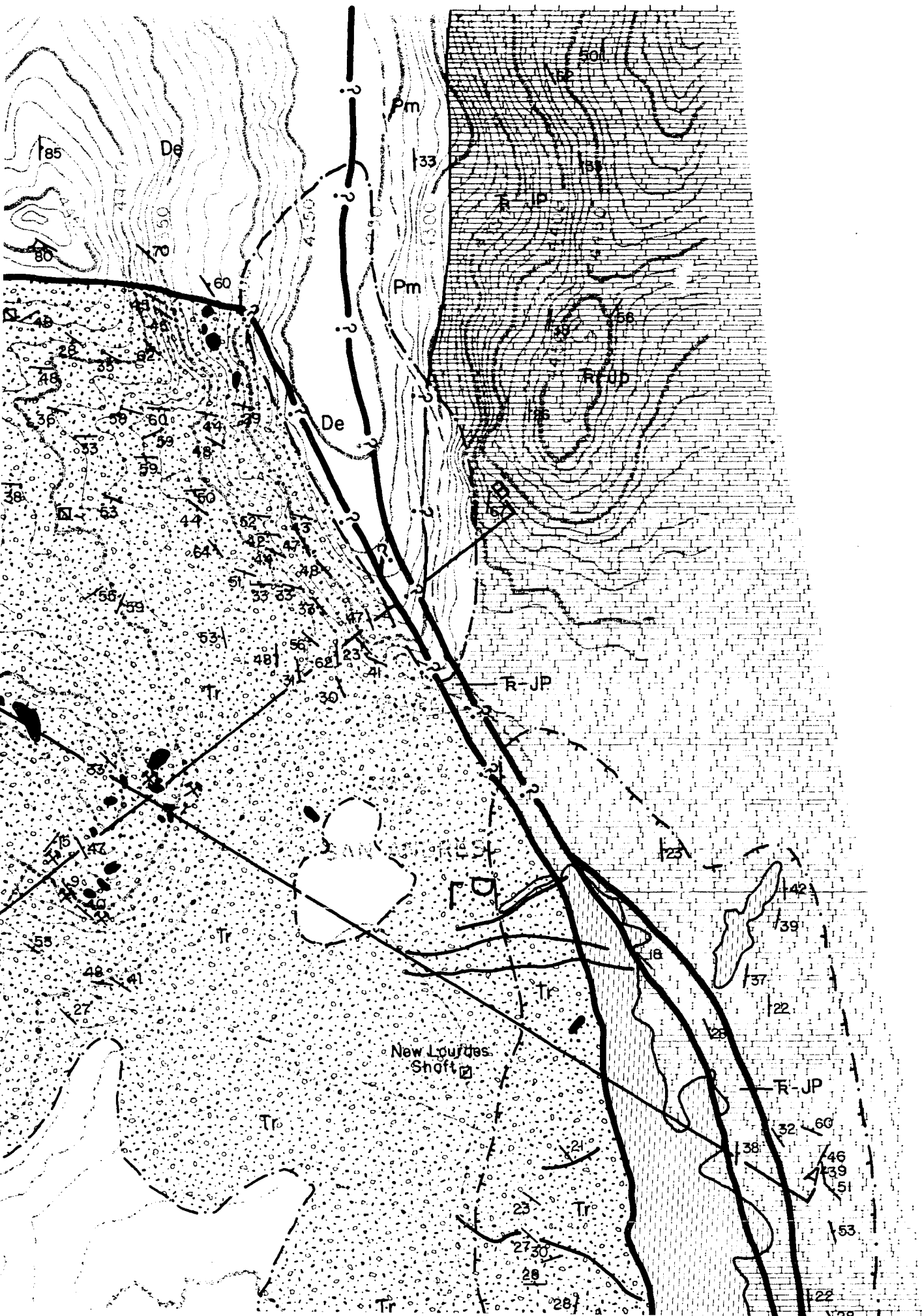
- Steven, T. A. and Ratte, 1965, Geology and structural control of ore deposition in the Creede District, San Juan Mountains, Colorado: U.S. Geol. Survey, Prof. Paper 487, 90 p.
- Szekely, T. S. and Grose, L. T., 1972, Stratigraphy of the carbonate, blackshale and phosphate of the Pucara Group (Upper Triassic-Lower Jurassic), Central Andes, Peru: Geol. Soc. America Bull., v. 83, p. 407-428.
- Tchalenko, J. S. and Ambraseys, N. N., 1970, Structural analysis of the Dasht-e Bayaz (Iran) earthquake fractures: Geol. Soc. America Bull., v. 81, p. 41-60.
- Ward, H. J., 1961, The pyrite body and copper ore bodies, Cerro de Pasco mine, central Peru: Econ. Geol., v. 56, p. 402-422.
- Weaver, C. E. and Pollard, L. D., 1973, The chemistry of clay minerals: Developments in Sedimentology, v. 15, Amsterdam, Elsevier, 213 p.
- Williams, H., 1932, The history and character of volcanic domes: Univ. California Pub. Geol. Sci., v. 21, p. 51-146.
- Williams, H., 1941, Calderas and their origin: California Univ. Pubs. Geol. Sci., v. 25, p. 239-246.
- Williams, H., 1942, Geology of Crater Lake National Park, Oregon: Carnegie Inst. Washington, Pub. 540.
- Williams, H. and McBirney, A. R., 1979, Volcanology: Freeman, Cooper and Co., San Francisco, 397 p.





FIGURE 12





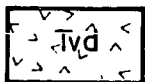




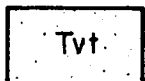
Massive Sulfide-Dominantly pyrite-silica with pipe-like bodies of galena-sphalerite.



Quartz monzonite porphyry dikes.



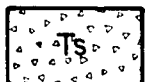
Dacite to Rhyodacite porphyries. Flow banding defines domal structure.



Intermediate to felsic tuffs. Locally welded.



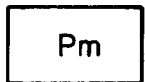
Rumiallana Agglomerate.



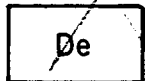
Shuco Conglomerate.



Pucara Group.



Mitu Group (?).



Excellsior Phyllite.



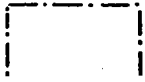
Veins - Projected from 600 foot level of mine.



Faults



Contacts



Stockpiles







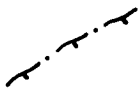













-  Contacts
-  Stockpiles
-  Pit edge
-  Strike & Dip of bedding.
-  Strike & Dip of foliation in volcanics & metamorphics.
-  20 Fold axis showing bearing & plunge.

 Diapiric structures

 Adit

 Shaft

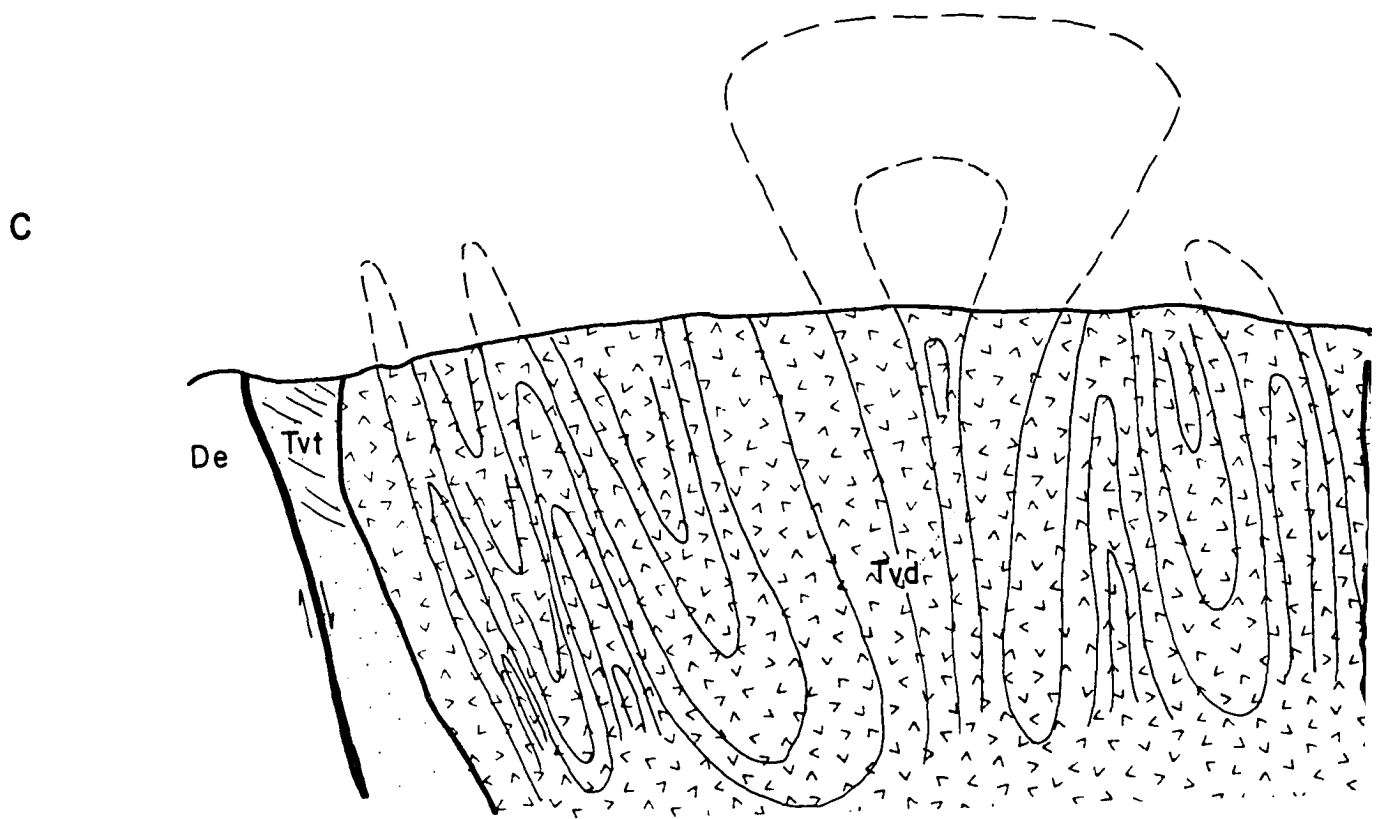
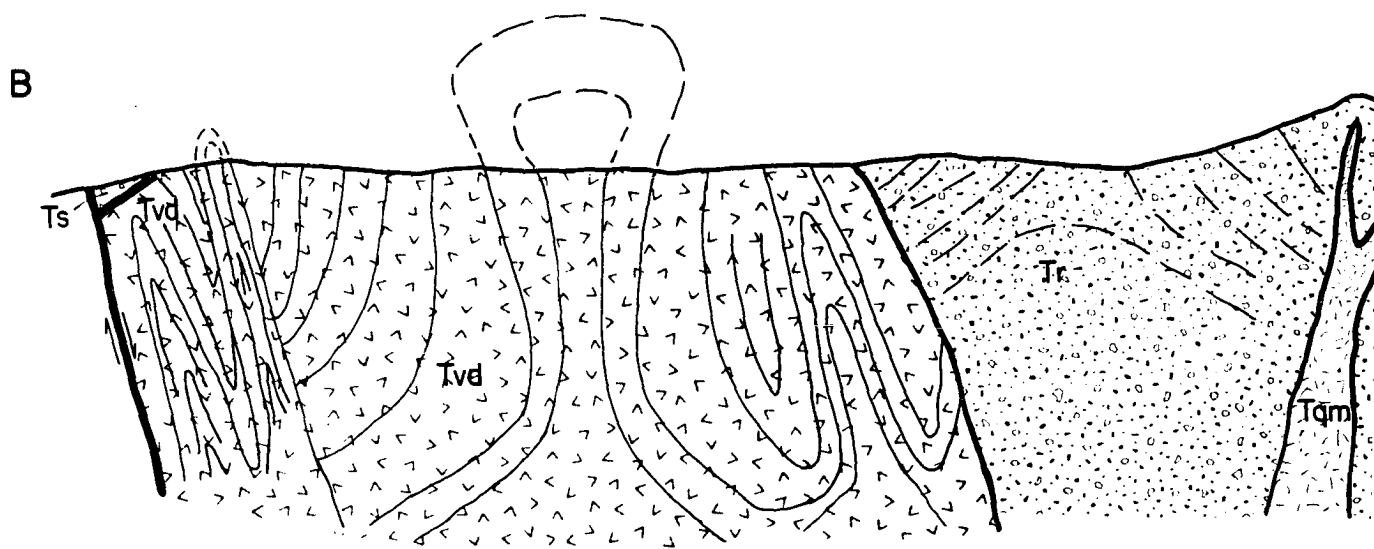
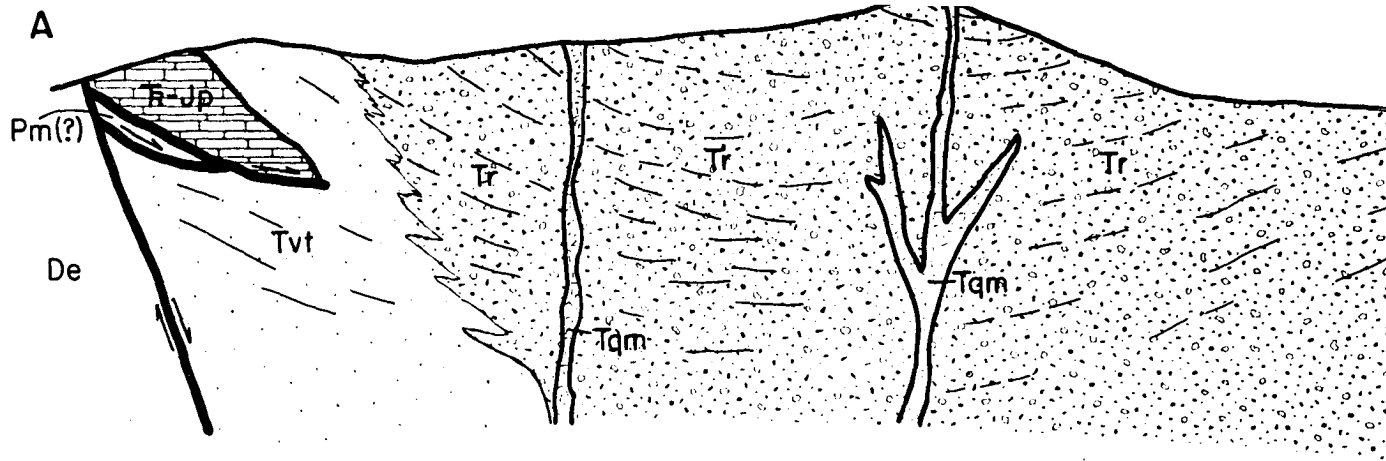
 Vertical component of net slip.

 Vertical component of net separation.



## GEOLOGIC MAP

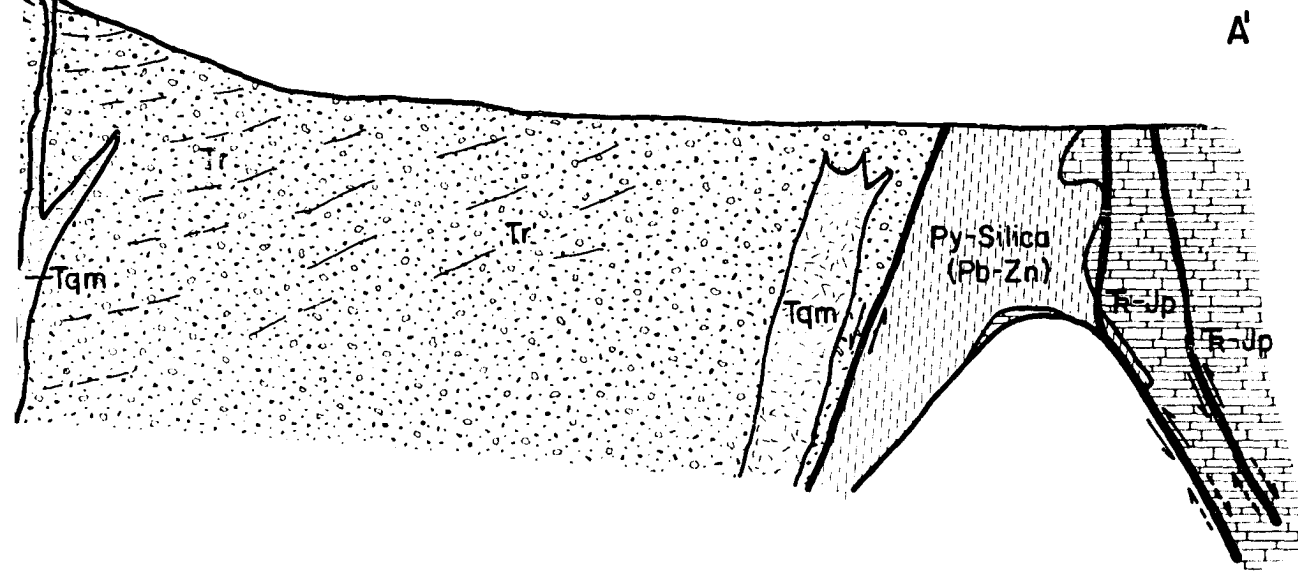




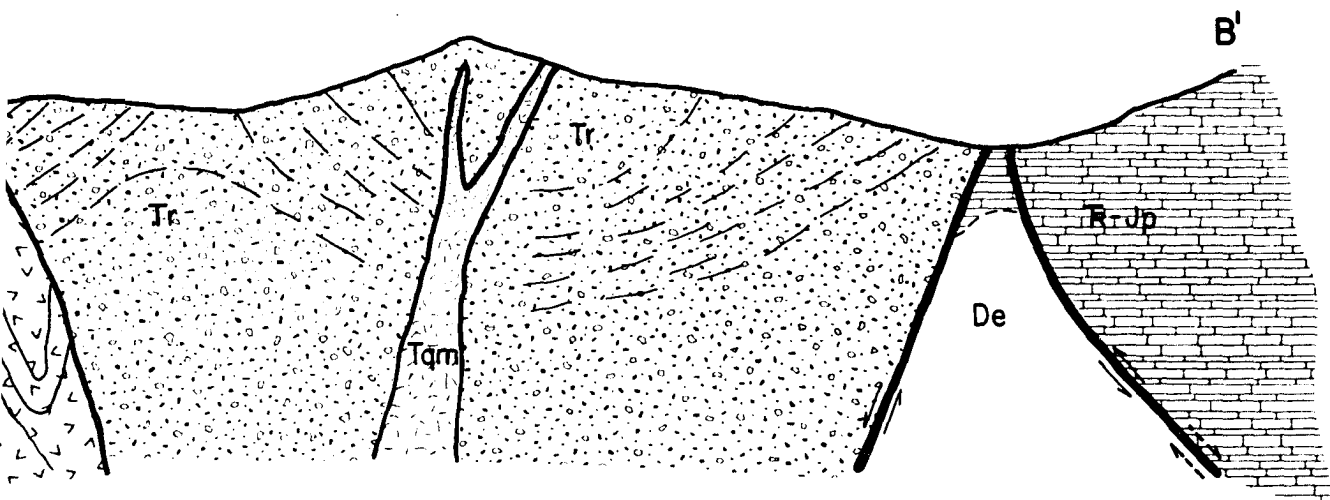




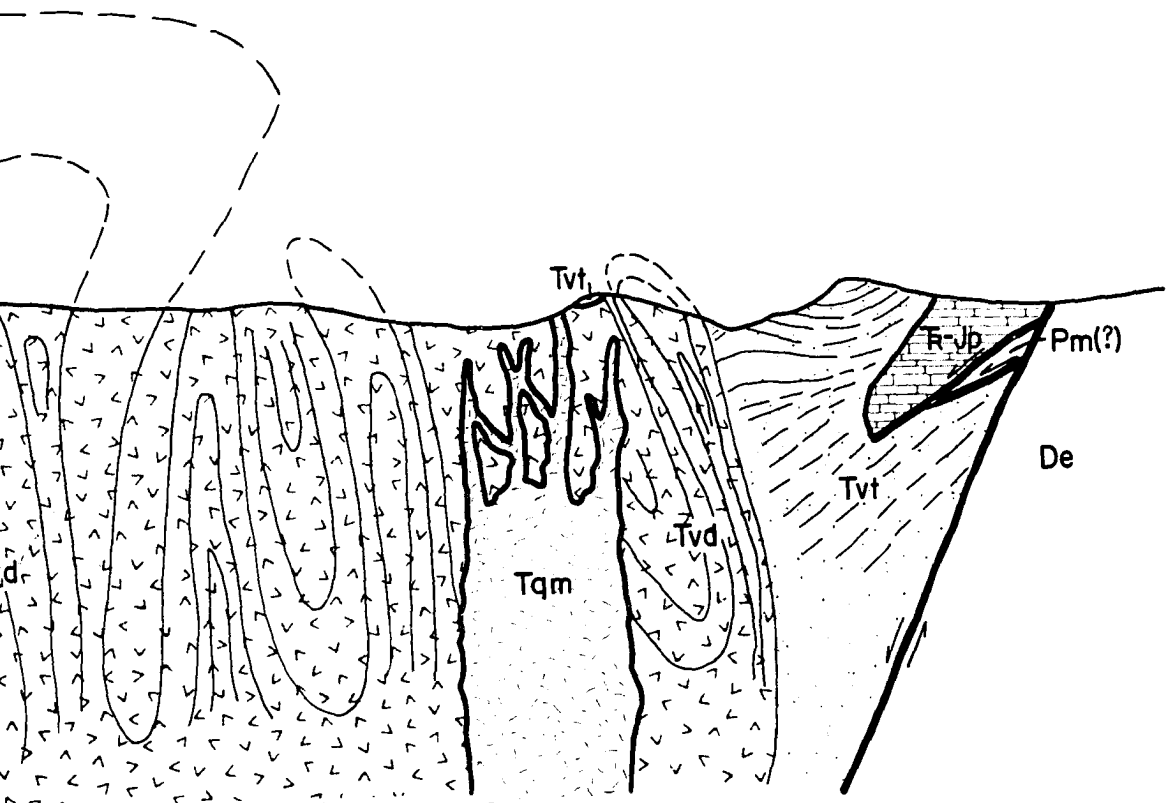
A'



B'



C'





**GEOLOGIC MAP  
and  
CROSS SECTIONS  
  
of the  
  
CERRO de PASCO DISTRICT  
PERU**

**Geology by: Ralph Rogers**

**June 1982**

**FIGURE 2**

*University of Arizona  
Department of Geosciences  
Ralph David Rogers  
Doctor of Philosophy  
1983*

